# Stony Brook University

# Quantum Computation and Quantum Measurements with Mesoscopic Superconducting Structures

A Dissertation Presented

by

**Qiang Deng**

to

The Graduate School

in Partial Fulfillment of the

Requirements

for the Degree of

**Doctor of Philosophy**

in

**Physics**

Stony Brook University

**August 2013**

**Stony Brook University**

The Graduate School

**Qiang Deng**

We, the dissertation committee for the above candidate for the Doctor of Philosophy degree, hereby recommend acceptance of this dissertation.

**Dmitri V. Averin**

**Department of Physics and Astronomy, SBU**

**Dissertation Director**

**Jacobus Verbaarschot**

**Department of Physics and Astronomy, SBU**

**Chairman of Dissertation**

**Xu Du**

**Department of Physics and Astronomy, SBU**

**Jiangyong Jia**

**Department of Chemistry, SBU**

**Serge Luryi**

**Department of Electrical and Computer Engineering, SBU**

This dissertation is accepted by the Graduate School

Charles Taber

Interim Dean of the Graduate School

Abstract of the Dissertation

**Quantum Computation and Quantum Measurements with Mesoscopic Superconducting Structures**

by

**Qiang Deng**

**Doctor of Philosophy**

in

**Physics**

Stony Brook University

**2013**

Systems of mesoscopic Josephson junctions are at present among the leading candidates for development of practical qubits for quantum information devices. Although different qubit structures have been realized with Josephson junctions, their common feature is the design that is optimized to overcome the problem of decoherence by the low-frequency noise that exists in all solid-state structures. In the presented dissertation research, we propose and study an alternative approach of direct suppression of noise by a feedback loop based on the low-frequency quantum measurements. The minimal noise induced in the qubit by such a feedback loop is calculated under the conditions of continuous quantum-limited measurements. Another obstacle facing the quantum Josephson junction circuits is the information transfer between the circuit elements. Here we study the quantum dynamics of dual-rail arrays of nSQUIDs characterized by a negative inductance between its arms, which hold promise for quantum information transfer. The scaling and decoherence properties of these arrays are analyzed. Information transfer along nSQUID

arrays can also be used to implement adiabatic quantum computation (AQC), an alternative to the gate-model approach to quantum computation that is expected to be more stable against the decoherence. Here we suggest fidelity of the ground state as the quantitative measure of the ultimate effect of decoherence on AQC. We show that decoherence-induced deformation of the ground state of an AQC algorithm is characterized by the same noise correlators as those that determine the decoherence time in the gate-model approach. Results for fidelity of a 16-qubit array at finite temperatures are obtained numerically.

# Contents

# List of Figures

# Acknowledgements

Here I want to thank everyone I met during the past five years, who made my life beautiful and memorable.

Among them, foremost, I am grateful to my advisor Prof. Dmitri V. Averin, whose guidance benefited me profoundly. Without his support, this work would not be possible. I also want to thank Prof. Mohammad H. Amin for the kind help and pleasant collaboration.

I also want to thank my family for the never-ending support. In the end, I want to thank my friends in B120 for the joyful discussion and inspiration, and all my friends for the unforgettable support and sharing.

# Publications

"Decoherence induced deformation of the ground state in adiabatic quantum computation", Qiang Deng, Dmitri V. Averin, Mohammad H. Amin and Peter Smith, *Scientific Reports* **3**, Article number: 1479, (2013).

# Chapter 1

# Introduction to Superconducting Quantum Computing

## 1.1 Introduction to quantum computing

The concept of quantum computation was proposed by David Deutsch[1] in 1985, when he was trying to find a physical foundation for the Church-Turing thesis[2, 3]. Also he attempted to define a computation model that can simulate arbitrary physical system efficiently. Naturally, he considered a computer based on quantum mechanics, i.e., the quantum computing, since quantum mechanics is the basic principle followed by the physical system. Since then this idea drew a lot of attention, especially in 1994 when Peter Shor[4] put forward the Shor's algorithm, showing that an integer factorization can be accomplished in polynomial time using a quantum computer. Afterward, several quantum algorithms were proposed, including the Grover's search algorithm[5] which is much faster (with complexity $O(\sqrt{N})$) in comparison to the classical searching algorithm (with complexity $O(N)$).

One of the most important features of these algorithms is quantum parallelism, loosely speaking, ability of a quantum computing device to evolve simultaneously along different classical computation trajectories. This ability implies that the sys-

tem stays coherent during the computation process, however, any parasitic interactions with other external degrees of freedom destroys the coherence of the quantum evolution of a computing device. This "decoherence" problem represents a big challenge faced by quantum computing. In 1996 Robert Calderbank and Peter Shor[7], and Andrew Steane[8] proposed the quantum error correcting codes to protect quantum states against the decoherence produced by unavoidable coupling to external environment. This CSS code is able to correct arbitrary errors in a single qubit by encoding one qubit of quantum information with several physical entangled qubits. Following this direction, an encouraging result - the threshold theorem[9, 10, 11, 12] - was found. This theorem asserts that as long as the error rate of individual quantum qubits and gates is below certain threshold, the fault-tolerant quantum computing can be realized with a poly-logarithmically larger quantum circuit. The precise value of the threshold depends on the assumed models of the environmental noise and desired capability of the computer, but typically the threshold value of the qubit quality factor value is estimated as $10^{-5} - 10^{-6}$. In 2005, it was proven that the threshold can be as high as $1 - 3\%$ [13] provided that the number of qubits can be made sufficiently large. Therefore, development of scalable qubits with relatively large quality factors is the main goal of solid-state qubit research.

## 1.2 Qubit: A Two Level System

The basic building block of a classical computer is a bit of information, which can take two values, 0 or 1, and a physical system with two possible states that represent these two values. For the quantum computing, the notion of a bit is replaced by the qubit, i.e., quantum bit. Physical qubit is a two-level quantum system and its possible states span a two-dimension Hilbert space. Assume the basis state of this system are $|0\rangle$ and $|1\rangle$, then an arbitrary state of the qubit $|\psi\rangle$ is a superposition of the two basis states: $|\psi\rangle = c_0|0\rangle + c_1|1\rangle$. This means that a logical qubit of information is encoded by the two coefficients $c_0$ and $c_1$. The quantum character of

these coefficients as amplitudes of probability can be used to dramatically enhance the computational capacity of a two-state system.

Although the theory of qubit advantages for information processing is quite straightforward, the only real two-level systems available in solid state experiments is spin-1/2, which is very difficult to isolate and manipulate individually because of the weakness of magnetic interactions. Typical systems employed in these experiments are all either "mesoscopic" or macroscopic, and have a very large number of degrees of freedom. In this respect, the majority of experimental solid-state qubits are effective two-level systems, which means that their dynamics is reduced to two levels in some range of (typically low) energies and corresponding characteristic time scales. For excitations on these time scales, employed in the computation process, transitions to other energy levels can be ignored. In practice, this is realized typically in a system with two lowest energy levels split by a small tunneling-produced energy gap, and separated from other energy levels by a much larger characteristic gap $\Delta E$. If the thermal energy and other excitation energies are small, e.g., $k_B T \ll \Delta E$ ($k_B$ is the Boltzmann's constant), the excitations can be suppressed exponentially and the system works effectively as a two-level system.

The Hamiltonian of a two level system is determined by the energy splitting $\epsilon$ and tunneling amplitude $\Delta$ with the following general form:

$$\hat{H} = \frac{\epsilon}{2}\hat{\sigma}_z + \frac{\Delta}{2}\hat{\sigma}_x = \frac{1}{2}\begin{pmatrix} \epsilon & \Delta \\ \Delta & -\epsilon \end{pmatrix} . \tag{1.1}$$

In the most basic designs of a qubit, the basis states $|0\rangle$ and $|1\rangle$ chosen to write down this Hamiltonian, can be characterized typically by different values of some classical collective degree of freedom, e.g., the number of Cooper pairs charging a superconducting island in a charge qubit[21, 22, 23], or magnetic flux through a superconducting loop in a flux qubit[24, 25, 26]. Tunneling between these two states mixes them together and creates a characteristic level-crossing spectrum (Fig. 1.1).

The eigenstates are generally a superposition of the $|0\rangle$ and $|1\rangle$ states, especially at the degeneracy point, where $\epsilon = 0$, and the eigenstates of $\hat{H}$ are the symmetric and antisymmetric superposition of $|0\rangle$ and $|1\rangle$, which gives an equal probability of occupying the two macroscopically distinct states. The time evolution of the

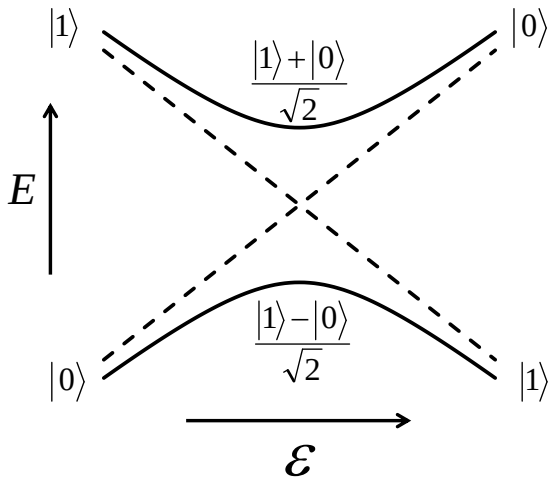


Figure 1.1: Eigenvalues of the Hamiltonian (1.1) for different values of the bias $\epsilon$. The eigenstates corresponding to these eigenvalues are generally a superposition of the basis states $|0\rangle$ and $|1\rangle$. At the degeneracy point, the eigenstates are the symmetric and anti-symmetric superposition of $|0\rangle$ and $|1\rangle$.

qubit (1.1) is governed by the Schrödinger equation. For an isolated system, the final state $|\psi(t)\rangle$ and initial state $|\psi(0)\rangle$ are related via a unitary transformation $|\psi(t)\rangle = \exp(-i\hat{H}t/\hbar)|\psi(0)\rangle$. For a generic initial state, this corresponds to the coherent oscillation between the two basis states. Assume $|\psi(0)\rangle = |0\rangle$, then

$$|\psi(t)\rangle = \cos(Et/\hbar)|0\rangle + i\sin(Et/\hbar)|1\rangle, \quad E = \frac{1}{2}\sqrt{\epsilon^2 + \Delta^2}\,. \tag{1.2}$$

The probability of occupying the state $|0\rangle$ oscillates with time $t$ as $\cos^2(Et/\hbar)$. Such coherent quantum oscillations represent the most basic manifestation of quantum coherence, which usually serves as the sign of the realization of coherent quantum dynamics in qubit experiments.

In real experiments, however, the qubits are always coupled to other "parasitic" degrees of freedom collection of which constitutes "external environment" that leads to eventual decoherence of coherent quantum qubit dynamics. A characteristic feature of such an environment is that it is coupled to a qubit through a dynamically fluctuating random force, "noise". In many cases, the nature of the environment generating the external noise is not essential, and the qubit decoherence can be understood directly in terms of the noise. To illustrate the concept of decoherence in more details, consider one of such cases, when a two-level system is weakly and diagonally coupled to a white noise:

$$H = \frac{\Omega}{2}\sigma_z + \frac{g}{2}\sigma_z \hat{f}(t)\,. \tag{1.3}$$

The coupling constant $g$ is assumed to be small. Since the system is not isolated from its environment anymore, the language of density matrix [15, 16] should be used, with its evolution equation

$$i\hbar\dot{\rho} = [H,\rho] = \left(\Omega + g\hat{f}(t)\right)\begin{pmatrix} 0 & \rho_{01} \\ \rho_{10} & 0. \end{pmatrix}\,. \tag{1.4}$$

The solution of this equation can be found immediately:

$$\rho_{01}(t) = \rho_{01}(0)\exp\left(-\frac{i\Omega t}{\hbar}\right)\exp\left(\frac{i}{\hbar}\int_0^t g\hat{f}(t')dt'\right)\,. \tag{1.5}$$

This equation has a clear physical meaning. When the two-level system is coupled to the external noise, the energy difference between its levels fluctuates around the noiseless value $\Omega$. Since the relative phase shift between the two energy levels is proportional to the energy difference, it becomes a random number, losing the definite structure $(\Omega/\hbar)t$ as before. The precise value of $\rho_{01}(t)$ depends on the path of $\hat{f}(t)$ which is a stochastic process, so only the average value can be determined. The average value of $\rho_{01}(t)$ is decided by the statistical properties of $\hat{f}(t)$, most impor-

tantly, the mean $\langle\hat{f}\rangle$ and the correlation function $\langle\hat{f}(t_1)\hat{f}(t_2)\rangle$. For the stationary white noise, these are:

$$\langle\hat{f}(t)\rangle = 0, \quad \langle\hat{f}(t_1)\hat{f}(t_2)\rangle = \langle\hat{f}(t_1 - t_2)\hat{f}(0)\rangle = 2\pi S_f \delta(t_1 - t_2)\,. \tag{1.6}$$

Here $\langle\ldots\rangle = Tr_{env}(\ldots)$. The average value can always be taken to be zero, because otherwise it can be combined with $\Omega$. The correlation function is described by the spectral density $S_f(\omega)$:

$$S_f(\omega) = \frac{1}{2\pi}\int_{-\infty}^{\infty}\langle\hat{f}(t)\hat{f}(0)\rangle e^{-i\omega t}\,. \tag{1.7}$$

For white noise the spectral density is constant. Average over the external degrees of freedom gives:

$$\langle\rho_{01}(t)\rangle = \langle\rho_{01}(0)\rangle \exp\left(-\frac{i\Omega t}{\hbar}\right)\exp\left(-\frac{t}{\tau_\varphi}\right), \quad \tau_\varphi^{-1} = \frac{\pi g^2}{\hbar^2}S_f\,. \tag{1.8}$$

i.e., $|\langle\rho_{01}(t)\rangle|$ decreases with time exponentially. Such exponential decay is characterized by the characteristic time $\tau_\varphi$ which is called coherence time. This time gives roughly the time scale on which the system stays coherent.

## 1.3 Superconducting Quantum Computing

As a best-studied macroscopic quantum phenomenon, superconductivity gives rise to several radically new effects. oNne of the most important examples is the Josephson effect in a "Josephson junction" - weak link between the two bulk superconductors [17, 18]. Josephson predicted for the first time that a dc current can flow across the junction even without the voltage bias applied to it (the DC Josephson effect), and an ac current is generated if there is a non-vanishing dc voltage drop across the junction (the AC Josephson effect). Inclusion of one or two Josephson junctions in a superconducting loop produces the SQUID(superconducting quantum interference

device) [20] which can be used to measure magnetic field with accuracy up to $10^{-15}T$ [19]. Another exciting application of Josephson junctions lies in quantum computing, which benefits from the dissipationless nature of current flow in superconductors. Several types of Josephson junction qubits: charge qubit[21, 22, 23], flux qubit[24, 25, 26], phase qubit [27], and their more recent generalizations have been realized. Quantum coherent oscillations, a signature of macroscopic quantum dynamics of these qubits, were observed in many experiments. As solid state devices, Josephson junction circuits also have the advantage of scalability because of the well-established microfabrication techniques like photo and electron beam lithography, and thin-film deposition. These techniques can in principle be developed into fabrication of the large scale circuits. Quantum Josephson junction circuits of several qubits were demonstrated to perform necessary gate operations and measurements, making present-day superconducting qubits one of the most promising qubit technologies.

One Josephson tunnel junction is a system of two mesoscopic superconducting islands separated by a layer of insulator. The insulator is thin enough, typically $1-2nm$, so the macroscopic wavefunction of the Cooper pair condensate can penetrate it, which leads to Cooper pair tunneling between the two superconducting islands connected by the tunnel junction. At energies smaller than the superconducting energy gap $\Delta$, only the Cooper pairs can tunnel in the junctions, while the dissipative quasiparticle tunneling is suppressed. Dissipationless tunneling of Cooper pairs plays an essential role in Josephson junction qubits of various types.

### 1.3.1 Charge qubit

The simplest scheme of a Josephson junction qubit is provided by the single-Cooper-pair box: a mesoscopic superconducting island coupled by a tunnel junction to a large superconducting electrode. The Hamiltonian of the systems contains two parts, charging energy and the Josephson coupling energy produced by the Cooper pair tunneling. The charging energy arises from the imbalance of the number of Cooper

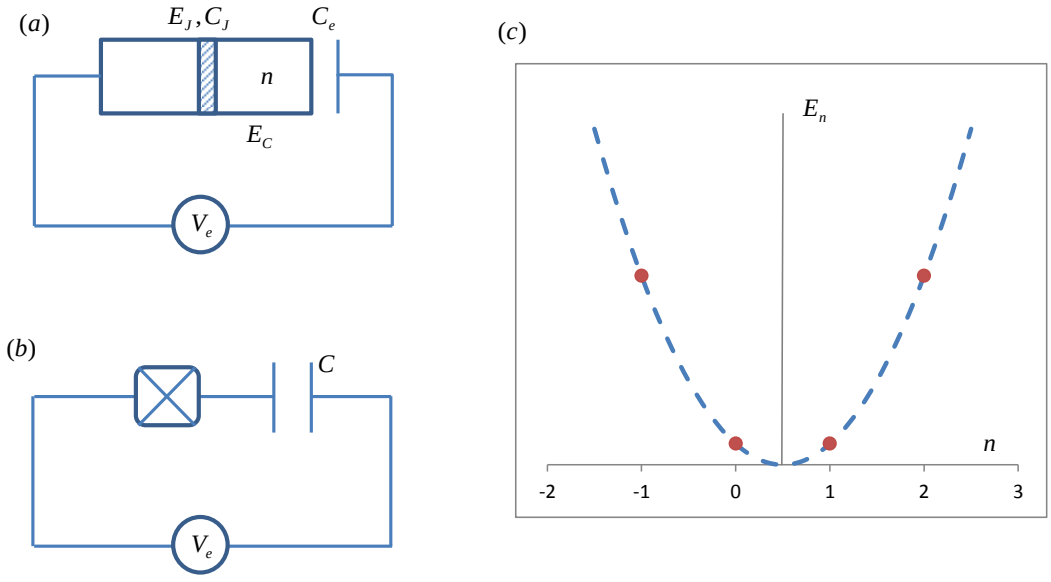


Figure 1.2: (a) Scheme of the charge qubit: a single Cooper pair box. The box is connected with the other superconducting island with an thin layer of insulator. The charge energy is $E_c \equiv (2e)^2/(2C)$, where $C$ is the overall capacitance $C = C_e + C_J$. The tunneling energy is $E_J$. The number of extra Cooper pairs in the box is a good quantum number. The balance number of the Cooper pairs in the box can be adjusted by the external voltage $V_e$. (b) The equivalent circuit diagram of the charge qubit: the box with a cross is the Josephson junction, which is coupled to the electrode capacitively. (c) The spectrum in the limit $E_c \gg E_J$ when $n_e = 0.5$ ($n_e$ is the polarization charge and can be adjusted by the gate voltage). The lowest two levels has $n = 0, 1$.

pairs on the island that gives rise to its finite electric charge. If the number of extra Cooper pairs on the island is $n$, the electrostatic charging energy can be written as $(n - n_e)^2 E_c$, where $E_c = (2e)^2/2(C_J + C_e)$ is the charing energy of one Cooper pair, $C_J$ is the capacitance of the tunnel junction, and $C_e$ is the capacitance between the island and external electrode. The external electrode also generates an electric field and induces a polarization charge $n_e$ on the capacitance $C_e$. The coupling energy arises from the Cooper pair tunneling between the two superconductors and is characterized with some tunneling amplitude which can be written as $-E_J/2$, where $E_J$ is called the Josephson energy. Then the total Hamiltonian of the Josephson

junction in the space of the number $n$ of extra Cooper pair on the island is [45, 46]:

$$H = (n - n_e)^2 E_c |n\rangle\langle n| - \frac{E_J}{2} \left( |n\rangle\langle n+1| + |n+1\rangle\langle n| \right) . \tag{1.9}$$

Changing the ratio of $E_c$ and $E_J$ leads to different behavior of the junction. In the regime of the charge qubit, the charging energy dominates the Hamiltonian, i.e., $E_c \gg E_J$, and the state of the system is well described by the number of the Cooper pairs in the box. The quantization of the energy corresponds to the quantization of number of Cooper pairs in the box in this case. It's easy to see from the Hamiltonian that it has a periodic structure as a function of the induced charge $n_e$. The charging energy spectrum stays the same under the change $n_e \to n_e + 1$, so without loss of generality, it's assumed in the following that $0 \leq n_e \leq 1$.

For charge qubit, the number $n$ of Cooper pairs is a good quantum number and it's convenient to work in the $n$ representation. The energies are roughly the parabolic function of the number of extra Cooper pairs $E_n \approx (n - n_e)^2 E_c$. If $n_e \approx 0.5$, the state $|0\rangle$ and $|1\rangle$ have the smallest energy and separate with other eigenstates by an energy gap $\Delta E \approx 2E_c$. If the thermal energy is low comparing to the energy gap, i.e., $E_c \gg k_B T$, the excitation to higher energy levels can be ignored, and the system reduces to a two-level system and serves as a qubit. The energy splitting of the two levels is around $2(n_e - 1/2)E_c$, and the tunneling amplitude between them is $-E_J/2$. So the Hamiltonian can be effectively written as:

$$H = (n_e - \frac{1}{2}) E_c \left( |0\rangle\langle 0| - |1\rangle\langle 1| \right) - \frac{E_J}{2} \left( |0\rangle\langle 1| + |1\rangle\langle 0| \right) . \tag{1.10}$$

The coherent oscillation of the single-Cooper-pair box has been observed in time domain by Nakamura *et* al.[21] for the first time. The period of the coherence oscillation was around 100ps, and the coherence time was around 2ns. The readout used in this experiment was a probe junction coupled to the box permanently, and the measurement process itself was a major contribution of dephasing.

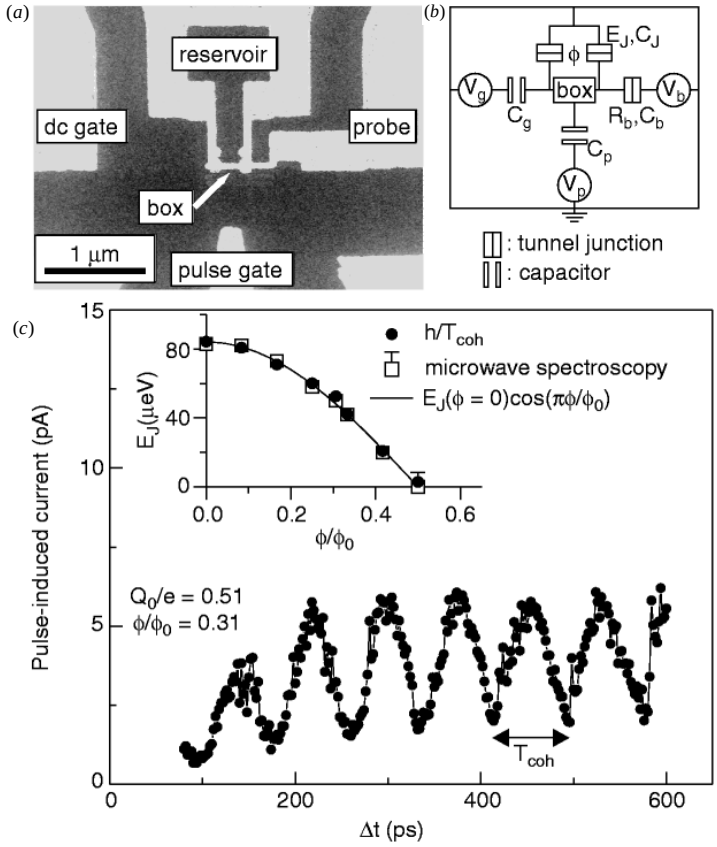


Figure 1.3: Singe-Cooper-pair box as a charge qubit[21]. (a) Micrography of the sample used in the experiment. The detector was a probe junction . (b) The equivalent circuit diagram of the charge qubit. (c) Coherent oscillation observed in the experiment, the period of the coherence oscillation was around 100ps, and the coherence time was around 2ns.

### 1.3.2 Flux qubit

Another paradigm of superconducting qubit is the flux qubit where the corresponding degree of the freedom used is flux instead of charge. An advantage of the flux qubit is that the magnetic background is much cleaner compared to the charge impurities produced during the fabrication. A scheme of the flux qubit is shown in Fig. 1.4. Instead of an isolated superconducting island, the Josephson junction is

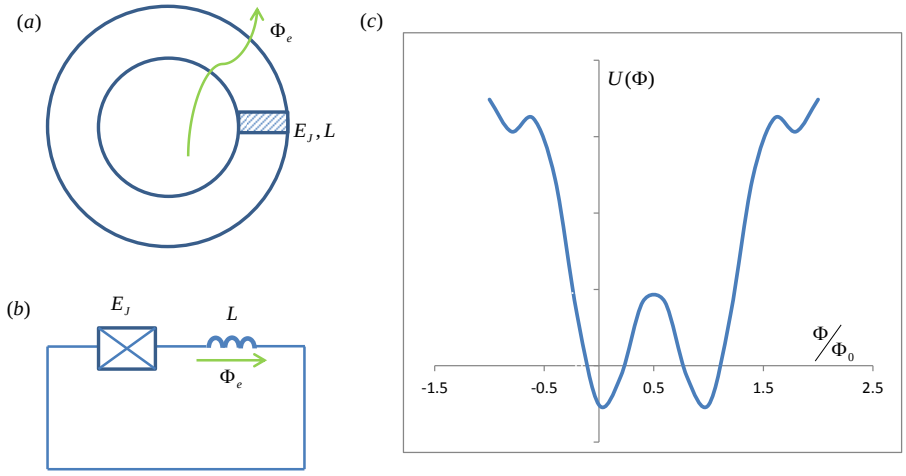


Figure 1.4: (a)Scheme of the flux qubit with a single Josephson junction (rf SQUID). The Josephson junction is included in a superconducting loop, thread by the external flux $\Phi_e$, which is used to adjust the balance flux number. (b) The equivalent circuit of the flux qubit. (c) The potential $U(\Phi)$ when $\beta = 10$ at $\Phi_e/\Phi_0 = 0.5$. There are two minimum around $0.5\Phi_0$. The two lowest level lie in these two minimas.

included into a superconducting loop. The flux qubit works in the region where $E_J \gg E_c$, and it's more convenient to work with the phase operator $\hat{\varphi}$. The phase operator is directly related to the flux operator $\Phi$, and the commutation with number operator $\hat{n}$ is well known:

$$\hat{\varphi} = 2\pi \frac{\hat{\Phi}}{\Phi_0}, \quad [\hat{n}, \hat{\varphi}] = i, \quad \hat{n} = i\frac{\partial}{\partial \varphi}\,. \tag{1.11}$$

where $\Phi_0 = \pi\hbar/e$ is the magnetic flux quantum, and $\hat{n}$ has been switched to the phase representation. The tunneling energy of the Josephson junction in phase representation is $-E_J \cos(\hat{\varphi})$. When the Josephson junction is included in the superconducting loop, the magnetic field energy of the loop inductance $L$ adds up to the charging and coupling energy. Since $E_J \gg E_c$, the Cooper pairs can move nearly continuously around the loop. The balance number of Cooper pairs $n_e$ becomes irrelevant with the system, and hence can be dropped from the Hamiltonian. So the

system's Hamiltonian becomes:

$$\hat{H} = n^2 E_c - E_J \cos(2\pi \frac{\Phi}{\Phi_0}) + \frac{(\Phi - \Phi_e)^2}{2L} \,. \tag{1.12}$$

Here $\Phi_e$ is the external flux and serves as the similar role as $n_e$ in charge qubit, and the flux quantization replaces the role of Cooper pairs in charge qubit. The dynamics of the flux is determined by the potential $U(\Phi)$, as is plotted in Fig. 1.4:

$$U(\Phi) = \frac{(\Phi - \Phi_e)^2}{2L} - E_J \cos(2\pi \frac{\Phi}{\Phi_0}) \,. \tag{1.13}$$

When $\beta \equiv E_J/(\Phi_0^2/4\pi^2 L) > 1$ and $\Phi_e \approx \Phi_0/2$, $U(\Phi)$ becomes a symmetric double well potential around $\Phi_e$. The two lowest eigenstates are localized around the two minima. The separation to higher energy levels has the order of the harmonic oscillation frequency around the minimal $\Delta E \sim (E_c E_J)^{1/2}$. If the temperature is much lower than this scale, the system reduces effectively to a two-level system, i.e., the qubit.

A physical realization of the flux qubit stated above was the rf SQUID[25], and the coherent superposition of the two states has been observed. In another experiment, where the flux qubit included multiple Josephson junctions instead of one, the coherent oscillation was also observed, and the observed dephasing time was $20ns$[26].

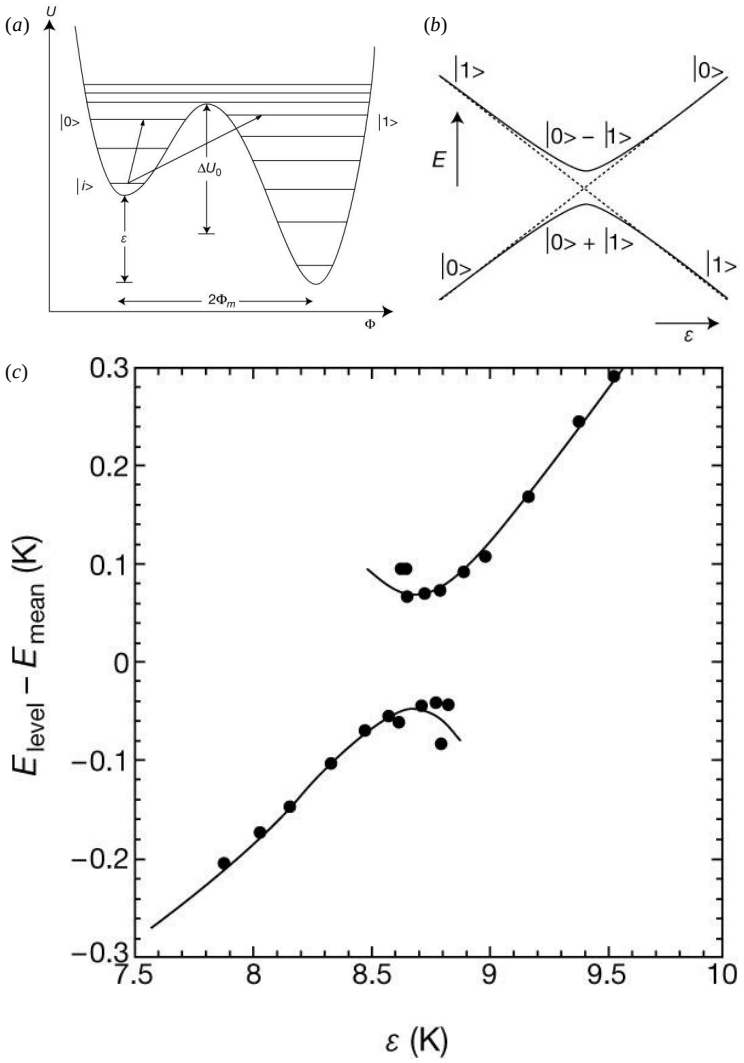


Figure 1.5: Observation of the coherent state in rf SQUID [25]. (a) rf SQUID Potential. The left well is the state with 0 flux and right well with one flux quantum. The two excited state $|0\rangle$ and $|1\rangle$ are generated from $|i\rangle$ by absorbing the photon. (b) Level-crossing of rf SQUID. Near the anti-crossing point, the eigenstates are the symmetric and anti-symmetric superposition of $|0\rangle$ and $|1\rangle$: $(|0\rangle + |1\rangle)/\sqrt{2}$ and $(|0\rangle - |1\rangle)/\sqrt{2}$. (c) The observed anti-crossing in the experiment.

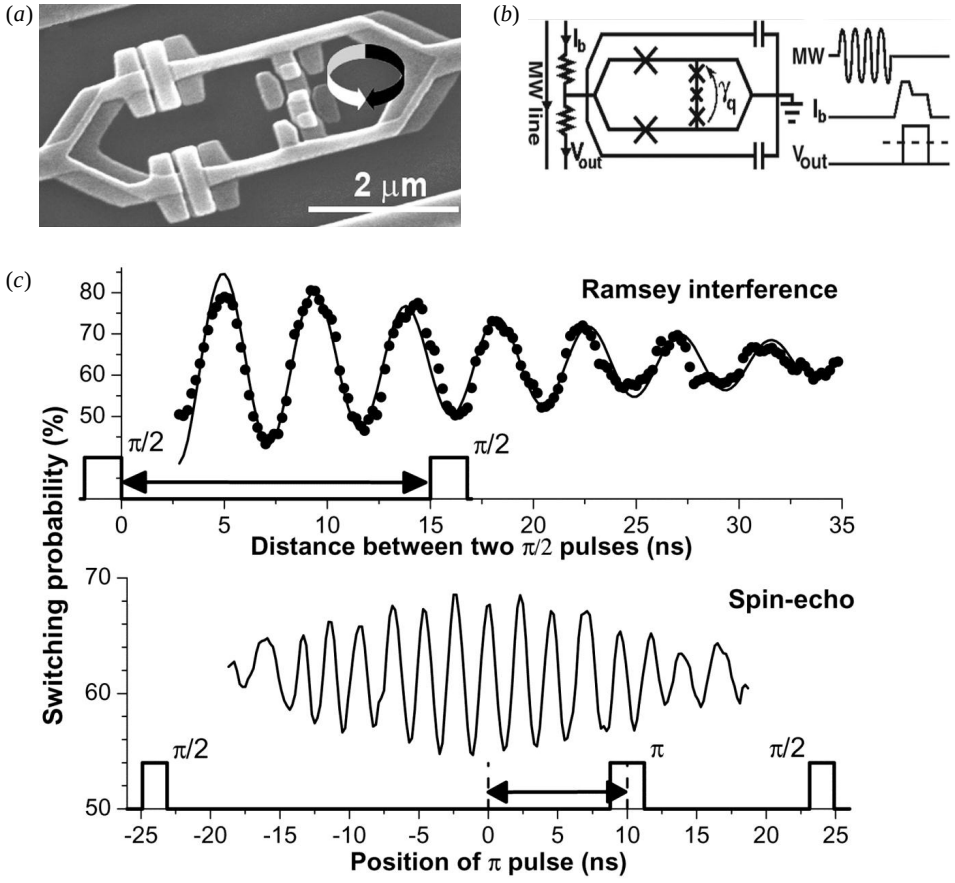


Figure 1.6: Coherent oscillation in flux qubit [26].(a) Scanning electron micrography of the flux qubit including three Josephson junctions(the small loop) and attached SQUID (the large loop). (b) The equivalent circuit of the flux qubit. (c) The observed coherent oscillation in the flux qubit, the coherence time was around 20ns.

### 1.3.3 Phase qubit and Transmon qubit

One of the main challenges of quantum computation is the short coherence time. Charge qubit, where $E_C \gg E_J$, is very sensitive to the charge noise caused by the fluctuation of offset charges; flux qubit, where $E_J \gg E_C$, is very sensitive to the external flux noise. One approach to this problem is to design the qubit in such a way that the degree of freedom used by the qubit system is separated from the external environment. Another approach is to eliminate the sensitivity by tailoring the quantum circuit and find a "sweet-spot" for operation. This section will briefly introduce two corresponding examples, phase qubit[27, 28] and transmon[29].

As the name indicated, the different states of the phase qubit are distinguished by phase difference across the Josephson junction. Consider the following circuit (Fig. 1.7) of a Josephson junction. The voltage, current and phase across the junc-

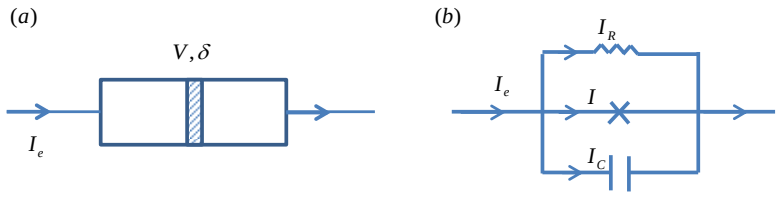


Figure 1.7: The schematic and equivalent circuit of the phase qubit. (a) Schematic of a Josephson junction, which serves as a phase qubit. The voltage and phase across the junction is $V$ and $\delta$. (b) The equivalent circuit Josephson junction. The external current is $I_e$, which equals the summation of the three branches: $I_R$, $I_C$ and $I$.

tion are $V$, $I$ and $\delta$, which are related by the relations $\dot{\delta} = 2\pi V/\Phi_0$ and $I = I_0 \sin\delta$; the self-inductance of the junction is $C$, and the junction is shunted by the resistance $R$. The external current $I_e$ equals the summation of the current in three branches:

$$I_e = I_C + I_R + I\,, \quad I = I_0 \sin\delta\,, \tag{1.14}$$

$$I_C = C\frac{\Phi_0}{2\pi}\ddot{\delta}\,, \quad I_R = \frac{\Phi_0}{2\pi}\frac{\dot{\delta}}{R}\,. \tag{1.15}$$

So the motion of the phase $\delta$ is governed by the following equation:

$$C\left(\frac{\Phi_0}{2\pi}\right)^2\ddot{\delta}+\frac{1}{R}\left(\frac{\Phi_0}{2\pi}\right)^2\dot{\delta}+\frac{\partial U}{\partial\delta}=0\,, \tag{1.16}$$

$$U(\delta)=-I_0\frac{\Phi_0}{2\pi}(\cos\delta+\frac{I_e}{I_0}\delta)\,. \tag{1.17}$$

The potential $U(\delta)$ has a washboard form (Fig. 1.8). For $I_e < I_0$, local minimum exists and quantized states can be trapped around the bottom of the well. The lowest two levels can serve as a qubit, i.e., phase qubit.

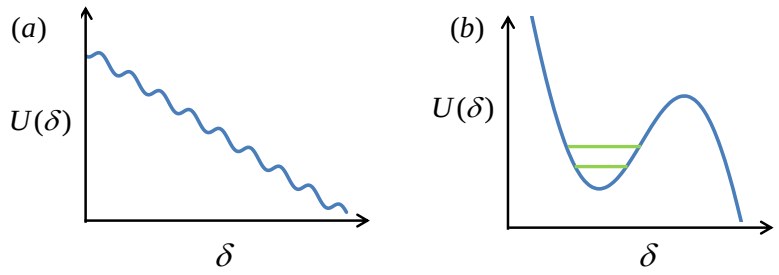


Figure 1.8: The potential $U(\delta)$. (a) $U(\delta)$ has a wash-board form, the local minimum could trap the phase if $I_e/I_0 < 1$. (b) The enlarged plot of a local minimum. Discrete quantum states lie around the bottom of the potential well and the lowest two serve as the qubit states.

The scheme and circuit of the transmon qubit are shown below. Similar to the charge qubit, the brick of the transmon qubit is a Cooper pair box. Also the Hamiltonian of the transmon qubit has the same form to the charge qubit:

$$\hat{H}=4E_C(\hat{n}-n_g)^2-E_J\cos\hat{\phi}\,. \tag{1.18}$$

where $E_C = e^2/2C_{net}$, $C_{net} = C_J + C_B + C_g$, $C_J$ and $C_g$ are junction capacitance and gate capacitance. The additional capacitance $C_B$ can be large and hence lower

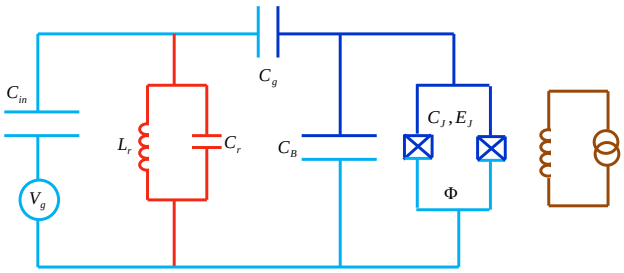


Figure 1.9: The circuit of a transmon qubit [29]. There are two Cooper pair boxes in the transmon qubit, the additional capacitance can lower the charging energy significantly.

$E_C$. The transmon benefits from the higher ratio of Josephson energy and charging energy $E_J/E_C$ (for transmon qubit, this ratio is several tens to several hundreds), because this ratio will suppress the charge dispersion exponentially and hence reduce the sensitivity to the charge noise significantly while lose the anharmonicity only in a weak power law. In other words, the transmon qubit trades a little anharmonicity for a huge increment in robustness. With the help of a three-dimensional superconducting cavity, the $T_2$ coherence time can be improved to $92\mu s$[30].

## 1.4 Adiabatic Quantum Computation

In 2001 Farhi, Goldstone, Gutmann and Sipser [31] proposed an quantum algorithm based on the adiabatic evolution of the quantum system to solve the classical optimization problems, which started a new direction of realization of quantum computation-adiabatic quantum computation (AQC). Unlike the usual gate-model quantum computation, where a sequence of discrete gate transformations are applied to the system, the calculation in AQC is "continuous". AQC encoded the solution of the problem into the ground state of a target Hamiltonian, and tracked the adiabatic quantum evolution to reach that ground state. Assume the target

Hamiltonian is $H_p$ whose ground state $|\psi_p\rangle$ is difficult to find, consider the following time-dependent Hamiltonian:

$$\hat{H}(s) = s\hat{H}_p + (1-s)\hat{H}_b\,. \tag{1.19}$$

where $\hat{H}_b$ is a simple Hamiltonian whose ground state $|\psi_b\rangle$ is readily known, and usually a superposition of all basis states. $s = t/t_f$ is normalized time with $t_f$ as the total time of the evolution. Based on the adiabatic theorem[32], if the evolution is slow enough and the ground state is non-degenerate during the evolution, starting from state $|\psi_b\rangle$, the system will stay on the ground state and finally arrives at $|\psi_p\rangle$. In order for the adiabatic theorem to hold, the evolution of the Hamiltonian should be slow enough, which could be related to the minimum energy gap between the ground state and first excited states $\Delta_{min}$. The time scale needed for a successful AQC roughly goes as $\Delta_{min}^{-2}$ [33].

A possible advantage of AQC is that the energy gap $\Delta_{min}$ gives a natural protection against the thermal noise if the temperature is small compared to the gap[34, 35]. Encouragingly, there is no less power of AQC than conventional quantum computation. Aharonov *et al.* proved the equivalence between AQC and conventional quantum computation, in the sense that any given quantum algorithm can be adiabatic simulated in polynomial complexity [36]. Furthermore, a set of Hamiltonians were proved to be universal [38, 39, 40, 41]. J.D. Biamonte and P.J. Love [41] showed that the following Hamiltonians are universal, i.e., any quantum circuit can be implemented adiabatically using the terms like these:

$$H_{ZZXX} = \sum_i h_i\sigma_i^z + \sum_i \Delta_i\sigma_i^x + \sum_{i,j} J_{ij}\sigma_i^z\sigma_j^z + \sum_{i,j} K_{ij}\sigma_i^x\sigma_j^x\,. \tag{1.20}$$

An effective method to find the ground state of some spin system of these type is quantum annealing [42, 43]. In [44] the ground state of an artificial Ising spin system with eight flux qubit and programmable spin-spin couplings were solved with the

quantum annealing method in experiment.

# Chapter 2

# Quantum Limited Measurement

Quantum measurement is a fundamental issue in quantum mechanics which also causes some deep philosophical problems, such as the nonlocality[47] or many-world interpretation[48]. But in a practical point of view, quantum measurement is a well formalized theory[49]. Any detector is a double edge sword: telling the value of the measured quantity while destroying the original state. This chapter focuses on the weak continuous measurement and shows that quantum mechanics puts a limit on detector, and this limit could be achieved in mesocopic detectors[59].

## 2.1 Measurement and Weak continuous Measurement

Quantum measurement was first rigorously formulated by John von Neumann[49], which is comprised by the probability interpretation of a wavefunction and the wavefunction reduction or collapse after the measurement. Consider the quantum measurement of a system with one degree of the freedom. The initial wavefunction is $|\psi\rangle = \sum_n p_n|\psi_p\rangle$, where $|\psi_p\rangle's$ are the eigenstates of the measured quantity $X$. The outcome is the eigenvalue of $X$, for example $X_m$, with probability $|p_m|^2$. The wavefunction collapses to $|\psi_m\rangle$ after the measurement.

This is an ideal description of measurement where a detector is assumed to have a perfect correlation with the measured system. Also this is called projected measurement because the wavefunction is projected to one of the eigenfunction with certainty after the measurement. Including the detector's degree of freedom, the wavefunction evolves as the following way :

$$|\psi\rangle \otimes |D\rangle = \left( \sum_n p_n |\psi_n\rangle \right) \otimes |D\rangle \longrightarrow \sum_n p_n \left( |\psi_n\rangle \otimes |D_n\rangle \right) . \tag{2.1}$$

where $|D\rangle$ is the initial state of the detector and $|D_n\rangle$ are the outcome state corresponding to $|\psi_n\rangle$, i.e., $D_n$ are the "reading's" of the detector and they are macroscopically distinguishable. Since the system and the detector are perfectly coupled together, the reading tells the state of the system. To realize a projected measurement, the coupling between the detector and measured system is usually very strong. To see a concrete example, consider the measurement of the spin of an electron.

During the measurement, the electron passes through a magnetic field in $\hat{z}$ direction, and suppose the electron is initially polarized in $x$ direction. The wavefunction of the electron evolves during the measurement as following:

$$|\psi_i\rangle = \frac{|\uparrow\rangle + |\downarrow\rangle}{\sqrt{2}} \otimes \phi(z) \longrightarrow |\psi_f\rangle = \frac{1}{\sqrt{2}} \left( |\uparrow\rangle \otimes \phi(z-a) + |\downarrow\rangle \otimes \phi(z+a) \right) . \tag{2.2}$$

where $\phi(z)$ is a localized envelope of electron in real space, for example, an Gaussian wavepacket $\phi(z) = \frac{1}{\sqrt{2\pi\lambda^2}} \exp(-\frac{z^2}{2\lambda^2})$. After passing the magnetic field, the centers of the wavepackets separate in real space, and each wavepacket has a definite value of $\sigma_z$. So the position of the electron reads out the spin. Note that in order to get a definite value of the spin, the two centers of the wavepackets should be distinguishable, i.e., the magnetic field should be strong enough.

Although the strong coupling between the measured system and the detector could pull out a large part of the information, usually it also disturbs the measured system a lot. Another paradigm of measurement is continuous weak

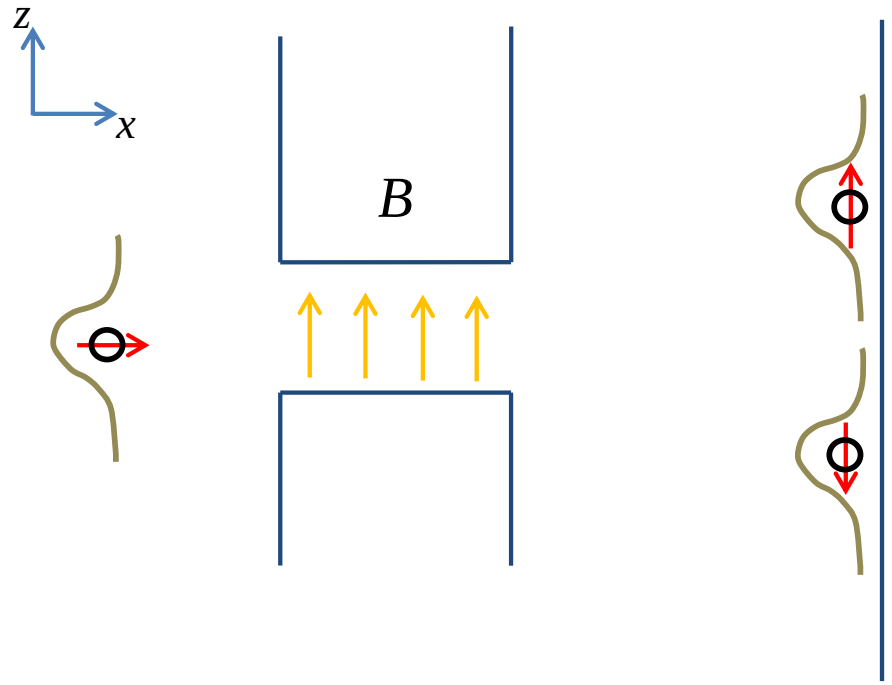


Figure 2.1: Measurement of the electron's spin. The electron passes through the magnetic field, and deflects to different positions due to the different spin state. In this case, the position and spin are coupled together. The reading of the position, which is macroscopic distinguishable, tells the electron's spin.

measurement[50], in which the coupling between the system and detector is weak. The measurement gives part of the information and gives little perturbation to the measured system. Consider the spin measurement in Fig. 2.1, if the magnetic field is weak and the two wavepackets overlap after passing the field, only a probable value could be given out by the measurement; in the meantime, the wavepackets are more similar to the original one.

Below is the general schema of the continuous weak measurement [51]. The quantity being measured is the system "coordinate" $\hat{x}$ whose eigenvalues are $x_j$, and $\hat{x}$ is coupled to the detector "force" $\hat{f}$. The coupling is weak enough so that the linear-response theory is applicable. The full Hamiltonian contains three parts: the system Hamiltonian $\hat{H}_s$, the detector Hamiltonian $\hat{H}_D$ and the coupling Hamiltonian

$\hat{H}_I \equiv \hat{x} \cdot \hat{f}$.

$$\hat{H} = \hat{H}_s + \hat{H}_D + \hat{H}_I \,. \tag{2.3}$$

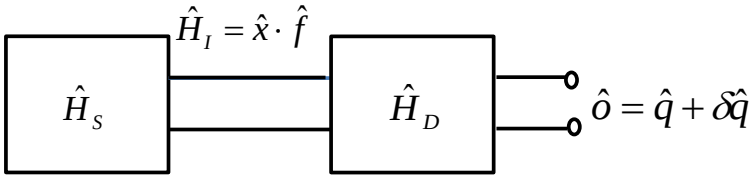


Figure 2.2: Schema of the continuous weak measurement. The measurable $\hat{x}$ is coupled to the detector via $\hat{H}_I = \hat{x}\hat{f}$. The output is $\hat{o}$, which is composed of the output noise $\hat{q}$ and response signal $\delta\hat{q}$. The characteristic of the detector is given by the commutation relation of $\hat{q}$ and $\hat{f}$: $[\hat{q}(t), \hat{f}(\tau)]$. The interaction $\hat{H}_I$ is weak enough that the perturbation to original system is weak; on the other side the information acquired is limited in finite time.

The output of the detector is $\hat{o}$. Using the perturbation theory[54], the output is:

$$\hat{o}(t) = \hat{q}(t) + \delta\hat{q}(t) = \hat{q}(t) - \frac{i}{\hbar}\int_0^t d\tau \left[\hat{q}(t), \hat{f}(\tau)\right] \hat{x}(\tau) \,. \tag{2.4}$$

Here $q(t) = \exp(iH_D t)\hat{o}(0)\exp(-iH_D t)$ is the output signal even no input is coupled to the detector, i.e., the output noise. The second term is the linear response to the input. In order to distinguish the response from the background noise, the magnitude of the second term should be large comparing to the first term.

Tracing out the degrees of the freedom of the detector, we could get the average

value of the output.

$$\langle \hat{o}(t) \rangle = \int_0^t d\tau \lambda(t-\tau)\hat{x}(\tau)\,, \tag{2.5}$$

$$\lambda(t-\tau) = -\frac{i}{\hbar}\left\langle \left[\hat{q}(t), \hat{f}(\tau)\right]\right\rangle\,. \tag{2.6}$$

where $\langle \ldots \rangle \equiv Tr_D(\ldots)$. In Eq. (2.5) $\langle \hat{q}(t) \rangle = 0$ is assumed, which means the mean value of the output is zero when there is no input. $\lambda(t-\tau)$ is the response function of the detector, it depends only on the time difference since the detector's state is stationary. Eq. (2.5) shows that the detector collects the information of the input continuously. The lower limit of the integrand in Eq. (2.5) is the starting time of the measurement and can be set to $-\infty$. Because of the causality, the response function should be 0 when $t < \tau$, the Eq. (2.5) and Eq. (2.6) can be reformulated as:

$$\langle \hat{o}(t) \rangle = \int_{-\infty}^{\infty} d\tau \lambda(t-\tau)\hat{x}(\tau)\,, \tag{2.7}$$

$$\lambda(t-\tau) = -\frac{i}{\hbar}\theta(t-\tau)\left\langle \left[\hat{q}(t), \hat{f}(\tau)\right]\right\rangle\,. \tag{2.8}$$

where $\theta(t)$ is the step function. For the simple example, consider the instantaneous detector where:

$$\lambda(t) = \lambda\delta(t-0^+)\,. \tag{2.9}$$

where $0^+$ is used to guarantee the causality. The output is $\langle \hat{o}(t) \rangle = \lambda x(t)$. In general, $\lambda(t)$ is a function decaying with certain time scale, and the measurement pulls out the information of the input continuously.

## 2.2 Quantum Limited Measurement

The Hamiltonian (2.3) is similar to the "system + reservoir" models studied in open quantum systems[55]. Replacing the detector with a large dissipative reservoir,

the well known fluctuation-dissipation theorem[56] can be derived from the linear response theory. However, the detector is different from the reservoir since the reservoir is usually very large and the interaction with system doesn't change itself. But as a detector, the response is the output and should be detectable to the coupling with the measured system. Also the detector is usually far away from thermal equilibrium in order to be sensitive to the input. Although there are differences between these two cases, the similar structure indeed leads to a general restriction to the detector, i.e., the quantum-limited detector[51, 52, 53].

### 2.2.1 Information Acquisition

For weak continuous measurement, the information of the input is collected gradually. Since there is output noise in the detector, a finite time is needed to acquire enough information to distinguish two different input signals. The information acquisition time is determined by the response function $\lambda(t)$, which describes how fast information can be collected, and the output noise, which sets the bottom line of how much information is needed to be separable from the noise.

To be concrete, consider the instantaneous detector $\lambda(t) = \lambda\delta(t - 0^+)$. If there are two different input signals $x_i$ and $x_j$, the difference between the outputs is $\Delta x = \lambda(x_i - x_j)$. This difference should be large compared to the variance of the output noise in order to be distinguished. The output noise is characterized by the spectral density:

$$S_{qq}(\omega) = \int_{-\infty}^{\infty} dt \langle \hat{q}(t)\hat{q}(0)\rangle e^{-i\omega t} \,. \tag{2.10}$$

For simplicity, here we consider the case of white noise $S_{qq}(\omega) = S_q$. The variance of the output in time $\Delta t$ is $\Delta o = \sqrt{S_q/\Delta t}$. The information acquisition time $\tau_m$ is defined to be the time needed for $\Delta o = 0.5\Delta x$. It's easy to get:

$$\tau_m = \frac{4S_q}{\lambda^2(x_i - x_j)^2} \,. \tag{2.11}$$

The results says that the acquisition time increases with the output noise and decreases with the response, which is physically obvious.

### 2.2.2 Back-action Dephasing

In Nakamura's experiment [21], the measurement process was a main source of decoherence. Although it was suppressed a lot later, the dephasing induced by the coupling to detector is inevitable, which make the measurement a double-edge sword: pulling out the information while causing the measured system dephasing. This back-action dephasing is similar to the dephasing caused by coupling to dissipative reservoir. The dephasing comes from the fluctuation of the relative energy between energy levels. Since the back action force commutes with degrees of freedom in the system, it can be treated as a classical force. The time-evolution of the density matrix is:

$$i\hbar\dot{\hat{\rho}}(t) = [\hat{\rho}(t), H_I] = [\hat{\rho}(t), \hat{x}(t)]f(t)\,. \tag{2.12}$$

To see the dephasing process, consider the element $\langle i|\hat{\rho}|j\rangle$, where $|i\rangle$ and $|j\rangle$ are the eigenstates of $\hat{x}$ corresponding to eigenvalues $x_i$ and $x_j$.

$$i\hbar\dot{\rho}_{ij}(t) = f(t)(x_i - x_j)\rho_{ij}(t)\,. \tag{2.13}$$

which can be solved easily:

$$\rho_{ij}(t) = \rho_{ij}(0)\exp\left(-\frac{x_i - x_j}{\hbar}\int_0^t d\tau f(\tau)\right)\,. \tag{2.14}$$

Similar to the quantum dynamics in usual dissipative quantum systems, this result depends on the statistical properties of the reservoir force $\hat{f}$. Without losing the generality, $\langle f(t)\rangle = 0$, since the average term can be absorbed into the system

Hamiltonian. The properties of the correlation is given by the spectral density:

$$S_{ff}(\omega) = \int_{-\infty}^{\infty} dt \langle f(t) f(0) \rangle e^{-i\omega t} \,. \tag{2.15}$$

For the simple case, assume the force is $\delta$-correlated, i.e., $S_{ff}(\omega) = S_f$. With the help of Wick theorem[55, 57], we get from Eq. (2.14) the following result:

$$\langle \rho_{ij}(t) \rangle = \langle \rho_{ij}(0) \rangle \, e^{-t/\tau_\phi} \,, \tag{2.16}$$

$$\tau_\phi^{-1} = \frac{(x_i - x_j)^2 S_f}{2\hbar^2} \,. \tag{2.17}$$

### 2.2.3 Quantum Limited Detector

The information acquisition time $\tau_m$ is the time needed to get enough information, i.e., the time at which the measurement should last; the backaction dephasing time $\tau_\phi$ is the time within which the information is destroyed by the measurement process. These two quantities are not independent, actually there is a fundamental limitation between these two. Combining $\tau_m$ and $\tau_\phi$ gives :

$$\frac{\tau_m}{\tau_\phi} = 2 \frac{S_q S_f}{\hbar^2 \lambda^2} \,. \tag{2.18}$$

The response $\lambda$ is related to $S_q$ and $S_f$ by linear-response theory. The Fourier transformation of Eq. (2.7) and Eq. (2.6) gives:

$$\langle \hat{o}(\omega) \rangle = \lambda(\omega) \hat{x}(\omega) \,, \tag{2.19}$$

$$i\hbar\lambda(\omega) = S_{qf}(\omega) - S_{qf}^*(-\omega) \,. \tag{2.20}$$

where

$$S_{qf}(\omega) = \int_{-\infty}^{\infty} dt e^{-i\omega t} \langle q(t) f(0) \rangle \,, \tag{2.21}$$

$$S_{qf}(\omega) = S_{fq}^*(\omega) \,. \tag{2.22}$$

As is noted before, $\langle \dots \rangle = Tr_D(\dots)$, which can be expressed by the density matrix of the detector $\hat{\rho}_D$. It's very natural to assume that the detector is stationary and diagonal in the energy basis of the detector, then Eq. (2.22) can be expressed microscopically:

$$\begin{aligned}
S_{qf}(\omega) &= \int_{-\infty}^{\infty} dt e^{-i\omega t} \langle q(t) f(0) \rangle \\
&= \int_{-\infty}^{\infty} dt e^{-i\omega t} \int d\epsilon \rho_D(\epsilon) \nu(\epsilon) \langle \epsilon | q(t) f | \epsilon \rangle \\
&= \int_{-\infty}^{\infty} dt e^{-i\omega t} \int d\epsilon d\epsilon^{'} \rho_D(\epsilon) \nu(\epsilon) \nu(\epsilon^{'}) \langle \epsilon | q(t) | \epsilon^{'} \rangle \langle \epsilon^{'} | f | \epsilon \rangle \\
&= \int_{-\infty}^{\infty} dt e^{-i\omega t} \int d\epsilon d\epsilon^{'} \rho_D(\epsilon) \nu(\epsilon) \nu(\epsilon^{'}) \langle \epsilon | e^{\frac{iH_D t}{\hbar}} q e^{\frac{-iH_D t}{\hbar}} | \epsilon^{'} \rangle \langle \epsilon^{'} | f | \epsilon \rangle \\
&= \int d\epsilon d\epsilon^{'} \rho_D(\epsilon) \nu(\epsilon) \nu(\epsilon^{'}) \int_{-\infty}^{\infty} dt \, \exp\left( -i \frac{\hbar\omega - \epsilon + \epsilon^{'}}{\hbar} t \right) \langle \epsilon | q | \epsilon^{'} \rangle \langle \epsilon^{'} | f | \epsilon \rangle \\
&= 2\pi\hbar \int d\epsilon \rho_D(\epsilon) \nu(\epsilon) \nu(\epsilon - \hbar\omega) \langle \epsilon | q | \epsilon - \hbar\omega \rangle \langle \epsilon - \hbar\omega | f | \epsilon \rangle \, . \qquad (2.23)
\end{aligned}$$

Here $\rho_D(\epsilon)$ is the probability of occupying a state with energy $\epsilon$; $\nu(\epsilon)$ is the density of states at $\epsilon$. Eq. (2.23) has the form of inner product:

$$S_{qf}(\omega) \equiv \langle q | f \rangle \, . \qquad (2.24)$$

Similarly, the spectral density of force $f$ and output $q$ can be expressed in the same way:

$$S_{qq}(\omega) = \langle q | q \rangle, \quad S_{ff}(\omega) = \langle f | f \rangle \, . \qquad (2.25)$$

The Schwarz inequality[58] puts a restriction of these three:

$$S_{qq}(\omega) S_{ff}(\omega) \geq |S_{qf}(\omega)|^2 \, . \qquad (2.26)$$

For classical noise, there are $S_{qq}(\omega) = S_{qq}(-\omega)$ and $S_{ff}(\omega) = S_{ff}(-\omega)$. For given $S_{qq}(\omega)$ and $S_{ff}(\omega)$, the magnitude of the response function $|\lambda(\omega)|$ is maximized if:

$$\begin{aligned} S_{qq}(\omega)S_{ff}(\omega) &= |S_{qf}(\omega)|^2\,, \\ S_{qq}(\omega)S_{ff}(\omega) &= |S_{qf}(-\omega)|^2\,, \\ S_{qf}(\omega) + S_{qf}^*(-\omega) &= 0\,. \end{aligned} \tag{2.27}$$

Under these conditions, there is:

$$i\hbar\lambda(\omega) = S_{qf}(\omega) - S_{qf}^*(-\omega) = 2S_{qf}(\omega)\,, \tag{2.28}$$

$$\hbar^2|\lambda(\omega)|^2 = 4|S_{qf}(\omega)|^2 = 4S_{qq}(\omega)S_{ff}(\omega)\,. \tag{2.29}$$

Applying these relations to the detector with instantaneous response, $\delta$-correlated back-action force and output, as discussed above, there is the limitation:

$$\frac{\tau_m}{\tau_\phi} = 2\frac{S_q S_f}{\hbar^2\lambda^2} \geq \frac{1}{2}\,. \tag{2.30}$$

This is the a fundamental restriction of the weak continuous measurement, and any detector satisfying the condition (2.27) is called quantum limited detector, which is the most efficient detector people could get. Indeed, we will see in the following section that this limit can be reached using mesoscopic structures.

## 2.3 QPC: a Physical Realization of Quantum Limited Detector

The section follows [59] to prove that quantum point contact (QPC) can be a physical realization of the quantum limited detector, and the spectral density of the input and output satisfy the condition found in last section at the quantum limited point. For clarity, the measured system has only two levels, i.e., a qubit. The schema

of the total system is shown below. A voltage is added across the QPC, the two level system generates a potential on the QPC and hence changes the current. The Hamiltonian is:

$$\hat{H} = -\frac{1}{2}(\epsilon\sigma_z + \Delta\sigma_x + \sigma_z U) + \sum_{i,k} \epsilon_k a_{ik}^\dagger a_{ik}\,, \tag{2.31}$$

$$U = \sum_{i,j} U_{ij} \sum_{k,p} a_{ik}^\dagger a_{jp}\,. \tag{2.32}$$

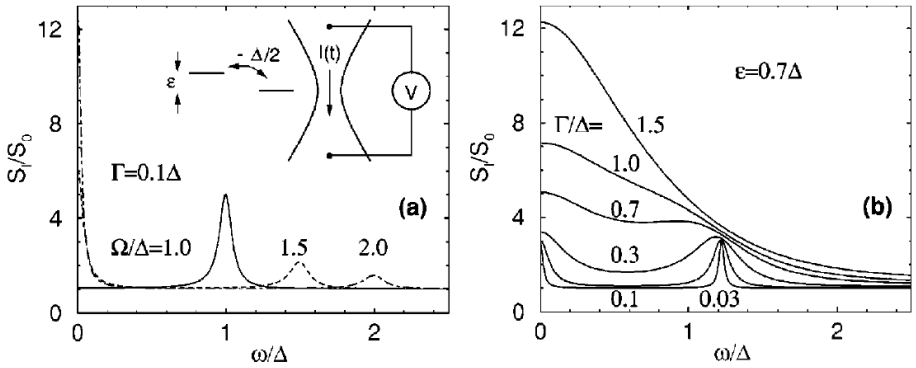


Figure 2.3: Schema of quantum point contact (QPC) [59]. $\epsilon$ is the energy split of the qubit, and $\Delta$ is the tunneling element. The qubit generates a potential on the electron and hence influence the current. The state of the qubit can be deducted from the electronic current. $\Gamma$ is the back-action dephasing rate. The curves are the spectrum of $S_{II}(\omega)$ for different $\epsilon$ and $\Gamma$, see Eq. (2.39).

Here the Hamiltonian of the detector is written in the scattering basis. $i, j$ can be 1 or 2, which stands for the two incident directions; $k, p$ are the magnitude of the momentum. The two-level system generates a potential on QPC. In the measurement, only the potential differences matter, since the average can be combined into the energy. Here the generated potentials are assumed to be $\pm 1/2U(x)$. When the bias energy and thermal energy are much smaller than Fermi energy, all momentum are near to the Fermi energy, hence the element $U_{ij}$ can be approximated the same for all $k's$. $U_{ij}$ is given by: $U_{ij} = \int dx \psi_i^*(x) U(x) \psi_j(x)$, here $\psi_i(x)$ is the scattering

state in real basis. The coupling term $\sigma_z U$ is assumed small enough to allow the linear response theory to work, and $U$ is the back-action force.

The output of the detector is the electric current. Near the Fermi sea, the spectrum can be approximated by $\epsilon_k = v_F k$, where $v_F$ is the Fermi velocity. Then the current operator in the scattering basis is :

$$I = \frac{ev_F}{L}\sum_{kp}[D(-a_{1k}^\dagger a_{1p} - a_{2k}^\dagger a_{2p}) + i\sqrt{DR}e^{-i(k-p)|x|}(-a_{1k}^\dagger a_{2p} - a_{2k}^\dagger a_{1p})]\,. \quad (2.33)$$

$D$ and $R$ are the transmission and reflection probability, $D+R=1$; they are assumed the same for all momentum since all $k's$, $p's$ are near the Fermi level, except for a phase variation.

In the linear-response regime, the difference of transmission probability $\delta D$ is related to the matrix element $U_{12}$ by:

$$U_{12} = \frac{v_F}{L}\frac{\delta D + iu}{2\sqrt{DR}}\,. \quad (2.34)$$

The imaginary part of $U_{12}$ has no effect on the current. It's related to the asymmetry of the coupling between the system and QPC. If $U(x)$ is symmetric, then $u=0$.

The correlation function for $U$ and $I$ are:

$$\begin{aligned}
\langle U(t)U(t+\tau)\rangle_0 &= \frac{eV}{4\pi}\frac{(\delta D)^2+u^2}{DR}\delta(\tau)\,, & (2.35)\\
\langle U(t)I(t+\tau)\rangle_0 &= \frac{e^2V}{2\pi}(i\delta D + u)\delta(\tau-\eta)\,, & (2.36)\\
\langle I(t)I(t+\tau)\rangle_0 - \langle I\rangle^2 &= e\langle I\rangle R\delta(\tau) = \frac{e^3VDR}{\pi}\delta(\tau)\,. & (2.37)
\end{aligned}$$

In these calculation, $eV \gg k_BT$, so the distribution is $\theta(\epsilon - eV_i)$.

The back-action dephasing rate is:

$$\Gamma = eV\frac{(\delta D)^2+u^2}{8\pi DR}\,. \quad (2.38)$$

The spectral density of the output $\hat{I}$ for $\epsilon = 0$ is:

$$S_{II}(\omega) = S_0 + \frac{\Gamma\Omega^2(\delta I)^2}{(\omega^2 - \Omega^2)^2 + \Gamma^2\omega^2}\,. \tag{2.39}$$

For $\epsilon \neq 0$, the plot of $S_{II}(\omega)$ is shown in Fig. 2.3 for different $\epsilon$ and $\Gamma$. For the continuous measurement, i.e., $\Gamma \ll \Delta$, $S_{II}$ is maximized at $\epsilon = 0$, whose value is shown below:

$$\frac{S_{max}}{S_0} = \frac{4(\delta D)^2}{(\delta D)^2 + u^2}\,. \tag{2.40}$$

This is a good indicator of the efficiency of the detector since it describes the ratio between the magnitude of the output in response to the input and the magnitude of the background noise. This signal-to-noise ratio is maximized when $u = 0$, and this corresponds to the case where the potential generated by the qubit is symmetric.

Another way to find the quantum-limitation of this detector is to use the quantum limited relation derived in last section. The spectral density of back-action force, output and their cross correlations:

$$S_{UU}(\omega) = \frac{eV}{4\pi}\frac{(\delta D)^2 + u^2}{DR}\,, \tag{2.41}$$

$$S_{UI} = \frac{e^2V}{2\pi}(i\delta D + u)e^{i\omega\eta}\,, \tag{2.42}$$

$$S_{II} = \frac{e^3VDR}{\pi}\,. \tag{2.43}$$

It's easy to see that the condition $S_{UU}(\omega)S_{II}(\omega) = |S_{UI}(\omega)|^2 = |S_{UI}(-\omega)|^2$ is satisfied automatically. The condition $S_{UI}(\omega) + S^*_{UI}(-\omega) = 0$ gives the condition of the quantum limited detector:

$$u = 0\,. \tag{2.44}$$

which is the same with the result by minimizing Eq. (2.40).

# Chapter 3

# Feedback Suppression of the Low Frequency Noise

Low-frequency noise (such as $1/f$ noise[60, 61, 62]) is one of the dominant sources of decoherence in superconducting qubit. One approach to overcome this problem is to employ the qubit structures with the basis states having the same values of the main qubit coordinate so that the noise will not cause decoherence. This chapter suggests another way by suppressing the low frequency directly using a feedback loop. Continuous quantum measurement is frequency dependent so the dynamics of the qubit could stay unchanged.

## 3.1 Noise in Superconducting Qubit

Decoherence, which is is caused by the coupling to external degrees of freedom, is one of the greatest challenges in quantum computation. As is shown in chapter 2, measurement itself will lead to decoherence of the system, but this is inevitable, and in some sense "necessary". In the view of information flow, this is a process of pumping the information from the measured system to the detector. Fortunately there is a limitation on this process and this limitation can be achieved by certain physical systems[59]. Another source of decoherence, however, is not welcomed at all.

That is the unwanted noise from the environment. The noise limits the coherence time of the system by two mechanisms: one is the relaxation process, in which the noise spectrum at the resonant frequency causes the system to transit between energy levels, the other is dephasing, in which the noise, especially low-frequency noise, that fluctuates the relative energy between energy levels and destroys the coherence. It would be helpful if the environment noise could be suppressed or eliminated. To find the ways of decreasing the noise, it's important to understand the characteristic and origin of the noise.

A qubit can be used as a noise spectrometer since it's behavior, relaxation and dephasing, is influenced by the noise. For example, consider a two-level system coupled to the reservoir:

$$\hat{H} = \frac{1}{2}\hbar\Omega\hat{\sigma}_z + \hat{\sigma}_x \cdot \hat{f}\,. \tag{3.1}$$

The transition rate between the two levels are:

$$\Gamma_{01} = \frac{1}{\hbar^2}S_{ff}(\Omega), \quad \Gamma_{10} = \frac{1}{\hbar^2}S_{ff}(-\Omega)\,. \tag{3.2}$$

The noise spectral density is related to the transition rate directly. By varying the energy splitting, tunneling amplitude and the coupling to the external degree of freedom, the spectrum of the noise can be derived from the relaxation and/or dephasing of the qubit system.

Using this method, it was found [60] that, unlike the classical noise, the quantum noise in charge qubit noise is asymmetric; at frequencies $\hbar\omega < k_BT$, the noise has the $1/f$ form; at frequencies $\hbar\omega > k_BT$, the noise is proportional to the frequency. In flux qubit the low-frequency flux noise spectrum also has a form of $1/f$ as low as to $1Hz$ [61][62], see Fig. 3.1. The general spectral density of the noise can be

written as:

$$S(\omega) = \frac{\gamma^2}{|\omega|} + \hbar^2 \frac{\eta\omega}{1 - e^{-\hbar\omega/k_B T}} \,. \tag{3.3}$$

In Chapter 5, we will use this spectral density for numerical simulation.

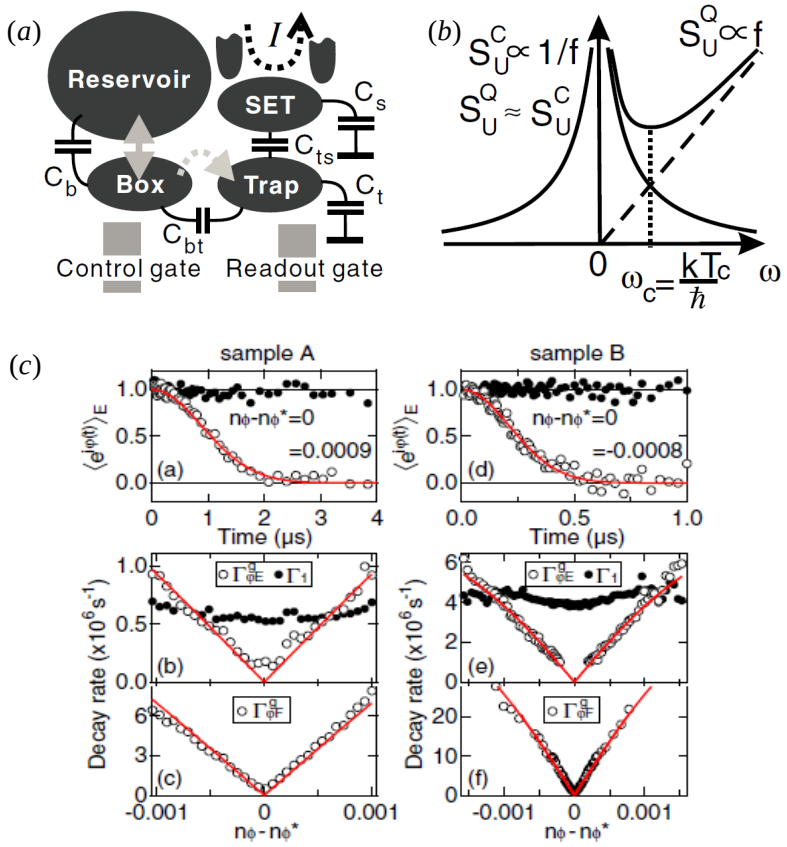


Figure 3.1: (a) Schematic of the charge qubit as the noise spectrometer. (b) The general behavior of the noise spectral density in the charge qubit. Here $S_U^C(\omega)$ and $S_U^Q(\omega)$ are classical and quantum noise. $S_U^C(\omega)$ is symmetric. $S_U^Q(\omega) \approx S_U^C(\omega)$ at $\hbar\omega < k_B T$ and has the form $1/f$; at $\hbar\omega > k_B T$, $S_U^Q(\omega)$ is proportional to $\omega$. See [60] and references therein for details.(c) Decoherence at various flux biases in the flux qubit. The red solid fitting curves are matches with the assumption of $1/f$ noise. See [61] and references therein for details.

## 3.2 Feedback Suppression of low-frequency noise

Feedback is well-studied in classical control theory and widely used in electronic apparatus design[63, 64]. One application is to use a negative feedback loop to increase the system robustness against external noise. Here we focus on the corresponding topic of suppressing the noise and increasing the coherence time via a negative feedback loop in quantum system. As is shown in the experiment, the main source of dephasing is low-frequency noise. Assume the typical frequency of the noise is $\omega_N$ and the energy splitting of the qubit is $\Omega$, there is $\omega_N \ll \Omega$. If the slowly changed noise could be measured quickly and been subtracted from the original noise, the net noise should be weaker. The classical feedback loop is shown below. The net input is $I_{net} = I_0/(1 - \lambda^{'}\lambda) < I_0$. There is no limitation on $|\lambda^{'}\lambda|$ in classical theory, so the input can be suppressed arbitrarily.

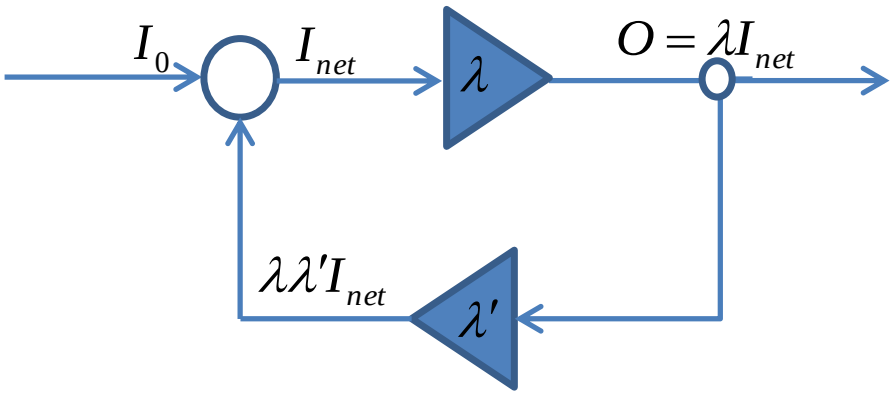


Figure 3.2: Schematics of the classical feedback loop. The original input is $I_0$, the detector has an instantaneous response $\lambda$, the output $O$ is send back by a feedback channel with response function $\lambda^{'}$. $I_{net}$ has two parts: $I_0$ and feedback signal $\lambda^{'}\lambda I_{net}$, i.e., $I_{net} = I_0 + \lambda^{'}\lambda I_{net}$. For a negative feedback, $\lambda^{'}\lambda < 0$. In the following quantum case, $\lambda^{'}$ is simply taken to be $-1$.

In the quantum regime, it's desirable to use the quantum limited detector in the measurement. The response function of the detector should be negligible beyond $\omega_N$, i.e., only the noise has been measured and the qubit dynamics is left unaffected. In classical regime, negative feedback has no fundamental limitation of the effectiveness, but it not clear in quantum regime how effective the negative feedback could be. As shown in chapter 2, the quantum measurement is a double-edged sword: on one side the detector acquires the information of the system, on the other the back-action destroys the coherence of the system. And quantum mechanics puts a fundamental limitation to the rate of information acquisition and decoherence. It's natural to ask how this quantum limited measurement affects the feedback suppression. This section tries to answer this question and addresses the ability of effectiveness of the feedback suppression of the low-frequency noise in quantum limited measurement.

### 3.2.1 Negative Feedback Suppression

A feedback loop is shown in Fig. 3.3. It includes a detector followed by a feedback channel. To be concrete, we consider a flux qubit sitting in an fluctuating external magnetic field with magnet flux $\hat{\Phi}^e$. The typical frequency of the noise in superconducting qubit $\omega_D$ is much smaller than the qubit energy splitting $\Omega$, i.e., $\omega_D \ll \Omega$. The response function of the detector $\lambda$ is chosen in such a way that it is negligible beyond frequency $\omega_D$, so the detector can measure the noise $\hat{\Phi}^e$ without disturbing the qubit dynamics. The output is send back to the qubit system and eliminate part of the original noise via the feedback loop. Then the net noise $\hat{\Phi}$ surrounding the qubit has three parts: external flux noise $\hat{\Phi}^n$, the back-action noise $\hat{\Phi}^{b.a.} = L_e\hat{I}^{b.a.}$, and the output $\hat{\Phi}^{out}$.

$$\hat{\Phi}(t) = \hat{\Phi}^n(t) + L_e\hat{I}^{b.a.}(t) - \hat{\Phi}^{out}(t)\,. \tag{3.4}$$

Here the detector is coupled to the system via the inductance $L_e$.

The dynamics of the system is governed by the response function $\lambda$, however the

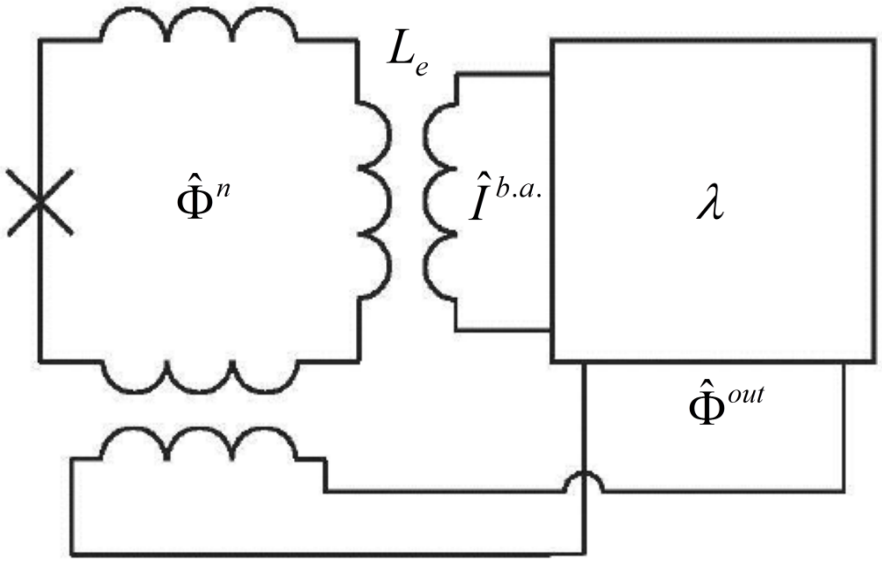


Figure 3.3: Schematics of the feedback loop.The detector dynamics is determined by the response function $\lambda$ which only measures the low-frequency noise $\hat{\Phi}^n$ in the qubit system. The back-action force of the detector $\hat{I}^{b.a.}$ is coupled inductively to the qubits and hence add extra noise. The output is sent back to the system via the feedback loop to eliminate the original noise.

input coupled to the back-action force $\hat{I}^{b.a.}$ consists both original flux noise $\hat{\Phi}^n$ and the feedback output $\hat{\Phi}^{out}$:

$$\hat{\Phi}^{out}(t) = \hat{\Phi}_0^{out}(t) + \int^t d\tau \lambda(t-\tau)\left(\hat{\Phi}^n(\tau) - \hat{\Phi}^{out}(\tau)\right) . \tag{3.5}$$

To get the final spectral density of the net flux noise in the qubit system, switch to frequency domain via Fourier transformation,

$$\hat{\Phi}(\omega) = \hat{\Phi}^n(\omega) + L_e\hat{I}^{b.a.}(\omega) - \hat{\Phi}^{out}(\omega) , \tag{3.6}$$

$$\hat{\Phi}^{out}(\omega) = \hat{\Phi}_0^{out}(\omega) + \lambda(\omega)\left(\hat{\Phi}^n(\omega) - \hat{\Phi}^{out}(\omega)\right) . \tag{3.7}$$

which related the net noise spectral density with the original noise, back-action force

and response function:

$$\hat{\Phi}(\omega) = \frac{\hat{\Phi}^n(\omega)}{1+\lambda(\omega)} + L_e \hat{I}^{b.a.}(\omega) - \frac{\hat{\Phi}_0^{out}(\omega)}{1+\lambda(\omega)} \,. \tag{3.8}$$

Since the original flux noise has a different origin with the back-action force and output noise, it's natural to assume that $\langle \hat{\Phi}^n(\omega) \hat{I}^{b.a.}(\omega') \rangle = \langle \hat{\Phi}^n(\omega) \hat{\Phi}_0^{out}(\omega') \rangle = 0$. Use the relationship $2\pi S_{qf}(\omega) = \langle \hat{q}(\omega) \hat{f}(-\omega) \rangle$, the spectral density of the net noise is:

$$S_\Phi(\omega) = \frac{S_\Phi^n(\omega)}{|1+\lambda(\omega)|^2} + S_\Phi^D(\omega) \,, \tag{3.9}$$

$$S_\Phi^D(\omega) = L_e^2 S_I(\omega) + \frac{S_{\Phi_0}(\omega)}{|1+\lambda(\omega)|^2} - 2L_e \mathcal{R}e \left( \frac{S_{\Phi_0 I}(\omega)}{1+\lambda(\omega)} \right) . \tag{3.10}$$

The physical meaning of this result is clear. The net noise spectral density has two parts. The first part is the suppressed original noise, and the second part $S_\Phi^D$ is the noise from the detector, which is the price paid for the feedback process. Since there is no limitation on the magnitude of response function, i.e. $|\lambda(\omega)|$ , the first part of the noise can be suppressed arbitrarily small and hence can be ignored, however, $S_\Phi^D$ has a fundamental limitation. Generally, the noise increases with the response function, but there is an optimal way to choose the input and output to minimize $S_\Phi^D$. Assume the input and output are all classical quantities, so the spectral density is symmetric. The minimization of the detector noise is given by the following conditions:

$$S_{I(\Phi_0)}(\omega) = S_{I(\Phi_0)}(-\omega) \,, \tag{3.11}$$

$$S_I(\omega) S_{\Phi_0}(\omega) = |S_{\Phi_0 I}(\omega)|^2 \,, \tag{3.12}$$

$$i\hbar\lambda(\omega) = S_{\Phi_0 I}(\omega) - S_{\Phi_0 I}^*(-\omega) \,, \tag{3.13}$$

$$S_{\Phi_0 I}(\omega) + S_{\Phi_0 I}^*(-\omega) = 0 \,. \tag{3.14}$$

Eq. (3.11) means the input and output are both classical noise; Eq. (3.12) means

the noise spectral density of the detector is quantum limited; Eq. (3.13) means the detector has no-reverse gain; Eq. (3.14) means the response function is maximized. Under these conditions, the noise spectral density $S_\Phi(\omega)$ can be formulated as following equation:

$$S_\Phi(\omega) = \frac{S_\Phi^n(\omega)}{|1+\lambda(\omega)|^2} + L_e^2 S_I(\omega) + \frac{1}{4S_I(\omega)}\left|\frac{\hbar\lambda(\omega)}{1+\lambda(\omega)}\right|^2 + \mathcal{I}m\left(\frac{\lambda(\omega)}{1+\lambda(\omega)}\right) L_e\hbar\,. \quad (3.15)$$

Varying $S_I(\omega)$ to minimize $S_\Phi(\omega)$:

$$S_\Phi(\omega) = \frac{S_\Phi^n(\omega)}{|1+\lambda(\omega)|^2} + \left|\frac{\lambda(\omega)}{1+\lambda(\omega)}\right| L_e\hbar + \mathcal{I}m\left(\frac{\lambda(\omega)}{1+\lambda(\omega)}\right) L_e\hbar\,. \quad (3.16)$$

where

$$2L_e S_I(\omega) = \left|\frac{\hbar\lambda(\omega)}{1+\lambda(\omega)}\right|. \quad (3.17)$$

The original noise could be suppressed to arbitrarily small and thus be negligible, then there is:

$$S_\Phi(\omega) = \left[\left|\frac{\lambda(\omega)}{1+\lambda(\omega)}\right| + \mathcal{I}m\left(\frac{\lambda(\omega)}{1+\lambda(\omega)}\right)\right] L_e\hbar \simeq L_e\hbar\,, \quad |\lambda| \gg 1\,. \quad (3.18)$$

Thus, in principle, any low-frequency flux noise can be suppressed by the negative feedback to this fundamental level, which corresponds to the zero-point motion of flux in the inductance $L_e$ spread over the frequency range up to the frequency of the zero-point motion.

## 3.3 Examples

### 3.3.1 Lorentzian Noise

A simple example of the low-frequency quantum detector is given below, where a Lorentzian form spectral density is assumed. The input and output has the same

frequency dependence decided by the typical time scale $\tau_D$; also $1/\tau_D$ is much smaller than the qubit energy splitting in order to retain the qubit dynamics. The magnitude of the response function is given by the quantum-limited detector condition, and the phase dependence over frequency can be determined with the help of Bode's relation. The results are:

$$\begin{aligned} S_I(\omega) &= \frac{S_I}{1+\omega^2\tau_D^2}, \quad S_{\Phi_0}(\omega) = \frac{S_{\Phi_0}}{1+\omega^2\tau_D^2}\,, \\ \lambda(\omega) &= \frac{K}{(1+i\omega\tau_D)^2}, \quad K = \sqrt{\frac{4S_I S_{\Phi_0}}{\hbar^2}}\,. \end{aligned} \tag{3.19}$$

The original noise is totally suppressed since $K$ can be arbitrarily large. So the noise spectrum is:

$$S_\Phi(\omega) \;=\; L_e^2 S_I(\omega) + \frac{S_{\Phi_0}(\omega)}{|1+\lambda(\omega)|^2}\,. \tag{3.20}$$

Now let's consider the fidelity of the system. The fidelity is given by the fluctuation of the phase difference $\delta E/\hbar$, which is proportional to the flux fluctuation $\delta\Phi$:

$$F \;=\; \langle exp\{\frac{i}{\hbar}\int_0^t \delta E ds\}\rangle = \langle exp\{i\frac{\nu}{\hbar}\int_0^t \delta\Phi(s) ds\}\rangle \tag{3.21}$$

$$\;=\; exp\{-\frac{\nu^2}{\hbar^2}\int_0^t dt_1 dt_2 \langle\delta\Phi(t_1)\delta\Phi(t_2)\rangle\}\,. \tag{3.22}$$

where $\delta E = \nu\delta\Phi$. At large time, the result is:

$$F \;=\; exp\{-\frac{\nu^2}{\hbar^2}\int_0^t dt_1 dt_2 \langle\delta\Phi(t_1)\delta\Phi(t_2)\rangle\} \propto exp\{-\gamma t\}\,, \tag{3.23}$$

$$\gamma \;=\; \frac{\nu^2}{2}\left(L_e^2 S_I + \frac{S_{\Phi_0}}{K^2}\right) \geq \frac{\nu^2 L_c \hbar}{2}\,. \tag{3.24}$$

The " = " holds when:

$$S_I = \frac{\hbar}{2L_e}\,. \tag{3.25}$$

To see the scale of dephasing time, use the experiment parameter:

$$\nu \approx 0.1GHz/m\Phi_0\,, \quad L_e \approx 100pH \rightarrow \gamma = (100ns)^{-1}\,. \tag{3.26}$$

### 3.3.2 $1/f$ Noise

$1/f$ noise is one of the dominant sources of decoherence in superconducting qubits[60, 61, 62]. For $1/f$ noise, the original noise is divergent at zero frequency and can't be suppressed completely. To avoid the divergence at zero-frequency, a low-frequency cut-off $\omega_c$ is assumed.

$$S_{\Phi_n}(\omega) = \frac{S_0}{|\omega|}\,, \quad |\omega| > \omega_c\,. \tag{3.27}$$

The fidelity under this noise decreases much faster than in the case of Lorentzian noise. Including the feedback loop, the net noise is:

$$S_\Phi(\omega) \;=\; \frac{1}{|1+\lambda(\omega)|^2}\frac{S_0}{|\omega|} + L_e^2 S_I(\omega) + \frac{S_{\Phi_0}(\omega)}{|1+\lambda(\omega)|^2}\,. \tag{3.28}$$

The fidelity at large time is:

$$\begin{aligned} -\ln F(t)/\nu^2 &= \frac{t}{2}\left(L_e^2 S_I + \frac{S_{\Phi_0}}{K^2}\right) + \frac{S_0}{K^2}t^2|\ln(\omega_0 t)| \\ &\geq \frac{L_e\hbar}{2}t + \frac{S_0}{K^2}t^2|\ln(\omega_0 t)|\,. \end{aligned} \tag{3.29}$$

The feedback loop adds a new term proportional to $t$ in the result, but strongly suppresses the much faster $t^2$ term.

# Chapter 4

# nSQUID array: a conveyer of quantum information

The problem of quantum information transfer along the mesoscopic quantum structures is one of the most important issues that needs to be solved in order to design and create scalable quantum computing circuits. This chapter suggests and evaluates a promising solution to this problem based on arrays of nSQUIDs[79, 80]. Negative mutual inductance between the two branches of an nSQUID assigns the two tasks of processing and transferring quantum information to different modes of the nSQUID circuit dynamics and therefore makes it possible to optimize parameters relevant for each mode for its particular task. The differential mode that corresponds to the current circulating along one is used to encode the qubit, while the common mode representing the total current through the nSQUID can be used to transport this qubit along the circuit. In one of the most important examples, dynamics of the common mode is similar to that of a fluxon propagating along the Josephson transmission line.

## 4.1 Introduction to Josephson transmission line

Superconducting qubits, including charge qubit [21, 22, 23], flux qubit[24, 25] and phase qubit[27], all make use of one or a few Josephson junctions. Another important circuit of Josephson junctions is a one-dimensional array of a large number of junctions, which supports propagation of fluxons carrying quanta of magnetic flux. Such a"Josephson transmission line" (JTL) is one of the family of rapid single-flux-quantum (RSFQ) devices [66] which were proposed as a promising technology for superconducting digital circuits [67, 68, 69]. In [70], JTL was suggested and analyzed as the quantum limited detector for flux qubits.

The Hamiltonian of the JTL, equivalent circuit of which is shown in Fig. 4.1, can be expressed through the charge $\hat{Q}$ and phase $\phi$ of each cell:

$$\hat{H} = \sum_i \left[ \frac{\hat{Q}_i^{\,2}}{2C} + E_J(1 - cos\hat{\phi}_i) + E_L(\hat{\phi}_{i+1} - \hat{\phi}_i - \hat{\phi}_i^e)^2 \right] , \tag{4.1}$$

where $E_J$ is the Josephson coupling energy, $E_L = \frac{1}{2L}(\frac{\Phi_0}{2\pi})^2$, $C$ and $L$ are the capacitance and inductance. In the continuum limit, as will be shown in the next section, the Hamiltonian reduces to that of the standard sine-Gordon model with its freely propagating fluxon excitations.

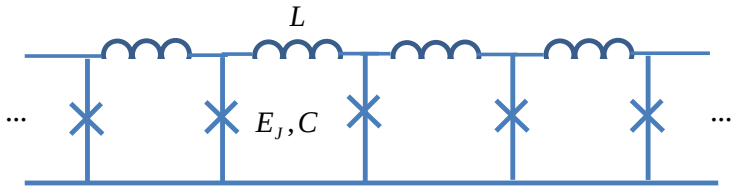


Figure 4.1: Equivalent circuit of Josephson transmisson line (JTL). The line with the "X" mark is a Josephson junction, and they are connected inductively. The collective mode of JTL is fluxon moving along the array.

In [71], a flux qubit detector was proposed using a closed JTL (Fig. 4.2). The fluxon moves around the circle with a velocity depending on the state of the flux qubit, and hence the frequency of the radiation of the fluxon includes the information of the qubit state (Fig. 4.2). The predicted dip at $\Phi_0/2$ is not clear enough, suggesting that further improvements are required.

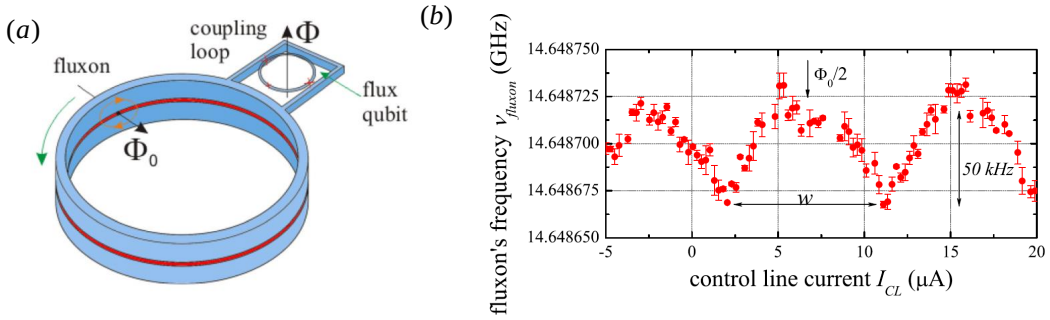


Figure 4.2: JTL as a flux qubit readout. (a) Scheme of the experiment setup in [71]. An annular Josephson junction with a trapped fluxon coupled to a flux qubit. (b) Modulation of the fluxon's oscillation frequency due to the coupling to the flux qubit.

## 4.2 nSQUID

In this section, we introduce a solution to the problem of transferring quantum information along a superconducting quantum circuit of the flux-based qubits that is based on nSQUID arrays. Such an array provides effectively the qubit implementation in the form of the dual-rail Josephson arrays. In details, the elementary cell of such an array consists of the two-junction SQUID with in general negative inductance between its two arms (Fig. 4.3). The time evolution of such a cell can be separated naturally into the dynamics of two degrees of freedom ("excitation

modes"). One is collective mode which represents total current flowing through the two junctions of the SQUID together, and the other is the differential mode which represents the current circulating along the SQUID loop. The negative mutual inductance between the SQUID arms enables one to make the effective inductance of the differential mode larger than the inductance of the common mode. As a result, the excitation frequency of the common mode becomes much larger than that of the differential mode, making it possible for the differential mode to exhibit non-trivial dynamic without exciting the common mode. In the particular case when the inductance of the differential mode is sufficiently large for it to have a bi-stable dynamics, this structure is equivalent to nSQUID in [79, 80] developed for classical reversible computing[72, 73] .

The Hamiltonian of the cell in in Fig. 4.3 includes the Hamiltonian of two Josephson junction and the inductive energy in the arm.

$$
\begin{aligned}
H &= \frac{Q_1^2}{2C} - E_J\cos\phi_1 + \frac{Q_2^2}{2C} - E_J\cos\phi_2 \\
&\quad + \frac{1}{2}\left(\frac{\Phi_0}{2\pi}\right)^2 \begin{pmatrix}\phi_1-\chi_e-\phi_e, & \phi_2-\chi_e+\phi_e\end{pmatrix} \hat{L}^{-1} \begin{pmatrix}\phi_1-\chi_e-\phi_e \\ \phi_2-\chi_e+\phi_e\end{pmatrix} \qquad (4.2) \\
&= \frac{K^2}{4C} + \frac{Q^2}{4C} - 2E_J\cos\chi\cos\phi \\
&\quad + \frac{1}{2(L^2-M^2)}\left(\frac{\Phi_0}{2\pi}\right)^2 \begin{pmatrix}\phi_1-\chi_e-\phi_e, & \phi_2-\chi_e+\phi_e\end{pmatrix} \begin{pmatrix}L & M \\ M & L\end{pmatrix} \begin{pmatrix}\phi_1-\chi_e-\phi_e \\ \phi_2-\chi_e+\phi_e\end{pmatrix} \qquad (4.3) \\
&= \frac{K^2}{2C_{tot}} + \frac{Q^2}{4C} - 2E_J\cos\chi\cos\phi + \left(\frac{\Phi_0}{2\pi}\right)^2 \left[\frac{(\chi-\chi_e)^2}{L-M} + \frac{(\phi-\phi_e)^2}{L+M}\right]. \qquad (4.4)
\end{aligned}
$$

Here $\Phi_0 = \pi\hbar/e$ is the magnetic flux quantum; $Q_{1(2)}$ is the charge on Josephson junction 1(2), $\phi_{1(2)}$ is the phase difference across each Josephson junction, $L$ is the inductance,$-M$ is the mutual inductance ($M > 0$, so the inductance is negative). $K$ and $\chi$ are the variables of the common mode: $K = Q_1 + Q_2$ is the total charge on the two capacitances of the SQUID junction, and $\chi = (\phi_1 + \phi_2)/2$ is the average Josephson phase difference across the junctions. The effective inductance of the

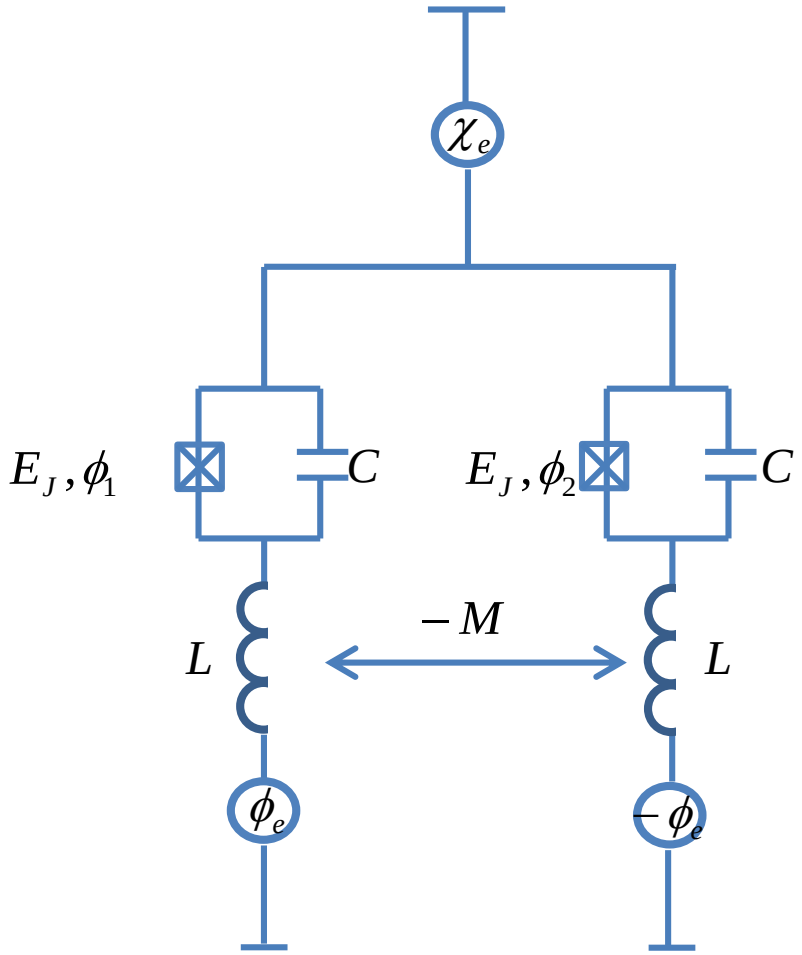


Figure 4.3: Equivalent circuit of an elementary cell of a dual-rail array: SQUID with two junctions of capacitances $C$ and Josephson coupling energies $E_J$ and the negative mutual inductance $M$ between its inductive arms with inductances $L$. The negative mutual inductance makes the effective inductance of the common mode of the SQUID dynamics much smaller than the inductance of the differential mode. Also shown are the phase bias $\chi_e$ of the common mode and the bias $\phi_e$ of the differential mode.

common mode is $(L-M)/2$ and capacitance $C_{tot}$ which can include additional contributions (see Fig. 4.4 below) besides the total capacitance $2C$ of the junctions. In quantum dynamic, $K$ and $\chi$ are canonically conjugated variables, $[\chi, K] = 2ei$. The corresponding variables of the differential mode are the charge difference $Q = Q_1 - Q_2$ and the phase difference $\phi = (\phi_1 - \phi_2)/2$ which have the same canonical commutation relation $[\phi, Q] = 2ei$. The effective inductance and capacitance of this mode are $(L+M)/2$ and $2C$ respectively.

The qualitative effect of the negative mutual inductance between the two SQUID branches (Fig. 4.3) is to make the dynamic properties of the common and the differential mode very different. For instance, if one neglects Josephson tunneling, the resonance frequencies of the two modes are $\omega_C = [2/(L-M)C_{tot}]^{1/2}$ and $\omega_D = 1/[(L+M)C]^{1/2}$, respectively, and for strong coupling, $M \to L$, the dynamics of the two modes can be clearly separated in frequency. This means that when the SQUID cells are connected in an array (Fig. 4.4) the two modes can be used to perform different functions. If the coupling inductances $L_C$ are designed to have negative mutual inductance $-M_C$ to preserve the character of the SQUID dynamics, the common mode remains rigid, i.e., it is not affected by the evolution of the differential mode, and is essentially fixed at some value $\chi_e(x,t)$, where x the coordinate along the array, which is either applied externally or generated dynamically. This phase plays then the role of the qubit control signal which is distributed along the array through , the "clock" line (upper horizontal line in Fig. 4.4). The differential mode has lower frequency and can be used to encode a classical or quantum bit of information in the current circulating along the coupled SQUID loops. Dynamics of the common mode ensures that the information encoded by the differential mode is transported along the array.

The Hamiltonian of the nSQUID array in the limit $M \to L$ is :

$$H = \sum_j \left\{ \frac{K_j^2}{2C_{tot}} + \frac{Q_j^2}{4C} - 2E_J \cos\chi_j \cos\phi_j + \left(\frac{\Phi_0}{2\pi}\right)^2 \left[ \frac{\phi_j^2}{L+M} + \frac{(\phi_j - \phi_{j-1})^2}{L_C + M_C} + \frac{(\chi_j - \chi_{j-1})^2}{2L_0} \right] \right\} . \quad (4.5$$

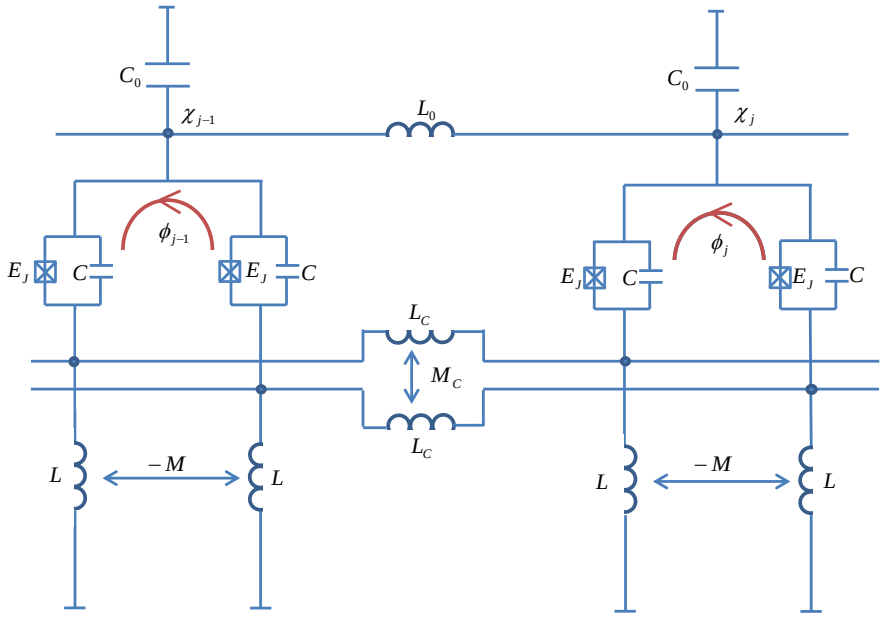


Figure 4.4: Dual-rail Josephson array made of nSQUID cells shown in Fig.(4.3). In the array configuration, both bias phases $\chi_e$ and $\phi_e$ can be generated by the array dynamics. In this dynamics, the common mode plays the role of the qubit control signal propagating along the control line with specific capacitance $C_0$ and inductance $L_0$, whereas the differential mode encodes the quantum information transferred between the cells coupled by inductances $L_C$, with negative mutual inductance $-M_C$ between them.

In the continuum limit, the Hamiltonian becomes:

$$H = \int dx \left\{ \left(\frac{\Phi_0}{2\pi}\right)^2 \left[\frac{1}{2} C_{tot} \left(\frac{\partial \chi}{\partial t}\right)^2 + \frac{1}{2L_0}\left(\frac{\partial \chi}{\partial x}\right)^2\right] - 2E_J \cos\chi \cos\phi \right.$$
$$\left. + \left(\frac{\Phi_0}{2\pi}\right)^2 \left[C\left(\frac{\partial \phi}{\partial t}\right)^2 + \frac{1}{L_C + M_C}\left(\frac{\partial \chi}{\partial x}\right)^2 + \frac{\phi^2}{L+M}\right] \right\}$$
$$= \int dx \left\{ E_C \left[\frac{1}{\omega_C^2}\left(\frac{\partial \chi}{\partial t}\right)^2 + \left(\frac{\partial \chi}{\partial x}\right)^2\right] - 2E_J \cos\chi\cos\phi + E_D \left[\frac{1}{\omega_D^2}\left(\frac{\partial \phi}{\partial t}\right)^2 + l\left(\frac{\partial \phi}{\partial x}\right)^2 + \phi^2\right] \right\} . (4.6$$

Here:

$$E_C = \frac{1}{2L_0}\left(\frac{\Phi_0}{2\pi}\right)^2, \quad E_D = \frac{1}{L+M}\left(\frac{\Phi_0}{2\pi}\right)^2, \quad \omega_C = \frac{1}{\sqrt{L_0 C_{tot}}},$$
$$\omega_D = \frac{1}{\sqrt{(L+M)C}}, \quad l = \frac{L+M}{L_c+M_c}. \tag{4.7}$$

This is a field of a massless particle $\chi$ and massive particle $\phi$ with mass $E_D$, where these two particles interacting via $\cos\chi\cos\phi$. Due to the mass term, field $\phi$ is small, the dynamics of the common mode $\chi$ is determined by the following Hamiltonian:

$$H_\chi = \int dx \Big\{ E_C \left[\frac{1}{\omega_C^2}\left(\frac{\partial\chi}{\partial t}\right)^2 + \left(\frac{\partial\chi}{\partial x}\right)^2\right] - 2E_J\cos\chi \Big\}. \tag{4.8}$$

The behavior of the common mode is given by the sine-Gordon model[76] of discrete Josephson junctions. This dynamically generalized common mode serves as a moving background for differential mode, and gives it a space structure along the array. The lowest-lying excitations of the differential mode that can serve as the basis state of a qubit propagating along the array are localized in the region where $\chi_j \simeq \pi$(see Eq.4.9), i.e., where the Josephson coupling has the largest negative value. Depending on the magnitude of this coupling, dynamics of the differential phase in this region is governed by a bi-stable potential required for encoding the qubit of information in two different flux states, as in regular qubits, or a mono-stable potential in which the information can be encoded in two different energy states, similarly to the phase qubits. In both situations, the qubit of information can be transported along the arrays by the dynamics of the clock phase.

In the continuous approximation, strictly valid when the effective Josephson penetration length $\lambda_J$ of the array, $\lambda_J \equiv (\hbar/2e)/[E_J(L_C+M_C)]^{1/2}$, is large, $\lambda_J \gg 1$, the common mode is given by the usual fluxon[74] solution:

$$\chi(x,t) = 4\tan^{-1}[\exp((x-vt)/\lambda_0)]. \tag{4.9}$$

where $\lambda_0 = (\hbar/2e)/[2E_J L_0]^{1/2}$. The fluxon propagates along the array with velocity $v$ determined by the dc bias voltage of the clock line. The Hamiltonian for differential mode becomes:

$$H_D = E_D \int dx \Big\{ \frac{1}{\omega_D^2} \left( \frac{\partial \phi}{\partial t} \right)^2 + l \left( \frac{\partial \phi}{\partial x} \right)^2 + \phi^2 - 2\beta \cos\chi \cos\phi \Big\} . \tag{4.10}$$

where $\beta \equiv E_J/E_D$. In these equations, inductances and capacitances are now defined per unit length of the array. For the quantum information transfer, one is interested in the regime of the array dynamics characterized by adiabatic evolution of $\chi$, when the excitation frequencies of $\phi$ which are on the order of $\omega_D$, are much larger than the frequency associated with the clock propagation, $\dot{\chi} \ll \omega_D$, ie, $v \ll \sqrt{L_0 C_{tot}}$.

## 4.3 Coherence property of the nSQUID

Let's start from the Hamiltonian for differential mode:

$$\hat{H}_D = \tilde{E}_D \int dz \Big\{ \frac{1}{\omega_D^2} \left( \frac{\partial \hat{\phi}}{\partial t} \right)^2 + \alpha \left( \frac{\partial \hat{\phi}}{\partial z} \right)^2 + \hat{\phi}^2 - 2\beta \cos\chi(z,t) \cos\hat{\phi} \Big\} . \tag{4.11}$$

where $z = x/\lambda_0$, $\tilde{E}_D = E_D \lambda_0$ and $\alpha \equiv l/\lambda_0^2$ . Here $\chi$ is the background potential given by the common mode.

$$\cos\chi = 1 - \frac{2}{\cosh^2 z} . \tag{4.12}$$

The two dimensionless parameter $\alpha$ and $\beta$ give a full description of the system. The potential $U(\phi)$ is:

$$\hat{U}(\hat{\phi}, z) = \hat{\phi}^2 - 2\beta \left( 1 - \frac{2}{\cosh^2 z} \right) \cos\hat{\phi} . \tag{4.13}$$

The potential $\hat{U}(\hat{\phi}, 0)$ is given below. There are two different cases according to the value of $\beta$.

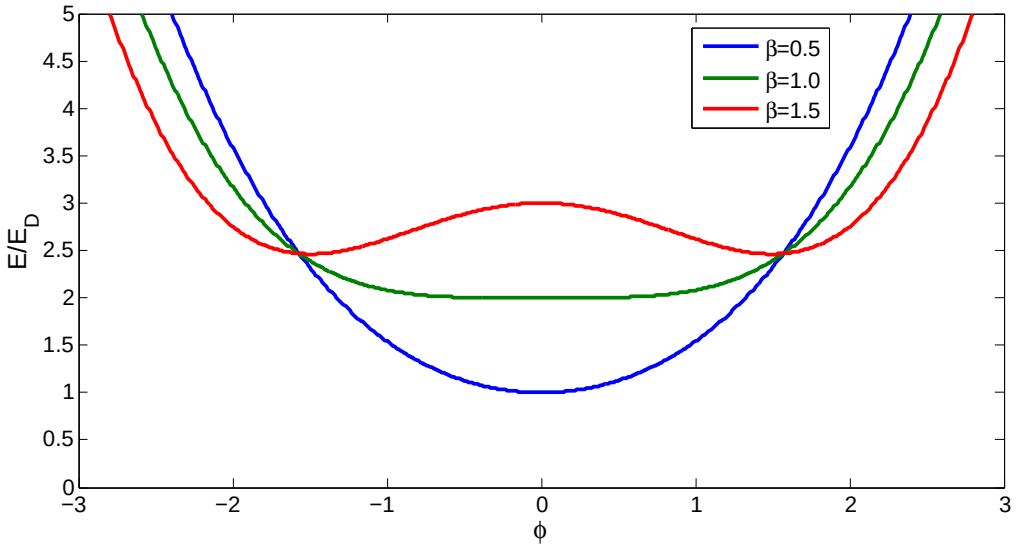


Figure 4.5: Potential at z=0: $\hat{U}(\hat{\phi}, 0)$. There are two qualitatively different cases: when $\beta < 1$, the potential has only one minimum at $\phi = 0$; when $\beta > 1$ , the potential has two minima symmetric to $\phi = 0$.

If $\beta < 1$, the potential always has only one minimum at $\phi = 0$, where the phase dynamics is similar to the phase qubit; if $\beta > 1$, the potential is bistable when $z$ is near to zero and information could be encoded in different flux states as in the flux qubit. In either case , the system is influenced by the noise and suffers a loss in the coherence.

### 4.3.1 Case I: $\beta < 1$

If the Josephson coupling in the array is chosen that $\beta < 1$, one can use the quadratic approximation to determine the space structure and frequencies for the $\phi$ excitations using the approximation $\cos\phi \approx 1 - \frac{\phi^2}{2}$, the classical equation of motion is then:

$$\alpha\phi'' = \omega_D^{-2}\ddot{\phi} + (1 + \beta - \frac{2\beta}{\cosh^2 z})\phi\} \,. \tag{4.14}$$

This equation is further reduced to a stationary Schrödinger equation after separating the variable by replacing $\ddot{\phi}$ with$-\omega^2\phi$. This equation is exactly solvable and gives the excitation modes $\phi_j(z)$ localized around $z \simeq 0$, and the frequencies $\omega_j$:

$$\omega_j = \omega_D\{1 + \beta - \alpha(s-j)^2\}^{1/2}\,. \tag{4.15}$$

where the integer $j$ is limited by the condition:

$$0 \le j \le s \equiv \frac{(1+8\beta/\alpha)^{1/2}-1}{2}\,. \tag{4.16}$$

Then the quantum dynamics of $\hat{\phi}$ and the Hamiltonian has then the following form:

$$\hat{\phi}(z,t) = \sum_j (\frac{e^2}{\hbar C\omega_j})^{1/2}\phi_j(z)(\hat{a}_j(t) + \hat{a}_j^\dagger(t))\,, \quad \hat{H}_0 = \sum_j \hbar\omega_j(\hat{a}^\dagger\hat{a} + \frac{1}{2})\,. \tag{4.17}$$

where a's are the usual creation/annihilation operators. The two level system used as a qubit is now the vacuum state $|0\rangle$ without phonon and the one phonon state $|1\rangle$ with the lowest excitation frequency $\omega_0$.

The noise is coupled directly to the phase $\phi$:

$$\hat{H}_I = \int dz F(z,t)\hat{\phi}(z,t) = \sum_j (\frac{e^2}{\hbar C\omega_j})^{\frac{1}{2}}F_j(t)(\hat{a}_j(t) + \hat{a}_j^\dagger(t))\,. \tag{4.18}$$

where $F_j(t) = \int dz F(z,t)\phi_j(z)$. So the qubit system together with the noise has the following form:

$$\hat{H} = \frac{\hbar\omega_0}{2}\hat{\sigma}_z + (\frac{e^2}{\hbar C\omega_0})^{\frac{1}{2}}F_0(t)\hat{\sigma}_x\,. \tag{4.19}$$

We assume that the noise for each N-SQUID is identical but independent from each other, so the noise $F(z,t)$ is $\delta$-correlated in space:

$$< F(z,t)F(z',t') >= \delta(z-z') < F(t-t')F(0) > \ . \tag{4.20}$$

The spectral density then is:

$$S_{FF}(\omega) = \int dt \langle F(t)F(0)\rangle e^{i\omega t} \,. \tag{4.21}$$

Since $F_0(t) = \int dz F(z,t)\phi_0(z)$, the spectral density for $F_0$ is:

$$\begin{aligned} S_{F_0F_0}(\omega) &= \int dt \langle F_0(t)F_0(0)\rangle e^{i\omega t} \\ &= \int dt dz dz' e^{i\omega t} \langle F(z,t)F(z',0)\rangle \phi_0(z)\phi_0(z') \\ &= \int dt dz dz' e^{i\omega t} \langle F(t)F(0)\rangle \delta(z-z')\phi_0(z)\phi_0(z') \\ &= \int dt e^{i\omega t} \langle F(t)F(0)\rangle \int dz [\phi_0(z)]^2 \\ &= S_{FF}(\omega) \,. \end{aligned} \tag{4.22}$$

Use the standard method, the tunneling rate between the two state and the decoherence rate are:

$$\Gamma_{10(01)} = \frac{e^2}{\hbar^3 C\omega_0} S_{F_0F_0}(\pm\omega_0) = \frac{e^2}{\hbar^3 C\omega_0} S_{FF}(\pm\omega_0) \,, \tag{4.23}$$

$$\gamma = \frac{\Gamma_{10} + \Gamma_{01}}{2} \,. \tag{4.24}$$

where the spectral density is given by:

Note that the space structure $\phi_0$ here doesn't play a role in the result. It's caused by the fact that the excitation has only one phonon, leads to $\int dz|\phi_0|^2 = 1$. Together with the $\delta$-correlated property of the noise, it has no explicit effect on the final result.

### 4.3.2 Case II: $\beta > 1$

When $\beta > 1$, the potential has one minimal when $|z|$ is large, and two minimals when $z \approx 0$ (Fig. 4.6(a)). Assume that the minimal of the potential is $\phi_m$, then $-\phi_m$ is also the minimals. Naively, one may say that there are two classical configurations

that minimize the energy, and hence the ground state is double-degenerate, with one state around $\phi_m$, the other around $-\phi_m$, but this is not always true. Consider a classical static classical configuration $\phi(z)$, then the energy (Hamiltonian) is:

$$H_S = (\frac{\Phi_0}{2\pi})^2 \frac{1}{L+M} \int dz \{\alpha(\phi')^2 + \phi^2 - 2\beta \cos\chi(z,t)\cos\phi\} \tag{4.25}$$

$$= (\frac{\Phi_0}{2\pi})^2 \frac{1}{L+M} \int dz \{\alpha(\phi')^2 + U(\phi)\}\,. \tag{4.26}$$

The energy has two competing parts: one is $\phi'$ which tends to keep $\phi$ constant, the other is potential $U(\phi)$ which tends to constraint $\phi$ to local minimal. Consider two extreme cases:

(1) $\alpha \to 0$:

$$H_S = (\frac{\Phi_0}{2\pi})^2 \frac{1}{L+M} \int dz \{\phi^2 - 2\beta \cos\chi(z,t)\cos\phi\}\,. \tag{4.27}$$

In this case, there are two minimums which coincide with the minimums of the potential, $\phi_m$ and $-\phi_m$.

(2) $\alpha \to +\infty$:

$$H_S = (\frac{\Phi_0}{2\pi})^2 \frac{\alpha}{L+M} \int dz (\phi')^2\,. \tag{4.28}$$

The minimum is $\phi = 0$.

So only for certain range of $\alpha$ and $\beta$, there are two minimums. This problem can be "solved" together with finding the minimal configuration via a variational method. Here we try the find $\phi_c(x)$ minimize $H_s$, assuming $\phi_c$ has the form: $\phi_c(z) = \phi_0/\cosh^\eta(z)$. Expand $\cos\phi$ to $\phi^4$ which includes the bistable character of the potential around $z \sim 0$, $H_S$ is exactly integrable. The result is:

$$\frac{H_0(L+M)}{(\phi_0/2\pi)^2} = \Big\{\phi_0^2 B(1/2,\eta)\frac{\alpha\eta^2 + 2(1-\beta)\eta + 1 + \beta}{2\eta+1} + \frac{\beta\phi_0^4}{12} B(1/2,2\eta)\frac{4\eta-1}{4\eta+1}\Big\}\,. \tag{4.29}$$

To get a nonzero minimum, it's necessary for the coefficient of $\phi_0^2$ to be negative and

$\phi_0^4$ to be positive, this leads to the condition:

$$\alpha < \frac{(\beta-1)^2}{1+\beta}, \quad \eta > 1/4\,. \tag{4.30}$$

To find the exact value of $\eta$ and $\phi_0$, numerical method is needed, see Fig.4.6 for result (in numerical method, it's not necessary to expand $\cos\phi$).

To minimize the energy, $\phi_c$ should be satisfied the following equation:

$$\alpha\phi_c'' = \phi_c + \beta\cos\chi\sin\phi_c\,. \tag{4.31}$$

For the $\phi_c$ found via variation method, $Fig.4.6(c)$ shows that, the $LHS$ of 4.31 is larger compared to the $LHS - RHS$.

From the symmetry of the Hamiltonian, it's easy to see $-\phi_c$ is also a minimum. States around these two minima have different flux and serves as a flux qubit. The energy splitting $\epsilon_0$ can be adjusted by external bias. Borrowing the result from quantum field theory $T = e^{-S_{cl}/\hbar}$, where $T$ is the transmission coefficient and $S_{cl}$ is the classical action connecting these two states, we can find the tunneling element $\Delta$ between these two minima as $T\epsilon_0/2\pi$. If $\phi_0$ is not very big, it's proper to assume that during the evolution it's roughly maintain the shape, only the amplitude changes. This approximation gives:

$$S_{cl} = (\frac{\Phi_0}{2\pi})^2\frac{1}{L+M}\frac{4\phi_0^3}{3\omega_D}\sqrt{(8\eta-2)B(1/2,\eta)B(3/2,2\eta)\beta} \sim (\frac{\Phi_0}{2\pi})^2\frac{1}{L+M}\frac{4\phi_0^3}{3\omega_D}\sqrt{\frac{\sqrt{2}\beta}{\eta}}\,.$$

The details of the calculation are given below. First let's review the instanton method[75]. Consider a particle moves under a bistable potential $V(x)$, the minimums are $x = \pm a$, given below:

The amplitude of transmission is:

$$|T| = \exp\left\{-\frac{1}{\hbar}\int_{-a}^{a} dx\sqrt{2m(V-E)}\right\}\,. \tag{4.32}$$

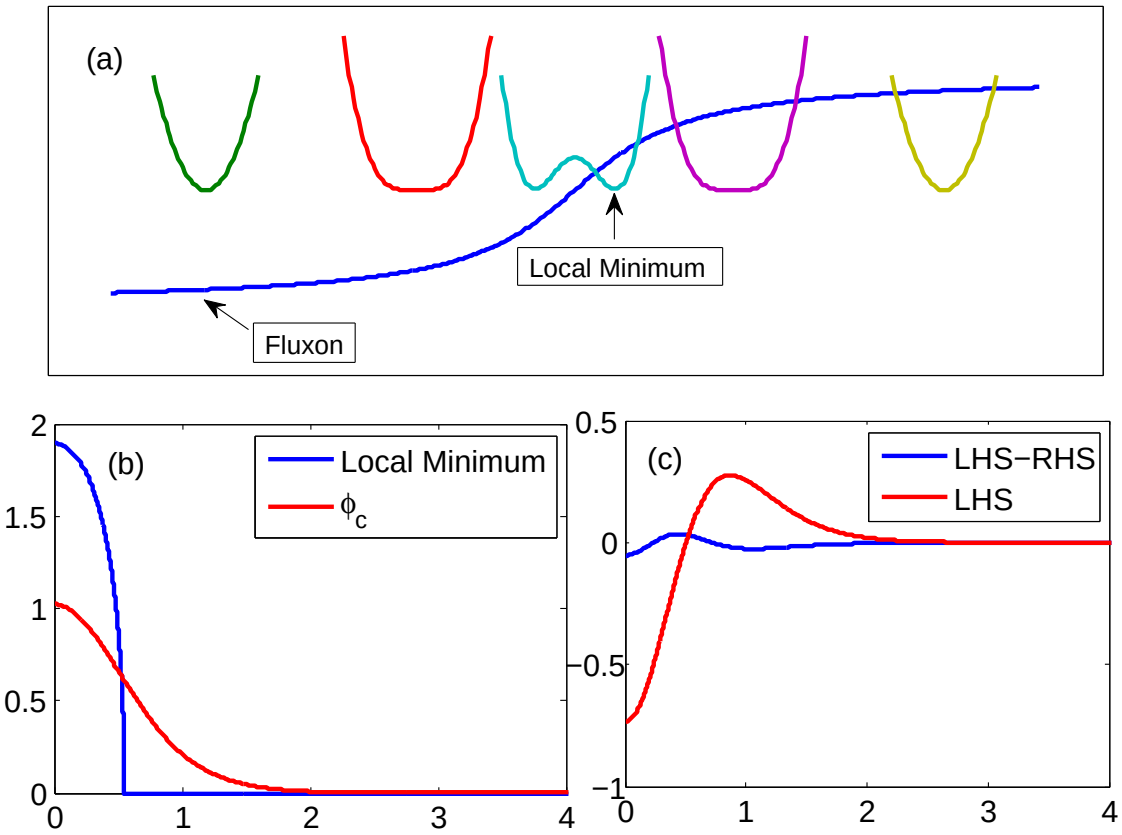


Figure 4.6: (a) Profile of the fluxon solution and the potential at different point; around $z \sim 0$, the potential is bistable; (b) Local minimum of the potential and $\phi_c$ given by variational method for $\beta = 2, \alpha = 0.2$; (c) $\phi_c$ should be a solution of equation $\alpha\phi_c'' = \phi_c + \beta\cos\chi\sin\phi_c$. Red line is LHS obtained $\phi_c$ got via variation, the blue curve is the difference between LHS and RHS. It can be seen that the variational method gives a good approximation.

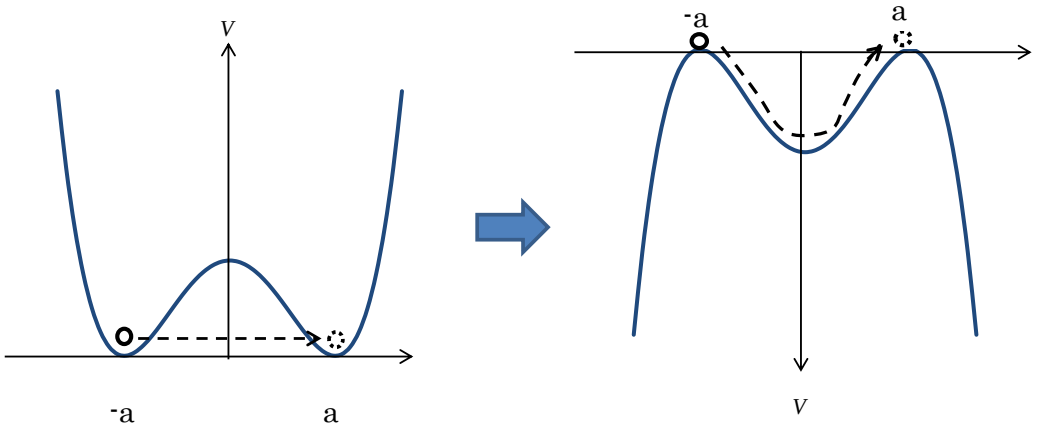


Figure 4.7: The instanton method. (a) A particle moving under potential $V$. (b) The inverse potential $-V$. The amplitude of transimission between the double well potential $V$ is given by the action of motion under the inverse potential $-V$.

This amplitude can be calculated using the instanton method: first, inverse the potential $V$ to $-V$, set the particle's energy $E$ to zero, and calculate the action $S_{cl}$ from $-a$ to $a$, then the amplitude is $\exp(-S_{Re}/\hbar)$. The Lagrangian after reversing the potential is $L_{Re}$ and the Hamiltonian is $H_{Re}$

$$H_{Re} = \frac{p^2}{2m} - V(x) = E = 0\,, \tag{4.33}$$

$$L_{Re} = \frac{p^2}{2m} + V(x) = 2V(x)\,. \tag{4.34}$$

The action is:

$$S_{Re} = \int dt L_{Re} = \int_{-a}^{a} \frac{dx}{\dot{x}} 2V(x)\,. \tag{4.35}$$

Due to the energy conservation:

$$\frac{1}{2}m\dot{x}^2 = E + V(x) = V(x)\,. \tag{4.36}$$

hence:

$$S_{Re} = \int dt L_{Re} = \int_{-a}^{a} \frac{dx}{\dot{x}} 2V(x) = \int_{-a}^{a} dx 2\sqrt{V(x)}\,. \tag{4.37}$$

which gives:

$$|T| = \exp\left\{-\frac{1}{\hbar}\int_{-a}^{a} dx\sqrt{2m(V-E)}\right\}\,. \tag{4.38}$$

Now get back to the original question. The Hamiltonian of the system is:

$$H_0 = (\frac{\Phi_0}{2\pi})^2 \frac{1}{L+M}\int dz\{\frac{\dot{\phi}^2}{\omega_D^2} + V(\phi,z)\}\,, \tag{4.39}$$

$$V(\phi,z) = \alpha(\phi')^2 + (1-\beta\cos\chi(z,t))\,\phi^2 - \frac{\beta}{12}\cos\chi\phi^4\,. \tag{4.40}$$

where $\int dz V(\phi)$ has two minimals $\pm\phi_c(z)$. There is a constraint on $phi_c$ that is useful in the following calculation. Assume $\phi(z) = k\phi_c(z)$, as a function of $k$, $\int dz V(\phi)$ should has two minimum at $k = \pm 1$ since $\phi_c$ minimize $\int dz V(\phi)$.

$$\begin{aligned}\int dz V(\phi) &= (\frac{\Phi_0}{2\pi})^2 \frac{1}{L+M}\int dz\left\{\left[\alpha(\phi_c')^2 + (1-\beta cos\chi(z,t))\,\phi_c^2\right]k^2 + \left[-\frac{\beta}{12}cos\chi\phi^4\right]k^4\right\} \\ &= Ak^2 + Bk^4\,.\end{aligned} \tag{4.41}$$

where

$$A = (\frac{\Phi_0}{2\pi})^2 \frac{1}{L+M}\int dz\left[\alpha(\phi_c')^2 + (1-\beta cos\chi(z,t))\,\phi_c^2\right]\,, \tag{4.42}$$

$$B = (\frac{\Phi_0}{2\pi})^2 \frac{1}{L+M}\int dz\left[-\frac{\beta}{12}cos\chi\phi_c^4\right]\,. \tag{4.43}$$

$k = \pm 1$ is minimum gives:

$$A + 2B = 0\,, \quad B > 0\,. \tag{4.44}$$

Now calculate the transmission amplitude, flip the potential and shift the energy

such that the energy at $\phi = \phi_c$ is zero. The new Hamiltonian and Lagrangian are:

$$H_F = (\frac{\Phi_0}{2\pi})^2 \frac{1}{L+M} \int dz \left[ \frac{\dot{\phi}^2}{\omega_D^2} - V(\phi, z) \right] + \delta E = 0 \,, \tag{4.45}$$

$$L_F = (\frac{\Phi_0}{2\pi})^2 \frac{1}{L+M} \int dz \left[ \frac{\dot{\phi}^2}{\omega_D^2} + V(\phi, z) \right] - \delta E \tag{4.46}$$

$$= (\frac{\Phi_0}{2\pi})^2 \frac{2}{L+M} \int dz \frac{\dot{\phi}^2}{\omega_D^2} \,, \tag{4.47}$$

$$S_F = \int dt L_F = (\frac{\Phi_0}{2\pi})^2 \frac{2}{L+M} \int dz dt \frac{\dot{\phi}^2}{\omega_D^2} \,. \tag{4.48}$$

Assume during the evolution the shape of the phase configuration is kept but with smaller amplitude, ie, $\phi(z,t) = f(t)\phi_c(z)$, where $f(t)$ involves from $-1$ to 1. Due to the energy conservation:

$$C\dot{f}^2 - Af^2 - Bf^4 = -A - B = B \,. \tag{4.49}$$

where

$$C = (\frac{\Phi_0}{2\pi})^2 \frac{1}{L+M} \int dz \frac{\phi_c^2}{\omega_D^2} \,. \tag{4.50}$$

Hence:

$$\dot{f} = \sqrt{\frac{B}{C}} (1 - f^2) \,. \tag{4.51}$$

and

$$S_F = 2C \int dt \dot{f}^2 = 2C \int_{-1}^{1} \frac{df}{\dot{f}} \dot{f}^2 \tag{4.52}$$

$$= 2C \int_{-1}^{1} df \dot{f} = 2C \int_{-1}^{1} df \sqrt{\frac{B}{C}} (1 - f^2) \tag{4.53}$$

$$= \frac{8}{3} \sqrt{BC} \,. \tag{4.54}$$

Here $A$, $B$, $C$ are all integrable and gives the result Eq. 4.32. After including the noise, the Hamiltonian for the qubit system is:

$$H = \frac{\epsilon_0}{2}\hat{\sigma}_z + \Delta\hat{\sigma}_x + f(t)\hat{\sigma}_z\,. \tag{4.55}$$

where $f(t) = \int dz\phi_c(z)F(z,t)$. It's easier to calculate the decoherence rate by diagonalize the qubit Hamiltonian,ie, rotate the system around y-axis by $\theta = \tan^{-1}[(E-\epsilon_0)/2\Delta]$, where $E = \sqrt{4\Delta^2+\epsilon_0^2}$:

$$H^N = U^\dagger H U = \frac{E}{2}\hat{\tau}_z + f_x(t)\hat{\tau}_x + f_z(t)\hat{\tau}_z, \quad U = \begin{pmatrix} \cos\theta & -\sin\theta \\ \sin\theta & \cos\theta \end{pmatrix}.$$

where $f_x(t) = \sin(2\theta)f(t)$ and $f_z(t) = \cos(2\theta)f(t)$. It's easy to calculate the transition and dephasing rate in this basis.

$$\Gamma^N_{01(10)} = \sin^2(2\theta)\frac{S_{ff}(-E/\hbar)}{\hbar^2}\,, \tag{4.56}$$

$$\gamma^N_{01} = \frac{\Gamma^N_{01}+\Gamma^N_{10}}{2} + \cos^2(2\theta)\frac{S_{ff}(0)}{\hbar^2}\,. \tag{4.57}$$

Here the spectral density $S_{ff}(\omega) = \int dz|\phi_c|^2 S_{FF}(\omega)$, is closely related to the space structure of the collective mode $\phi_c(z)$.

## 4.4 Moving Fluxons

In the above discussion, it's assumed that the fluxon evolves adiabatically and can be treated as static. But in the application, it's hoped the fluxon could move fast enough to accomplish the information transfer within the coherence time; in another aspect, the velocity should still be small in the sense that the separation between common mode and differential mode is clear and safe. Assume the fluxon's velocity $v$ satisfies the restriction. This finite velocity changed the noise felt by the qubit system and hence changed the dephasing rate. We will show in the following that

due to the independence of the noise at different space point, the velocity actually suppresses the dephasing rate. For simplicity of the statement, $\phi_c(z)$ is taken to be a rectangular with width $a$ and height $\phi_m$ around $z = vt$. Since the localized character of the profile is the essential point for the result, the detail of the collective mode gives only a prefactor.

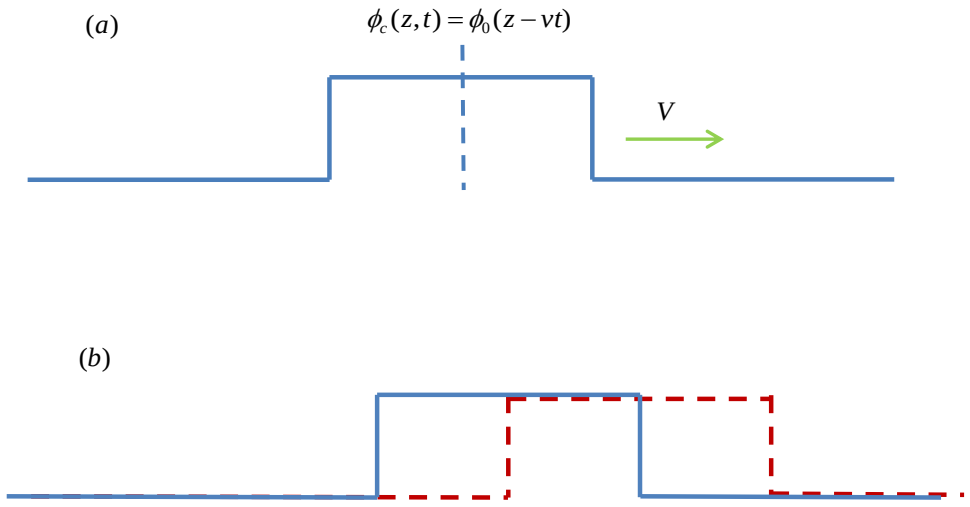


Figure 4.8: (a) Moving fluxons. (b) when the fluxon moves, only the overlap part contributes to the decoherence because the noise are independent at difference positions.

The quantity to be calculated is fidelity of the system, $\mathcal{F}(t) = \langle \exp[-i\int_0^t dt_1 \delta\epsilon(t_1)/\hbar]\rangle$, the fluctuation of the energy is $\delta\epsilon(\tau) = \int dz \phi_c(z,t) F(z,t)$. It's easy to find that:

$$\begin{aligned} -\ln \mathcal{F} &= \int_0^t dt_1 dt_2 \frac{\langle \delta\epsilon(t_1)\delta\epsilon(t_2)\rangle}{2\hbar^2} \\ &= \frac{2\phi_m^2}{\hbar^2}\Big[vT\int \frac{d\omega}{2\pi} S_{FF}(\omega)\frac{\sin^2(\omega\tau/2)}{\omega^2} - v\tau\int \frac{d\omega}{2\pi} S_{FF}(\omega) \\ &\quad * \frac{\frac{2}{\omega\tau}\sin(\omega\tau/2)\cos(\omega\tau/2) - \cos^2(\omega\tau/2)}{\omega^2}\Big]. \end{aligned} \tag{4.58}$$

where $T = Max\{t, a/v\}$, $\tau = Min\{t, a/v\}$. Meanwhile, the result for the static fluxon case ($v = 0, vT = a, \tau = t$) is :

$$-\ln \mathcal{F} = \frac{2\phi_m^2 a}{\hbar^2} \int \frac{d\omega}{2\pi} S_{FF}(\omega) \frac{\sin^2(\omega t/2)}{\omega^2} \,. \tag{4.59}$$

For low-frequency noise, Eq. (4.58) is smaller than Eq. (4.59), ie, the dephasing rate is suppressed when the fluxon has a finite velocity. This effect is essential for large time, when the low-frequency part of the noise accumulates and contributes most to dephasing. When $t \gg a/v$, the low-frequency noise accumulate linearly with time in moving fluxon, but quadratically with time in static fluxon. Here are two examples to see the effect explicitly.

First consider a noise spectrum mainly in low-frequency $\omega \leq \omega_D$, but still finite in zero frequency: $S_{FF}(\omega) = S_f \frac{\omega_D^2}{\omega^2 + \omega_D^2}$, the results at large time are:

$$-\ln \mathcal{F} \sim \frac{a\phi_m^2 S_f \cdot t}{2\hbar^2} \left[ \frac{\exp(-\omega_D \tau) - 1 + \omega_D \tau}{\omega_D \tau} \right] , \quad moving\, case \,, \tag{4.60}$$

$$-\ln \mathcal{F} \sim \frac{a\phi_m^2 S_f \cdot t}{2\hbar^2} \left[ \frac{\exp(-\omega_D t) - 1 + \omega_D t}{\omega_D t} \right] , \quad static\, case \,. \tag{4.61}$$

The factor within the square bracket increases with $t$ and approaches 1 in the static fluxon, but keeps constant in moving case. If the velocity is large that $v/a \gg \omega_D$, the dephasing time in moving fluxon case is enlarged by a factor $v/\omega_D a$ comparing the that of the static case.

The noise spectrum mentioned above is a toy model and it's known that $1/f$ noise is the main source of dephasing in flux qubit. Assume the noise has the following spectrum $S_{FF}(\omega) = S_f/\omega$, the lower cutoff is $\omega_c$, the fidelity at large time is:

$$-\ln \mathcal{F} \sim \frac{a\phi_m^2 S_f}{\pi\hbar^2} \left[ t\frac{a}{v}(3 - 2\gamma - 2\ln(\omega_c \frac{a}{v}) \right] , \quad moving\, case \,, \tag{4.62}$$

$$-\ln \mathcal{F} \sim \frac{a\phi_m^2 S_f}{\pi\hbar^2} \left[ t^2(3 - 2\gamma - 2\ln(\omega_c t) \right] , \quad static\, case \,. \tag{4.63}$$

The fidelity is much larger for moving fluxon carrier. For real profile of $\phi_c$, the result

should be a little bit different, but the qualitative picture stays the same.

**APPENDIX**

This subsection includes the detail of the calculation of Eq.4.58

$$\begin{aligned}
-\ln\mathcal{F} &= \int_0^t dt_1 dt_2 \frac{\langle\delta\epsilon(t_1)\delta\epsilon(t_2)\rangle}{2\hbar^2} \\
&= \frac{1}{2\hbar^2}\int_0^t dt_1 dt_2 dz_1 dz_2 \langle F(z_1,t_1)F(z_2,t_2)\rangle \phi_c(z_1,t_1)\phi_c(z_2,t_2) \\
&= \frac{1}{2\hbar^2}\int_0^t dt_1 dt_2 \langle F(t_1-t_2)F(0)\rangle \int dz \phi_c(z-vt_1)\phi_c(z-vt_2) \\
&= \frac{1}{2\hbar^2}\int \frac{d\omega}{2\pi} S_{FF}(\omega) \int_0^t dt_1 dt_2 e^{-i\omega(t_1-t_2)} \int dz \phi_c(z-vt_1)\phi_c(z-vt_2) \\
&= \frac{2\phi_m^2}{\hbar^2}\Big[vT\int\frac{d\omega}{2\pi}S_{FF}(\omega)\frac{\sin^2(\omega\tau/2)}{\omega^2} - v\tau\int\frac{d\omega}{2\pi}S_{FF}(\omega) \\
&\quad * \frac{\frac{2}{\omega\tau}\sin(\omega\tau/2)\cos(\omega\tau/2) - \cos^2(\omega\tau/2)}{\omega^2}\Big]. \qquad (4.64)
\end{aligned}$$

where the integral over $\phi_c$ is given below:

$$\begin{aligned}
&\int_0^t dt_1 dt_2 e^{-i\omega(t_1-t_2)} \int dz \phi_c(z-vt_1)\phi_c(z-vt_2) \\
&= \phi_m^2 \int_0^t dt_1 dt_2 e^{-i\omega(t_1-t_2)}(a - v|t_1-t_2|)\theta(a/v - |t_1-t_2|) \\
&= 2\phi_m^2\left\{\int_0^t dt_1 \int_0^{t_1} dt_2 \cos(\omega(t_1-t_2))(a-v|t_1-t_2|)\theta(a/v-|t_1-t_2|)\right\} \\
&= 2\phi_m^2\left\{\int_0^t dt_1 \int_0^{t_1} dt_2 \cos(\omega t_2)(a-vt_2)\theta(a/v-t_2)\right\}. \qquad (4.65)
\end{aligned}$$

When $t < a/v$, Eq.4.65 equals:

$$\begin{aligned}
&2\phi_m^2\left\{\int_0^t dt_1 \int_0^{t_1} dt_2 \cos(\omega t_2)(a-vt_2)\right\} \\
&= 2\phi_m^2 \frac{a+vt+(vt-a)\cos(\omega t) - (2v/\omega)\sin(\omega t)}{\omega^2} \\
&= 2\phi_m^2\left\{a\frac{1-\cos(\omega t)}{\omega^2} + vt\frac{1+\cos(\omega t) - 2\sin(\omega t)/(\omega t)}{\omega^2}\right\} \\
&= 4\phi_m^2\left\{a\frac{\sin^2(\omega t/2)}{\omega^2} + vt\frac{\cos^2(\omega t/2) - 2\sin(\omega t/2)\cos(\omega t/2)/(\omega t)}{\omega^2}\right\}. \qquad (4.66)
\end{aligned}$$

When $t > a/v$, Eq.4.65 equals:

$$
\begin{aligned}
& 2\phi_m^2 \left\{ \int_0^{a/v} dt_1 \int_0^{t_1} dt_2 \cos(\omega t_2)(a - vt_2) + \int_{a/v}^{t} dt_1 \int_0^{a/v} dt_2 \cos(\omega t_2)(a - vt_2) \right\} \\
= \; & 2\phi_m^2 \left\{ \frac{2a - (2v/\omega)\sin(\omega a/v)}{\omega^2} + \left(t - \frac{a}{v}\right) \frac{v - v\cos(\omega a/v)}{\omega^2} \right\} \\
= \; & 2\phi_m^2 \left\{ \frac{a + vt - (2v/\omega)\sin(\omega a/v) + (a - vt)\cos(\omega a/v)}{\omega^2} \right\} \\
= \; & 2\phi_m^2 \left\{ vt \frac{1 - \cos(\omega a/v)}{\omega^2} + a \frac{1 + \cos(\omega a/v) - \frac{2v}{\omega a}\sin(\omega a/v)}{\omega^2} \right\} \\
= \; & 4\phi_m^2 \left\{ vt \frac{\sin^2(\omega a/2v)}{\omega^2} + a \frac{\cos^2(\omega a/2v) - \frac{2v}{\omega a}\sin(\omega a/2v)\cos(\omega a/2v)}{\omega^2} \right\} . \qquad (4.67)
\end{aligned}
$$

So generally the result is:

$$
\begin{aligned}
-\ln \mathcal{F} \;=\; & \frac{2\phi_m^2}{\hbar^2} \Big[ vT \int \frac{d\omega}{2\pi} S_{FF}(\omega) \frac{\sin^2(\omega\tau/2)}{\omega^2} - v\tau \int \frac{d\omega}{2\pi} S_{FF}(\omega) \\
& * \frac{\frac{2}{\omega\tau}\sin(\omega\tau/2)\cos(\omega\tau/2) - \cos^2(\omega\tau/2)}{\omega^2} \Big] . \qquad (4.68)
\end{aligned}
$$

where $T = Max\{t, a/v\}$, $\tau = Min\{t, a/v\}$.

# Chapter 5

# Decoherence Induced Deformation of the Ground State in Adiabatic Quantum Computation

Adiabatic quantum computation (AQC) [31], either in its universal form [36, 37], or in the form of adiabatic quantum optimization [81], or quantum simulations [82], presents a viable alternative to gate-model quantum computation (GMQC). Although a part of the original motivation for introduction of the AQC [35] was the promise of the increased stability against decoherence due to the energy gap between the ground and excited states, the question of the role of decoherence in AQC remains an open one. This uncertainty makes it important to quantify more precisely the decoherence properties of AQC. A crucial step towards this would be to define a quantitative characteristic of the decoherence strength in AQC, that plays a role similar to the decoherence time for GMQC. However, in the case of AQC, decoherence has qualitatively different, static effect on the qubits, not limiting the operation time of an algorithm [83]. Here we propose the ground state fidelity, defined as the distance between the open and closed system reduced density matrices normalized to the Boltzmann ground state probability, as a quantitative

measure of decoherence-induced deformation of the ground state in AQC, analogous to the decoherence time for GMQC. We calculate the fidelity perturbatively at finite temperatures and express it through the same environmental noise correlators that determine the decoherence times in GMQC. We discuss the relation between fidelity and the relaxation and dephasing times of the qubits, and its projected scaling properties with the number of qubits.

## 5.1 Ground Sate Fidelity

In AQC, adiabatic evolution of the ground state of a qubit system realizes the solution of a computational problem represented by an appropriately designed Hamiltonian, which is typically written as

$$H_S = A(s)H_U + B(s)H_P, \tag{5.1}$$

where $s = t/t_f$ with $t_f$ being the total evolution time. At $s = 0$, one has $A(0) = 1$, $B(0) = 0$, and the system is initialized in the ground state of the Hamiltonian $H_U$, which usually consists of the uniform superposition of all computational basis states. The energy scales $A(s)$ and $B(s)$ are varied monotonically so that at $s = 1$, $A(1) = 0$ and $B(1) = 1$. If the evolution is slow enough, an isolated qubit system stays in the ground state with high fidelity throughout the evolution, and at $s = 1$ reaches the ground state of $H_P$, which provides a solution to a computational problem.

If the qubit system is weakly coupled to a dissipative environment, two effects are expected. First, the low-frequency part of the environmental noise moves the system energy levels relative to each other. This results in a dephasing of the energy eigenstates that eventually suppresses all off-diagonal elements of the qubit density matrix in the energy basis. However, since the population of the ground state is the only important part of the computation and the relative phases of the energy eigenstates do not carry any information, this does not affect AQC. Second effect of

the coupling to the environment is that it induces the thermal transitions between the qubit energy levels pushing the qubit system towards thermal equilibrium at a temperature $T$. For slow evolution, the instantaneous probability to be in the ground state is given approximately by the Boltzmann distribution, and so the qubit system loses some of the ground state probability due to thermal occupation of the excited states. Such a thermal loss of probability can be compensated by multiple iterations of an AQC algorithm as long as it does not scale exponentially with the size of the system, i.e. as long as the number of excited states within roughly the energy $k_BT$ above the ground state does not grow exponentially.

The preceding arguments provide an intuitive explanation for the predicted robustness of AQC against local environmental noise in the limit of weak coupling [34, 83, 88, 87, 86, 85, 84, 33]. When the strength of the coupling to the environment is increased without changing either the Hamiltonian or the temperature, the qubit Boltzmann distribution is still not directly affected. However, it is known that the decoherence time of the qubits decreases with increased coupling, and strong coupling to the environment eventually makes the qubits completely incoherent, rendering them useless for quantum computation. In GMQC, qubit decoherence leads to computation errors which, without error correction, completely destroy the computation process. This is why the qubits' quality factor, which is the ratio of the decoherence time and the gate operation time, provides a good measure of the qubit performance in GMQC. It is, however, unclear how an increase in coupling to the environment, or equivalently decrease in qubit quality factor, affects AQC.

In this section, we look closely at what happens to the eigenstates of the qubit system in AQC when coupling to the environment is non-negligible. To ensure consistent notation throughout this chapter, symbols with (without) "$\sim$" denote quantities related to the coupled (uncoupled) qubit system and environment. We use letters $m, n$ to enumerate the eigenstates and eigenvalues of the qubits (e.g., $|n\rangle$, $E_n$), letters $\nu, \mu$ to enumerate the eigenstates and eigenvalues of the environmental degrees of freedom, and letters $a, b$ to enumerate the eigenstates and eigenvalues of

the *total* system (qubits+environment). The total Hamiltonian is $\widetilde{H} = H_S + H_B + H_I$, where $H_B$ and $H_I$ are the environment and interaction Hamiltonians, respectively. In the absence of coupling, $H_I = 0$, and the eigenstates of the total system are $|a\rangle = |n\rangle \otimes |\nu\rangle$ with eigenvalues $E_a = E_n + E_\nu$. When $H_I \neq 0$, the new eigenstates are $|\widetilde{a}\rangle$, which typically are entangled superpositions of the unperturbed states $|a\rangle$. For weak coupling, $|\widetilde{a}\rangle$ is very close to $|a\rangle$ and the effect of the environment is thermalization of the qubit system. Once the environment is averaged out, the equilibrium of the total system gives the Boltzmann distribution for the qubits:

$$P_n = \sum_\nu \frac{e^{-(E_n+E_\nu)/T}}{Z_S Z_B} = \frac{e^{-E_n/T}}{Z_S}, \tag{5.2}$$

where $Z_S = \sum_n e^{-E_n/T}$ and $Z_B = \sum_\nu e^{-E_\nu/T}$ are the partition functions of the qubit system and the environment.

As the coupling increases, the deviation of $|\widetilde{a}\rangle$ from $|a\rangle$ grows. In equilibrium, the density matrix of the total system still has the Boltzmann form $\widetilde{\rho}_{SB} = \sum_a \widetilde{P}_a |\widetilde{a}\rangle\langle\widetilde{a}|$, where $\widetilde{P}_a = e^{-\widetilde{E}_a/T}/\widetilde{Z}_{SB}$, with $\widetilde{Z}_{SB} = \sum_a e^{-\widetilde{E}_a/T}$ being the partition function of the total system. However, the reduced density matrix $\widetilde{\rho}_S = Tr_B[\widetilde{\rho}_{SB}]$ of the qubit system alone is no longer given by the Boltzmann distribution. The deviation from the Boltzmann form provides a good qualitative measure of how strongly the eigenstates $|\widetilde{a}\rangle$ are deformed in comparison to the unperturbed states.

To be consistent with the notation in the main text, we use symbols with (without) "$\sim$" to denote quantities related to the coupled (uncoupled) qubit system and environment. We also use $m, n, k$ to enumerate qubit system's eigenstates and eigenvalues (e.g., $|n\rangle$, $E_n$). Similarly, the letters $\nu, \mu$ correspond to environment eigenstates and eigenvalues, and letters $a, b$ correspond to *total* system (qubits+environment) eigenstates and eigenvalues. The total Hamiltonian is written as $\widetilde{H} = H_S + H_B + H_I$, which includes the qubit system Hamiltonian

$$H_S = \sum_n E_n |n\rangle\langle n| \,, \tag{5.3}$$

and interaction Hamiltonian

$$H_I = \sum_{\alpha,j} q_j^\alpha \sigma_j^\alpha, \tag{5.4}$$

where $\sigma_j^\alpha$ are the Pauli matrices, $\alpha = x, y, z$, and $q_j^\alpha$ are the noise operators dependent on the heat bath variables coupled to the $j$-th qubit. The bath Hamiltonian $H_B$ is not specified, but the bath is assumed to be in thermal equilibrium at temperature $T$. For the purpose of perturbative calculations of fidelity in this work, the properties of $q_j^\alpha$ are completely characterized by its spectral density

$$S_j^\alpha(\omega) = \int_{-\infty}^{\infty} dt e^{i\omega t} \langle q_j^\alpha(t) q_j^\alpha(0) \rangle \tag{5.5}$$

where $q_j^\alpha(t) = e^{iH_B t} q_j^\alpha e^{-iH_B t}$, and vanishing average $\langle q_j^\alpha(t) \rangle \equiv 0$.

Even if the dissipative environment does not excite the system out of its ground state, the non-vanishing $H_I$ term changes the structure of the ground state wavefunction in comparison with the unperturbed ground state of the Hamiltonian $H_S$. The magnitude of this change can be characterized quantitatively by fidelity. For two general density matrices $\rho$ and $\rho'$ acting on the same Hilbert space, the fidelity (sometimes called Uhlmann's fidelity) is given by

$$\mathcal{F}(\rho, \rho') = Tr \sqrt{\sqrt{\rho} \rho' \sqrt{\rho}}\,. \tag{5.6}$$

If one of the states is a pure state, e.g., $\rho = |\psi\rangle\langle\psi|$, then we can use the property $\sqrt{\rho} = \rho = \rho^2$ to write

$$\begin{aligned} \mathcal{F}(\rho, \rho') &= Tr \sqrt{|\psi\rangle\langle\psi|\rho'|\psi\rangle\langle\psi|} = \sqrt{\langle\psi|\rho'|\psi\rangle} \\ &= \{\mathrm{Tr}[\rho\rho']\}^{1/2}. \end{aligned} \tag{5.7}$$

Let $|a\rangle$ and $|\widetilde{a}\rangle$ denote the unperturbed and perturbed states of the total system, respectively. The total density matrix of the combined system is $\rho_{SB} = \sum_a \widetilde{P}_a |\widetilde{a}\rangle\langle\widetilde{a}|$, where $\widetilde{P}_a$ is the probability of finding the total system in the state $|\widetilde{a}\rangle$. We define the

reduced density matrix as $\widetilde{\rho}_S = Tr_B[\rho_{SB}]$, where the partial trace is taken only over the environmental degrees of freedom. We also define the pure state density matrix $\rho_0 = |0\rangle\langle 0|$, where $|0\rangle$ is the ground state of the (isolated) qubit system Hamiltonian $H_S$. Then, we express the fidelity $\mathcal{F}$ between $\rho_0 = |0\rangle\langle 0|$ and $\widetilde{\rho}_S$ as

$$\mathcal{F}(\rho_0, \widetilde{\rho}_S)^2 = \langle 0|\widetilde{\rho}_S|0\rangle = \widetilde{P}_0\,, \tag{5.8}$$

where $\widetilde{P}_0$ is the probability of finding the open system in state $|0\rangle$. In equilibrium, this probability is determined by the thermal distribution over the system eigenstates and also by the effects of the non-vanishing coupling to the environment. To separate these two contributions, we define the ground state fidelity as

$$F \equiv P_0^{-1/2}\mathcal{F}(\rho_0, \widetilde{\rho}_S) = \sqrt{\frac{\widetilde{P}_0}{P_0}}, \tag{5.9}$$

where $P_0 = e^{-E_0/T}/Z$ is the Boltzmann probability of the ground state $|0\rangle$ with partition function $Z = \sum_n e^{-E_n/T}$ in the case of an isolated qubit system.

Quantitatively, we define the ground state fidelity as the Uhlmann fidelity [89] between the reduced density matrix $\widetilde{\rho}_S$ and the "ideal" ground state density matrix $\rho_0 = |0\rangle\langle 0|$, normalized to the Boltzmann ground state probability $P_0$:

$$F = P_0^{-1/2} Tr\sqrt{\sqrt{\rho_0}\,\widetilde{\rho}_S\sqrt{\rho_0}} = \sqrt{\widetilde{P}_0/P_0}\,, \tag{5.10}$$

where $\widetilde{P}_0 = \langle 0|\widetilde{\rho}_S|0\rangle$ is the equilibrium probability for the qubits to be in the ideal ground state when coupled to the environment. In the weak-coupling limit, no deformation of the eigenstates is expected. Then $\widetilde{P}_0 = P_0$, and Eq. (5.10) gives $F = 1$. This shows that Eq. (5.10) correctly separates the effect of the quantum deformation of the ground state, which can be viewed as the result of virtual transitions to the excited states, from the thermal loss of probability. Qualitatively, the effect of the virtual transitions, expressed in $F$, is different from that of the thermal transitions

in two important aspects. First, it persists even at $T = 0$, when all the thermal transitions are suppressed. Second, it depends on the strength of coupling to environment (or decoherence time of the qubits), while thermal equilibrium probabilities only depend on the energy eigenvalues and temperature. Nevertheless, similarly to thermal transitions, the virtual transitions reduce the occupation probability of the ground state by transferring it to the higher-energy states.

## 5.2 Perturbation Calculation of Ground State Fidelity

In this section, we calculate the fidelity (5.10) perturbatively and relate it to measurable parameters of the qubit system and environment. As appropriate for AQC, we assume that the coupling $H_I$ is weak. This allows us to employ the perturbation theory in $H_I$ around the non-interacting state of the qubit system and the environment with both of them in equilibrium at the same temperature $T$, i.e., density matrices $\rho_S = \sum_n P_n|n\rangle\langle n|$ and $\rho_B = \sum_\nu P_\nu|\nu\rangle\langle\nu|$, where $P_n$ and $P_\nu$ are the Boltzmann probabilities. The reduction of the ground state probability due to finite $H_I$ is caused by a change $\delta P_0$ in the equilibrium probability $P_0$ as a result of renormalization of the energy eigenvalues (Lamb shifts), and probability transfers into and out of the ground state due to renormalization of the wavefunctions. The probability $\widetilde{P}_0$ that defines the fidelity (5.10) can be expressed as

$$\widetilde{P}_0 = Tr_{B,S}\Big[|0\rangle\langle 0| \sum_a \widetilde{P}_a|\widetilde{a}\rangle\langle\widetilde{a}|\Big]. \tag{5.11}$$

Introducing interaction-induced corrections to the equilibrium probabilities $\widetilde{P}_a = P_a + \delta P_a$, where $P_a = P_n P_\nu$, and wavefunctions: $|\widetilde{a}(n,\nu)\rangle = |n\rangle\otimes|\nu\rangle + |\delta\widetilde{a}(n,\nu)\rangle$, we

can rewrite this expression to the lowest non-vanishing order in $H_I$ as

$$\widetilde{P}_0 = \delta P_0 + \sum_n P_n Tr_{B,S}\left[|0\rangle\langle 0| \otimes \rho_B \cdot |\widetilde{a}(n,\nu)\rangle\langle\widetilde{a}(n,\nu)|\right] . \tag{5.12}$$

Using the relation $|0\rangle\langle 0| = 1 - \sum_{m\neq 0} |m\rangle\langle m|$ to transform the $n = 0$ term in Eq. (5.12) we obtain

$$\widetilde{P}_0 = P_0 + \delta P_0 - \sum_{n\neq 0} \left(\Gamma_{0n} P_0 - \Gamma_{n0} P_n\right) , \tag{5.13}$$

where

$$\Gamma_{mn} \equiv \langle n| Tr_B[|\delta\widetilde{a}(m,\nu)\rangle\langle\delta\widetilde{a}(m,\nu)|\rho_B]|n\rangle .$$

The terms proportional to $\Gamma$ in Eq. (5.13) describe the reduction of the ground state probability as a result of renormalization of the qubit system wavefunctions by their interaction with the environment.

Next, we calculate $\delta P_0$ and $\Gamma_{mn}$. Quite generally, the interaction Hamiltonian $H_I$ is

$$H_I = \sum_{j,\alpha} q_j^\alpha \sigma_j^\alpha , \tag{5.14}$$

where $\sigma_j^\alpha$ are the Pauli matrices for the $j$th qubit, $\alpha = x, y, z$, and $q_j^\alpha$ are the corresponding operators of the noise generated by the environment. As usual, the averages of the noise operators vanish, $\langle q_j^\alpha\rangle = 0$. Then, in the weak coupling regime, the effect of environment is fully characterized by the noise spectral densities:

$$S_j^\alpha(\omega) = \int dt\ e^{i\omega t}\langle q_j^\alpha(t) q_j^\alpha(0)\rangle , \tag{5.15}$$

where $\langle ...\rangle = Tr_B\{\rho_B ...\}$ is the average over the environmental degrees of freedom. For simplicity, we limit our discussion to the most typical case when the noises with different $\alpha$ or $j$ are uncorrelated.

In the situation relevant to quantum computation, the coupling $H_I$ is weak and

can be treated by perturbation theory around the non-interacting state of the qubit system and environment. In the context of AQC, one can also assume that both the qubits and environment are in equilibrium at the same temperature $T$. These are characterized by the density matrices $\rho_S = \sum_n P_n|n\rangle\langle n|$ and $\rho_B = \sum_\nu P_\nu|\nu\rangle\langle\nu|$ without the interaction, while the total interacting system has the density matrix $\widetilde{\rho}_{SB} = \sum_a \widetilde{P}_a|\widetilde{a}\rangle\langle\widetilde{a}|$, where $\widetilde{P}_a$, $P_n$, and $P_\nu$ are the Boltzmann probabilities. The probability $\widetilde{P}_n$ of finding the qubit system in the state $|n\rangle$ in the presence of interaction can be written as

$$\widetilde{P}_n = Tr_{B,S}[|n\rangle\langle n|\widetilde{\rho}_{SB}]\,. \tag{5.16}$$

The interaction $H_I$ creates corrections to the equilibrium probabilities $\widetilde{P}_a = P_a + \delta P_a$, where $P_a = P_n P_\nu$, and to the wavefunctions: $|\widetilde{a}(n,\nu)\rangle = |a(n,\nu)\rangle + |\delta\widetilde{a}(n,\nu)\rangle$, where $|a(n,\nu)\rangle = |n\rangle\otimes|\nu\rangle$. In the lowest non-vanishing order in $H_I$, one can separate these corrections in the total density matrix of the system:

$$\widetilde{\rho}_{SB} = \sum_a [\delta P_a|a\rangle\langle a| + P_a|\widetilde{a}\rangle\langle\widetilde{a}|]\,. \tag{5.17}$$

This expression reduces Eq. (5.16) for the probability $\widetilde{P}_n$ to:

$$\widetilde{P}_n = \delta P_n + \sum_m P_m Tr_{B,S}\big[|n\rangle\langle n|\otimes\rho_B\cdot|\widetilde{a}(m,\nu)\rangle\langle\widetilde{a}(m,\nu)|\big]\,. \tag{5.18}$$

Using the relation $|n\rangle\langle n| = 1 - \sum_{k\neq 0}|k\rangle\langle k|$ to transform the $n = m$ term in Eq. (5.18), we obtain

$$\widetilde{P}_n = P_n + \delta P_n - \sum_{m\neq n}\left(\Gamma_{nm}P_n - \Gamma_{mn}P_m\right)\,, \tag{5.19}$$

where

$$\Gamma_{mn} \equiv \langle n|Tr_B[|\delta\widetilde{a}(m,\nu)\rangle\langle\delta\widetilde{a}(m,\nu)|\rho_B]|n\rangle\,. \tag{5.20}$$

The $\Gamma$-factors in (5.20) represent the fractions of the probability transfer from the

state $|m\rangle$ to the state $|n\rangle$ of the qubit system due renormalization of the qubit system wavefunctions by non-vanishing coupling to the environment. Equation (5.19) shows that, in addition to these transfers, environment-induced change of the probabilities $\widetilde{P}_n$ is also caused by the change in the equilibrium probability $\delta P_n$ due to renormalization of the energy eigenvalues (Lamb shift).

Next, we calculate these two contributions explicitly using the perturbation expansion. We start with $\delta P_n$. As shown below, the changes of the equilibrium occupation probabilities $\delta P_n$ of the qubits states are determined by the changes $\delta E_a$ of the total system energies *averaged* over the equilibrium state of the environment. Since $\langle q_j^\alpha \rangle = 0$, the linear corrections to the qubit system energies vanish, and the relevant energy changes are given by second-order perturbation:

$$\delta E_a = \sum_{b \neq a} \frac{|\langle a|H_I|b\rangle|^2}{E_a - E_b} = \sum_{\alpha,j,m,\mu}{}' \frac{|\sigma^\alpha_{j,nm}|^2 |\langle \nu|q_j^\alpha|\mu\rangle|^2}{\omega_{nm} + E_\nu - E_\mu}\,. \tag{5.21}$$

The prime sign over the sum excludes terms with zero denominator. The average change of the qubit system energy eigenvalues due to coupling to the environment, which determines $\delta P_n$, is therefore

$$\delta E_n = \sum_\nu P_\nu \delta E_{n,\nu} = \sum_{\alpha,j,m,\nu,\mu}{}' P_\nu \frac{|\sigma^\alpha_{j,nm}|^2 |\langle \nu|q_j^\alpha|\mu\rangle|^2}{\omega_{nm} + E_\nu - E_\mu}. \tag{5.22}$$

We express this result in terms of the noise spectral densities. In this calculation, we assume that the noises with different $\alpha$ and $j$ are uncorrelated. The standard spectral decomposition,

$$S_j^\alpha(\omega) = 2\pi \sum_{\nu,\mu} P_\nu |\langle \nu|q_j^\alpha|\mu\rangle|^2 \delta(\omega + E_\nu - E_\mu)\,, \tag{5.23}$$

transforms Eq. (5.22) into

$$\delta E_n = \sum_{j,\alpha,m} \int \frac{d\omega}{2\pi} \frac{|\sigma^\alpha_{j,nm}|^2 S_j^\alpha(\omega)}{\omega_{nm} - \omega}\,. \tag{5.24}$$

Now, we relate the changes in the occupation probabilities of the qubit states to the energy changes of the total system. Expanding the Boltzmann probabilities, we get

$$\begin{aligned}\delta P_a &= -\beta\frac{e^{-\beta E_a}\delta E_a}{\sum_b e^{-\beta E_b}} + \beta\frac{e^{-\beta E_a}\sum_b e^{-\beta E_b}\delta E_b}{\left(\sum_b e^{-\beta E_b}\right)^2} \\ &= -\beta P_a \delta E_a + \beta P_a \sum_b P_b \delta E_b \\ &= \beta P_a \sum_b (P_b - \delta_{ab})\delta E_b \,. \end{aligned} \tag{5.25}$$

Using $P_a = P_n P_\nu$, $P_b = P_m P_\mu$, and $\delta_{ab} = \delta_{nm}\delta_{\nu\mu}$, we see that $\delta P_n$ is indeed determined by the energy shifts averaged over the environment:

$$\begin{aligned}\delta P_n &= \sum_\nu \delta P_a = \beta \sum_\nu P_n P_\nu \sum_{m,\mu} (P_m P_\mu - \delta_{nm}\delta_{\nu\mu})\delta E_{m,\mu} \\ &= \beta P_n \sum_{m,\mu} (P_m - \delta_{nm}) P_\mu \delta E_{m,\mu} \\ &= \beta P_n \sum_m (P_m - \delta_{nm})\delta E_m \,. \end{aligned} \tag{5.26}$$

Combining Eqs. (5.24) and (5.26), we obtain

$$\delta P_n = -\beta P_n \sum_{j,\alpha,m,k} (P_m - \delta_{mn})|\sigma^\alpha_{j,mk}|^2 \int \frac{d\omega}{2\pi}\frac{S^\alpha_j(\omega)}{\omega_{km}+\omega}. \tag{5.27}$$

Next, we calculate the probability transfer fractions $\Gamma_{mn}$ (5.20). It is convenient to view the relation between the states with and without interaction as arising from the adiabatic switching on of the interaction:

$$|\widetilde{a}\rangle = U|a\rangle \,, \tag{5.28}$$

where

$$U = \mathcal{T}\exp\left\{-i\int_{-\infty}^{0} dt e^{\lambda t} H_I(t)\right\}. \tag{5.29}$$

Here $\lambda$ is a small positive number which ensures an adiabatic increase of the coupling, and

$$\begin{aligned} H_I(t) &= e^{i(H_S+H_B)t} H_I e^{-i(H_S+H_B)t} \\ &= \sum_{\alpha,j,n,m} \sigma^\alpha_{j,nm} e^{i\omega_{nm}t} q^\alpha_j(t) |n\rangle\langle m| \end{aligned} \tag{5.30}$$

with $H_I$ given by Eq. (5.4).

Using Eq. (5.28) together with (5.29) limited to the lowest order in $H_I$ in Eq. (5.20), we obtain

$$\begin{aligned} &\Gamma_{mn} = Tr_B[\langle n|U|m\rangle \rho_B \langle m|U^\dagger|n\rangle] \\ &= \int_{-\infty}^{0} dt \int_{-\infty}^{0} dt' Tr_B[\langle n|e^{\lambda t} H_I(t)|m\rangle \rho_B \langle m|e^{\lambda t'} H_I(t')|n\rangle] \\ &= \int_{-\infty}^{0} dt \int_{-\infty}^{0} dt' \sum_{j,\alpha} |\sigma^\alpha_{j,nm}|^2 e^{\lambda(t+t')+i\omega_{nm}(t-t')} \langle q^\alpha_j(t') q^\alpha_j(t)\rangle. \end{aligned}$$

We combine this expression with Eq. (5.5) for spectral densities to get

$$\begin{aligned} \Gamma_{mn} &= \sum_{j,\alpha} |\sigma^\alpha_{j,nm}|^2 \int \frac{d\omega}{2\pi} S^\alpha_j(\omega) \\ &\quad \times \int_{-\infty}^{0} dt \int_{-\infty}^{0} dt' e^{\lambda(t+t')+i(\omega_{nm}+\omega)(t-t')} \\ &= \sum_{j,\alpha} |\sigma^\alpha_{j,nm}|^2 \int \frac{d\omega}{2\pi} \frac{S^\alpha_j(\omega)}{\lambda^2 + (\omega_{nm}+\omega)^2} \,. \end{aligned} \tag{5.31}$$

In the limit $\lambda \to 0$, this gives

$$\Gamma_{mn} = \sum_{j,\alpha} |\sigma^\alpha_{j,nm}|^2 \int \frac{d\omega}{2\pi} \frac{S^\alpha_j(\omega)}{(\omega_{nm}+\omega)^2} \,. \tag{5.32}$$

The final result is

$$\widetilde{P}_n = P_n - \beta P_n \sum_{j,\alpha,m,k} |\sigma^\alpha_{j,mk}|^2 \int \frac{d\omega}{2\pi} \frac{S^\alpha_j(\omega)(P_m - \delta_{mn})}{\omega_{km} + \omega}$$
$$- \sum_{j,\alpha,m\neq n} |\sigma^\alpha_{j,mn}|^2 \int \frac{d\omega}{2\pi} \frac{P_n S^\alpha_j(\omega) - P_m S^\alpha_j(-\omega)}{(\omega_{mn} + \omega)^2}. \tag{5.33}$$

This equation gives the normalized fidelity of the ground state $n = 0$ as

$$F = \sqrt{\frac{\widetilde{P}_0}{P_0}} = 1 - \beta \sum_{j,\alpha,n,m} |\sigma^\alpha_{j,nm}|^2 \int \frac{d\omega}{4\pi} \frac{S^\alpha_j(\omega)(P_n - \delta_{n0})}{\omega_{mn} + \omega}$$
$$- \sum_{j,\alpha,n>0} |\sigma^\alpha_{j,n0}|^2 \int \frac{d\omega}{4\pi} \frac{S^\alpha_j(\omega) - (P_n/P_0) S^\alpha_j(-\omega)}{(\omega_{n0} + \omega)^2}. \tag{5.34}$$

This is our central equation, which is used in the numerical calculations. As shown in the next subsection, it can also be obtained directly from the partition function of the total system. However, the physical interpretation of the following derivation is less transparent than the derivation presented above.

### 5.2.1 Alternative derivation using partition function

Consider the partition function

$$\widetilde{Z} = Tr\left(e^{-\beta \widetilde{H}}\right). \tag{5.35}$$

Using Eq. (5.3) one can express the occupation probabilities $\widetilde{P}_n$ directly through $\widetilde{Z}$

$$\begin{aligned} -\frac{1}{\beta} \frac{\partial}{\partial E_n} \ln \widetilde{Z} &= \frac{1}{\widetilde{Z}} Tr\left(e^{-\beta \widetilde{H}} \frac{\partial \widetilde{H}}{\partial E_n}\right) = Tr\left(\widetilde{\rho}_{SB} |n\rangle\langle n|\right) \\ &= \langle n | Tr_B(\widetilde{\rho}_{SB}) | n\rangle = \langle n | \widetilde{\rho}_S | n\rangle = \widetilde{P}_n, \end{aligned} \tag{5.36}$$

where

$$\widetilde{\rho}_{SB} = \frac{e^{-\beta \widetilde{H}}}{\widetilde{Z}} \tag{5.37}$$

is the total density matrix of the system plus environment.

First, we calculate the partition function in the interaction representation,

$$e^{-\beta\widetilde{H}} = e^{-\beta H}\left(\mathcal{T}\exp\int_0^\beta d\tau H_I(\tau)\right), \tag{5.38}$$

where $H = H_S + H_B$ is the non-interacting part of the Hamiltonian and $H_I(\tau) = e^{\beta H}H_I e^{-\beta H}$. Therefore,

$$\begin{aligned}\widetilde{Z} &= Tr\left(e^{-\beta\widetilde{H}}\right) = Tr\left[e^{-\beta H}\left(\mathcal{T}\exp\textstyle\int_0^\beta d\tau H_I(\tau)\right)\right] \\ &= Z\,Tr\left[\rho_{SB}\left(\mathcal{T}\exp\textstyle\int_0^\beta d\tau H_I(\tau)\right)\right] \\ &= Z\left\langle\mathcal{T}\exp\int_0^\beta d\tau H_I(\tau)\right\rangle,\end{aligned} \tag{5.39}$$

where $\langle ...\rangle = Tr[\rho_{SB}...]$ and $\rho_{SB} = e^{-\beta H}/Z$ is the density matrix for the non-interacting qubit system plus environment, which has the form $\rho_{SB} = \rho_S \otimes \rho_B = \sum_n P_n|n\rangle\langle n| \otimes \rho_B$, where $P_n$ is the occupation probability of state $|n\rangle$ and $\rho_B$ is the density matrix of the environment alone. Expanding to second order, we have

$$\begin{aligned}\widetilde{Z} &= Z\left(1 + \int_0^\beta d\tau\int_0^\tau d\tau'\,\langle H_I(\tau)H_I(\tau')\rangle\right) \\ &= Z\left(1 + \int_0^\beta d\tau\int_0^\tau d\tau'\,\left\langle q_j^\alpha(\tau)q_j^\alpha(\tau')\right\rangle_B\right. \\ &\left.\cdot\sum_{j,\alpha,n} P_n\langle n|\sigma_j^z(\tau)\sigma_j^z(\tau')|n\rangle\right),\end{aligned} \tag{5.40}$$

where $\langle ...\rangle_B = Tr_B[\rho_B...]$. We write the integral in this expression in terms of the environment spectral density using

$$\left\langle q_j^\alpha(\tau)q_j^\alpha(\tau')\right\rangle_B = \int\frac{d\omega}{2\pi}S_j^\alpha(\omega)e^{-\omega(\tau-\tau')}. \tag{5.41}$$

Defining $\sigma^{\alpha}_{j,nm} = \langle n|\sigma^{z}_{j}|m\rangle$ and $\omega_{nm} = E_n - E_m$, we find

$$
\begin{aligned}
&Integral = \textstyle\sum_{j,\alpha,n,m} \int \frac{d\omega}{2\pi} P_n |\sigma^{\alpha}_{j,nm}|^2 S^{\alpha}_{j}(\omega) \\
&\times \int_0^{\beta} d\tau \int_0^{\tau} d\tau' e^{(\omega_{nm}-\omega)(\tau-\tau')} \\
&= \sum_{j,\alpha,n,m} \int \frac{d\omega}{2\pi} P_n |\sigma^{\alpha}_{j,nm}|^2 S^{\alpha}_{j}(\omega) \\
&\times \frac{e^{\beta(\omega_{nm}-\omega)} - 1 - \beta(\omega_{nm}-\omega)}{(\omega_{nm}-\omega)^2} \\
&= \sum_{j,\alpha,n,m} \int \frac{d\omega}{2\pi} \frac{|\sigma^{\alpha}_{j,nm}|^2}{(\omega_{nm}-\omega)^2} [P_m S^{\alpha}_{j}(-\omega) - P_n S^{\alpha}_{j}(\omega)] \\
&- \sum_{j,\alpha,n,m} \int \frac{d\omega}{2\pi} \frac{\beta P_n |\sigma^{\alpha}_{j,nm}|^2 S^{\alpha}_{j}(\omega)}{\omega_{nm}-\omega}
\end{aligned}
\tag{5.42}
$$

In the last step we used $P_m = e^{\beta\omega_{nm}} P_n$, which is valid for the Boltzmann distribution, and $S^{\alpha}_{j}(-\omega) = S^{\alpha}_{j}(\omega) e^{-\beta\omega}$. The first integral in the last equation vanishes, giving

$$
\widetilde{Z} = Z \left( 1 - \sum_{j,\alpha,n,m} \int \frac{d\omega}{2\pi} \frac{\beta P_n |\sigma^{\alpha}_{j,nm}|^2 S^{\alpha}_{j}(\omega)}{\omega_{nm}-\omega} \right). \tag{5.43}
$$

Therefore,

$$
\ln \widetilde{Z} = \ln Z + \sum_{j,\alpha,n,m} \int \frac{d\omega}{2\pi} \frac{\beta P_n |\sigma^{\alpha}_{j,nm}|^2 S^{\alpha}_{j}(\omega)}{\omega_{mn}+\omega} \, , [P_n S^{\alpha}_{j}(\omega) - P_m S^{\alpha}_{j}(-\omega)]
$$

and

$$
\begin{aligned}
\widetilde{P}_n \;\; = \;\; & -\frac{1}{\beta} \frac{\partial}{\partial E_n} \ln \widetilde{Z} = -\frac{1}{\beta} \frac{\partial}{\partial E_n} \ln Z \\
& - \frac{\partial}{\partial E_n} \sum_{j,\alpha,m,k} \int \frac{d\omega}{2\pi} \frac{P_m |\sigma^{\alpha}_{j,mk}|^2 S^{\alpha}_{j}(\omega)}{\omega_{km}+\omega} \, .
\end{aligned}
\tag{5.44}
$$

Finally, we transform this equation using the relations

$$\begin{aligned} -\frac{1}{\beta}\frac{\partial}{\partial E_n}\ln Z &= P_n\,, \\ \frac{\partial}{\partial E_n}\frac{1}{\omega_{km}+\omega} &= \frac{\delta_{mn}-\delta_{kn}}{(\omega_{km}+\omega)^2}\,, \\ \frac{\partial P_m}{\partial E_n} &= \beta P_n(P_m-\delta_{mn})\,, \end{aligned} \tag{5.45}$$

to obtain

$$\begin{aligned} \widetilde{P}_n = P_n - \beta \sum_{j,\alpha,m,k} |\sigma^\alpha_{j,mk}|^2 \int \frac{d\omega}{2\pi} \frac{S^\alpha_j(\omega) P_n(P_m-\delta_{mn})}{\omega_{km}+\omega} \\ - \sum_{j,\alpha,m\neq n} |\sigma^\alpha_{j,mn}|^2 \int \frac{d\omega}{2\pi} \frac{P_n S^\alpha_j(\omega) - P_m S^\alpha_j(-\omega)}{(\omega_{mn}+\omega)^2}\,. \end{aligned} \tag{5.46}$$

This is the same equation as (5.33). Using (5.9), one recovers Eq. (5.34) for fidelity. Therefore

$$\begin{aligned} F = \sqrt{\frac{\widetilde{P}_0}{P_0}} = 1 - \beta \sum_{j,\alpha,n,m} |\sigma^\alpha_{j,nm}|^2 \int \frac{d\omega}{4\pi} \frac{S^\alpha_j(\omega)(P_n-\delta_{n0})}{\omega_{mn}+\omega} \\ - \sum_{j,\alpha,n>0} |\sigma^\alpha_{j,n0}|^2 \int \frac{d\omega}{2\pi} \frac{S^\alpha_j(\omega) - (P_n/P_0) S^\alpha_j(-\omega)}{(\omega_{n0}+\omega)^2}, \end{aligned} \tag{5.47}$$

which is the same as (5.34).

## 5.3 General properties of Ground State Fidelity

As is shown above, the perturbation expansion in $H_I$ in this situation gives

$$\begin{aligned} \delta P_0 &= -\beta P_0 \sum_{j,\alpha,n,m} (P_n-\delta_{n0}) |\sigma^\alpha_{j,nm}|^2 \int \frac{d\omega}{2\pi} \frac{S^\alpha_j(\omega)}{\omega_{mn}+\omega}\,, \\ \Gamma_{mn} &= \sum_{j,\alpha} |\sigma^\alpha_{j,nm}|^2 \int \frac{d\omega}{2\pi} \frac{S^\alpha_j(\omega)}{(\omega_{nm}+\omega)^2}\,, \end{aligned} \tag{5.48}$$

where $\sigma^\alpha_{j,nm} \equiv \langle n|\sigma^\alpha_j|m\rangle$ and $\omega_{nm} \equiv E_n - E_m$. Substituting (5.48) into (5.13) and then into (5.10), we obtain

$$F = 1 - \beta \sum_{j,\alpha,n,m} |\sigma^\alpha_{j,nm}|^2 \int \frac{d\omega}{4\pi} \frac{S^\alpha_j(\omega)(P_n - \delta_{n0})}{\omega_{mn} + \omega}$$
$$- \sum_{j,\alpha,n>0} |\sigma^\alpha_{j,n0}|^2 \int \frac{d\omega}{4\pi} \frac{S^\alpha_j(\omega) - (P_n/P_0) S^\alpha_j(-\omega)}{(\omega_{n0} + \omega)^2}. \tag{5.49}$$

Equation (5.49) is our main result. It is well-defined at $T = 0$, when all thermal excitations are suppressed, i.e., $P_n = 0$ for $n > 0$ and $S^\alpha_j(\omega) \equiv 0$ at $\omega < 0$. Hence, the values of $\omega$ around $-\omega_{m0}$, when the denominator in (5.49) vanishes, do not contribute to the integral. When $T \neq 0$, the divergences that appear at $\omega = -\omega_{m0}$ reflect the fact that environment can also create real thermal excitations of the qubit system. However, the detailed balance relation, $S^\alpha_j(-\omega) = e^{-\beta\omega} S^\alpha_j(\omega)$, ensures that these divergences cancel each other out and Eq. (5.49) is well-defined also at $T \neq 0$.

Equation (5.49) is now applied to specific problems. The first example we consider is a typical *individual qubit* with the Hamiltonian

$$H_S = -[\epsilon\sigma^z + \Delta\sigma^x]/2 \tag{5.50}$$

coupled as in Eq. (5.14), but only through $\sigma^z$, to the environmental noise with spectral density $S(\omega)$ (5.15). In the usual weak-coupling approximation [see, e.g., [16]], the qubit decoherence time $T_2^*$ is given by

$$\frac{1}{T_2^*} = \frac{1}{2T_1} + \frac{1}{T_\varphi}\,, \tag{5.51}$$

where $T_1$ and $T_\varphi$ are the relaxation and pure dephasing times, given by

$$T_1^{-1} = (\Delta^2/\Omega^2)[S(\Omega) + S(-\Omega)]\,, \tag{5.52}$$
$$T_\varphi^{-1} = (\epsilon^2/\Omega^2) S(0)\,, \tag{5.53}$$

with $\Omega = \sqrt{\Delta^2 + \epsilon^2}$. The standard expressions for the eigenstates of the Hamiltonian (5.50) reduce Eq. (5.49) for the fidelity to $F = 1 - \Delta^2 K/2\Omega^2$, where

$$K = \int \frac{d\omega S(\omega-\Omega)}{2\pi\omega} \left\{ \frac{1-e^{-\omega/T}}{\omega} - \frac{e^{-\Omega/T}+e^{-\omega/T}}{T(e^{-\Omega/T}+1)} \right\}. \tag{5.54}$$

We see that the same noise spectral density that defines the relaxation and dephasing rates (5.52) and (5.53) of the qubits in the GMQC determines the reduction of the ground-state fidelity in AQC. In this respect, the main difference between the reduction of fidelity and the real-time relaxation and dephasing is that even in the lowest-order perturbation theory, the fidelity is reduced by the whole spectrum of environmental excitations, and not just by limited spectral groups resonant with the qubit energy differences or the low-frequency excitations, as in Eqs. (5.52) and (5.53).

To strengthen this comparison, we consider an Ohmic bath characterized by the noise

$$S(\omega) = \eta\omega/(1 - e^{-\omega/T}) \tag{5.55}$$

with cutoff frequency $\omega_c$. In this case, the relaxation time is $T_1^{-1} = \eta(\Delta^2/\Omega)\coth(\Omega/2T)$ and the fidelity is expressed as

$$F = 1 - \frac{k}{Q}, \qquad k \equiv \frac{K}{2\eta} \tanh \frac{\Omega}{2T}, \tag{5.56}$$

where $Q = T_1\Omega$ is the qubit quality factor due to relaxation. Equation (5.54) gives the following expressions for the factor $k$ at low and high temperatures:

$$k = \frac{1}{4\pi} \begin{cases} \ln(\omega_c/\Omega) - 1 + \pi^2 T^2/3\Omega^2, & T \ll \Omega, \\ (\Omega/T)^2 \ln(\omega_c/T), & T \gg \Omega. \end{cases} \tag{5.57}$$

Equation (5.56) relates the ground state fidelity to the qubit quality factor, $Q$, as calculated due to relaxation only. This shows that the fidelity can be related more closely to the relaxation ($T_1$) and not dephasing ($T_\varphi$) processes. Adding a $1/f$ low-

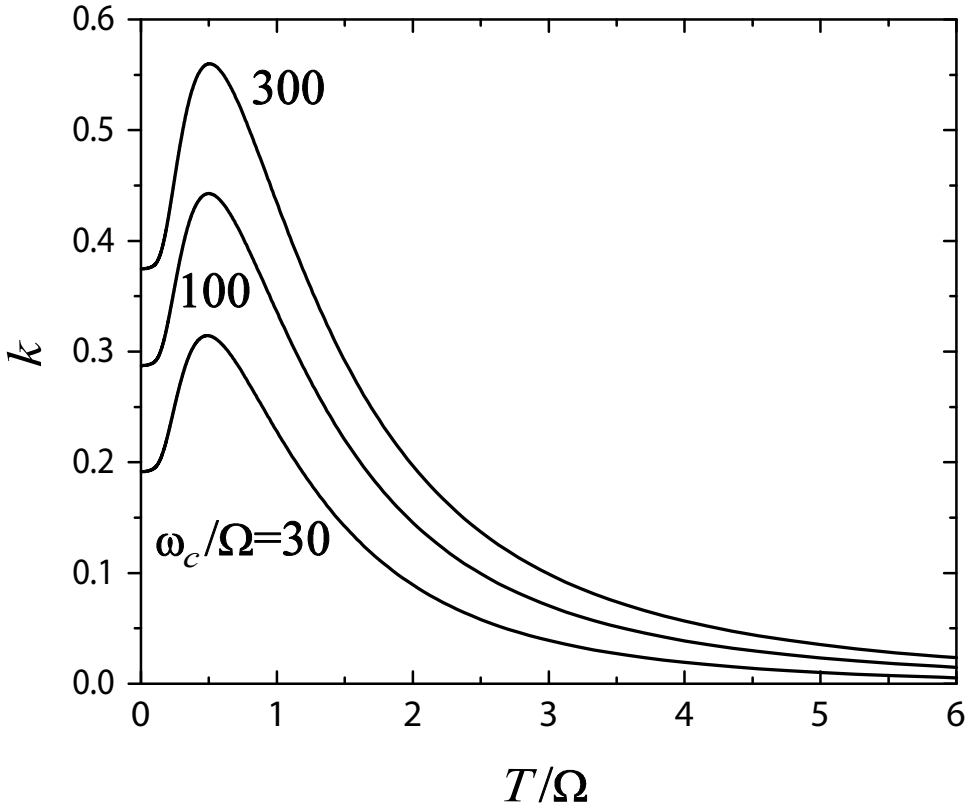


Figure 5.1: The temperature-dependent factor $k$ in the expression (5.56) for the ground state fidelity of an individual qubit in the presence of Ohmic environment with cut-off frequency $\omega_c$.

frequency noise of a realistic magnitude does not change this conclusion (as discussed in more details in the numerical examples below). As expected, a larger $Q$ leads to a better ground state fidelity. Figure 5.1 shows the factor $k$ in Eq. (5.56) as a function of temperature for different cut-off frequencies $\omega_c$. It exhibits the non-monotonic $T$-dependence, and only weak, logarithmic, dependence on $\omega_c$, which allows one to estimate the fidelity without precisely specifying $\omega_c$. The factor $k$ is maximal around $k_{\max} \simeq 0.5$ at $T \simeq 0.5\Omega$, which leads to a minimum fidelity $F \simeq 1 - (2Q)^{-1}$. Notice that even a qubit quality factor as low as $Q = 10$, which is practically useless for

GMQC, leads to $F > 95\%$ ground state fidelity.

The fact that fidelity is dominated by the relaxation (as opposed to dephasing) and, more generally, high-frequency noise, remains true even if we take into account the low-frequency (e.g., $1/f$) noise. In addition to an Ohmic component (5.55), for a typical mesoscopic solid-state qubit, environmental noise contains a low-frequency component (see, e.g., [91]). Under an appropriate approximation that the low-frequency noise is concentrated at frequencies $\omega \ll \Omega, T$, Eq. (5.54) for the fidelity in presence of the low-frequency noise can be expressed through the total noise intensity $W^2 = \int d\omega S(\omega)/2\pi$, and gives:

$$F = 1 - \frac{1}{2}(\frac{\Delta W}{\Omega^2})^2\big[1 - e^{-\Omega/T} - \frac{2\Omega/T}{e^{\Omega/T}+1}\big]\,. \tag{5.58}$$

For realistic parameters, suppression of fidelity (5.58) is small compared to that due to the high-frequency Ohmic noise. This is a very important difference between AQC and the GMQC, as the latter is very sensitive to the dephasing dominated by the low-frequency noise.

We now consider *multi-qubit systems*, starting with a system of $N$ *uncoupled* qubits. In this case, the trace in the definition of fidelity (5.10) can be taken independently over separate qubits, so that the total fidelity $F$ is the product of fidelities $F_j$, $j = 1, ..., N$ of the individual qubits: $F = \prod_j F_j$. For instance, a typical starting point of AQC algorithms is to initialize the system in the ground state of the Hamiltonian $H_U$ (5.71). Then, the state of all qubits is the same and can be characterized by the same fidelity (5.56). Then,

$$F = (1 - k/Q)^N\Big|_{Q\gg k} \simeq e^{-kN/Q}. \tag{5.59}$$

For independent qubits, fidelity scales exponentially with $N$ as a result of the exponential scaling of the probability for all qubits to remain in their corresponding ground states. Since $Q$ is inversely proportional to the noise strength $\eta$, by decreas-

ing the noise by a factors of, e.g., 10, one can achieve the same fidelity with 10 times more qubits.

## 5.4 Numerical calculations

In this section, we derive the equations that form the basis of our numerical calculation of the ground state fidelity $F$. We assume that the noise is coupled only to $\sigma_j^z$ operators and $S_j^z(\omega) = S(\omega)$ is the same for all qubits. We also define $M_{mn} = \sum_j |\sigma_{j,mn}^z|^2$. Equation (5.34) can be rewritten as

$$\begin{aligned} F^2 = 1 &- \beta \sum_{m,n>0} M_{mn} \int \frac{d\omega}{2\pi} \frac{S(\omega) P_n}{\omega_{mn} + \omega} \\ &- \beta \sum_{n>0} M_{0n} \int \frac{d\omega}{2\pi} \frac{S(\omega) P_n}{\omega_{0n} + \omega} \\ &- \beta \sum_{m} M_{m0} \int \frac{d\omega}{2\pi} \frac{S(\omega)(P_0 - 1)}{\omega_{m0} + \omega} \\ &- \sum_{n>0} M_{n0} \int \frac{d\omega}{2\pi} \frac{S(\omega) - (P_n/P_0) S(-\omega)}{(\omega_{n0} + \omega)^2} \,. \end{aligned} \tag{5.60}$$

We use $M_{nm} = M_{mn}$ and change $\omega$ to $-\omega$ in some integrals to get

$$\begin{aligned} F^2 = 1 &- \beta \sum_{m,n>0} M_{mn} \int \frac{d\omega}{2\pi} \frac{S(\omega) P_n}{\omega_{mn} + \omega} \\ &- \beta \sum_{n>0} M_{n0} \int \frac{d\omega}{2\pi} \frac{P_0 S(\omega) - P_n S(-\omega)}{\omega_{n0} + \omega} \\ &- \beta (P_0 - 1) M_{00} \int \frac{d\omega}{2\pi} \frac{S(\omega)}{\omega} - \sum_{n>0} M_{n0} \\ &\cdot \int \frac{d\omega}{2\pi} \frac{S(\omega)[1 - \beta(\omega_{n0} + \omega)] - (P_n/P_0) S(-\omega)}{(\omega_{n0} + \omega)^2} \,. \end{aligned} \tag{5.61}$$

Next, we symmetrize this equation by using the fact that $\sum_{m>0} P_m = 1 - P_0$:

$$
\begin{aligned}
F^2 = 1 &- \beta \sum_{m>n>0} M_{mn} \int \frac{d\omega}{2\pi} \frac{S(\omega)P_n - S(-\omega)P_m}{\omega_{mn} + \omega} \\
&- \frac{\beta}{2} \sum_{m>0} P_m (M_{mm} - M_{00}) \int \frac{d\omega}{2\pi} \frac{S(\omega) - S(-\omega)}{\omega} \\
&- \sum_{m>0} M_{m0} \int \frac{d\omega}{2\pi} \frac{S(\omega)[1 - \beta(\omega_{m0} + \omega)] - (P_m/P_0)S(-\omega)}{(\omega_{m0} + \omega)^2} \\
&- \sum_{m>0} M_{m0} \int \frac{d\omega}{2\pi} \frac{\beta(\omega_{m0} + \omega)[P_0 S(\omega) - P_m S(-\omega)]}{(\omega_{m0} + \omega)^2}.
\end{aligned}
\tag{5.62}
$$

Note that each line in Eq. (5.62) has the form $S(\omega)/\omega$ at large $\omega$ and hence diverges together with the high-frequency cutoff in the used model of environmental noise (see below). When all the states of the qubit system are included, these divergences cancel each other. However, only part of the eigenstates are used in the numerical calculations, so the divergence does not vanish if one employs directly Eq. (5.62).

Using the property $\sum_n |\langle |n|\sigma_j^z|m\rangle|^2 = 1$, it can be shown that

$$
\begin{aligned}
\sum_{m>0} P_m (M_{mm} - M_{00}) = &\sum_{m>0} M_{m0}(1 - P_0 - P_m) \\
&- \sum_{m>n>0} (P_m + P_n) M_{mn} \,.
\end{aligned}
\tag{5.63}
$$

Combining (5.62) and (5.63), we get the final result for fidelity:

$$
F^2 = 1 - \int \frac{d\omega}{2\pi} f(\omega) \,,
$$

or, in our perturbation approximation,

$$
F = 1 - \frac{1}{4\pi} \int d\omega f(\omega) \,,
\tag{5.64}
$$

with

$$f(\omega) = \beta \sum_{m>n>0} M_{mn} f_{mn}(\omega) + \sum_{m>0} M_{m0} g_m(\omega)\,.$$

Here

$$\begin{aligned} f_{mn}(\omega) &= \frac{S(\omega)P_n - S(-\omega)P_m}{\omega_{mn}+\omega} - \frac{P_m+P_n}{2} \\ &\times \frac{S(\omega)-S(-\omega)}{\omega}\,, \\ g_m(\omega) &= \frac{[1+(P_0{-}1)\beta(\omega_{m0}{+}\omega)]S(\omega)}{(\omega_{m0}{+}\omega)^2} \\ &- \frac{[1+P_0\beta(\omega_{m0}{+}\omega)](P_m/P_0)S(-\omega)}{(\omega_{m0}{+}\omega)^2} \\ &+ \beta\frac{1-P_0-P_m}{2}\frac{S(\omega)-S(-\omega)}{\omega}\,. \end{aligned} \tag{5.65}$$

One can see that

$$f_{mn}(\omega) \to P_n S(\omega) + \frac{P_m+P_n}{2}\frac{S(\omega)+S(-\omega)}{\omega}$$

as $\omega \to -\omega_{mn}$, and

$$g_m(\omega) \to \beta^2(P_0{-}1/2)S(\omega) + \beta\frac{1-P_0-P_m}{2}\frac{S(\omega)-S(-\omega)}{\omega}$$

as $\omega \to -\omega_{m0}$. This implies that the poles are removed and the $S(\omega)/\omega$ divergence at infinity also disappears for each term, thus improving the convergence properties of this expression for the numerical evaluation of fidelity.

### 5.4.1 Noise spectral density

For numerical calculations in this work, we consider the flux noise in a rf-SQUID. The noise operator $q = I_p \delta\Phi_x$ is therefore related to the flux noise $\delta\Phi_x$ through the rf-SQUID, where $I_p$ is the persistent current of the rf-SQUID. The noise is

characterized by its correlation function through the spectral density

$$S(\omega) = \int_{-\infty}^{\infty} dt\ e^{i\omega t} \langle q(t)q(0)\rangle = I_p^2 S_\Phi(\omega) \tag{5.66}$$

where

$$S_\Phi(\omega) = \int_{-\infty}^{\infty} dt\ e^{i\omega t} \langle \delta\Phi_{1x}(t)\delta\Phi_{1x}(0)\rangle \tag{5.67}$$

is the spectral density of the flux noise. Since the actual noise is of the form of flux noise, the spectral density, $S(\omega) \propto I_p^2$, should depend on the bias point through $I_p$. Then,

$$S(\omega) = \kappa \left[ \frac{\gamma^2}{|\omega|} + \hbar^2 \frac{\eta\omega e^{-|\omega|/\omega_c}}{1 - e^{-\hbar\omega/k_B T}} \right], \tag{5.68}$$

with

$$\kappa = (I_p/I_{pm})^2, \tag{5.69}$$

where $I_{pm}$ is the maximum value for $I_p$, $\eta$ is a dimensionless coefficient characterizing the Ohmic noise and $\gamma$ is an energy scale characterizing the $1/f$ noise.

In the actual quantum annealing system described by Eq. (1) of the main text, the persistent current $I_p$ and the tunneling amplitude of qubits are time-dependent. As described in Ref. 18 of the main text, the energy scale $B(s)$ depends on $I_p$ as $B(s) = M_0 I_p^2$, where $M_0$ is the maximum mutual inductance between the qubits through the tunable couplers and $s = t/t_f$. Therefore, one can write $\kappa(s) = B(s)/B(s_m)$, where $B(s_m) = M_0 I_{pm}^2$. It is therefore sufficient to determine $s_m$ to calculate $\kappa(s)$ at all $s$.

Measurement of the $1/f$ noise reveals a flux noise spectral density of the form $S_\Phi(2\pi f) = A^2/|f|^\alpha$, with $\alpha \approx 1$. From (5.66) we find

$$\gamma \approx \sqrt{2\pi} I_{pm} A\,. \tag{5.70}$$

For the qubits in the current D-Wave processors we have $\eta \approx 0.1$, $A \approx 3\mu\Phi_0$, and $I_{pm} \approx 1\ \mu$A at $s_m = 0.636$, which gives $\gamma/h \approx 23$ MHz $\approx 0.02$ GHz.

### 5.4.2 Results

Next, we focus on how the ground state fidelity behaves in practical AQC systems. We use as an example the *D-Wave One* quantum annealing processor installed at the University of Southern California (see [96]). The Hamiltonian implemented by the processor has the form of Eq. (5.1), with

$$H_U = -\sum_{i=1}^{N} \sigma_i^x \,, \quad H_P = \sum_{i=1}^{N} h_i \sigma_i^z + \sum_{i,j=1}^{N} J_{ij} \sigma_i^z \sigma_j^z \,, \tag{5.71}$$

where $h_i$ and $J_{ij}$ are tunable dimensionless bias and coupling coefficients. The parameters $A(s)$ and $B(s)$ for this processor are plotted in Fig. 5.2**b**. We calculate fidelity of the ground state for a ferromagnetic chain (illustrated in Fig. 5.2**a**) with $h_i = 0$ and $J_{i,i+1} = -1$, otherwise known as a quantum Ising model in a transverse field. Here, the length of the chain is varied from $N = 2$ to 16. Although this model is exactly solvable (see, e.g., [97] and references therein), fidelity cannot be calculated exactly for practical noise models in which the coupling to environment is dominated by the $\sigma_j^z$ terms. Hence, we calculate the fidelity numerically. In the limit $N \to \infty$, the model is known to have a *quantum critical point* at $A(s) = B(s)$. At this point, the chain goes through a quantum phase transition between paramagnetic and ferromagnetic phases. In the ferromagnetic phase, the ground state is doubly degenerate with respect to simultaneous change of signs of all $\sigma_i^z$ terms. Figure 5.2**c** plots several of the lowest energy levels of a 10-qubit chain relative to the ground state energy $E_0$. As seen in this plot, the quantum critical point manifests itself as the appearance of the doubly-degenerate ground state and the minimum in the energy gap between the ground and the second excited states.

To calculate fidelity for this system, we use a realistic noise model relevant to the *D-Wave* qubits [90]. In this case, the dominant environmental coupling is to the magnetic flux noise, which couples directly to the qubit computational basis states represented by the $\sigma_j^z$ operators. The noise spectral density $S(\omega)$ was characterized

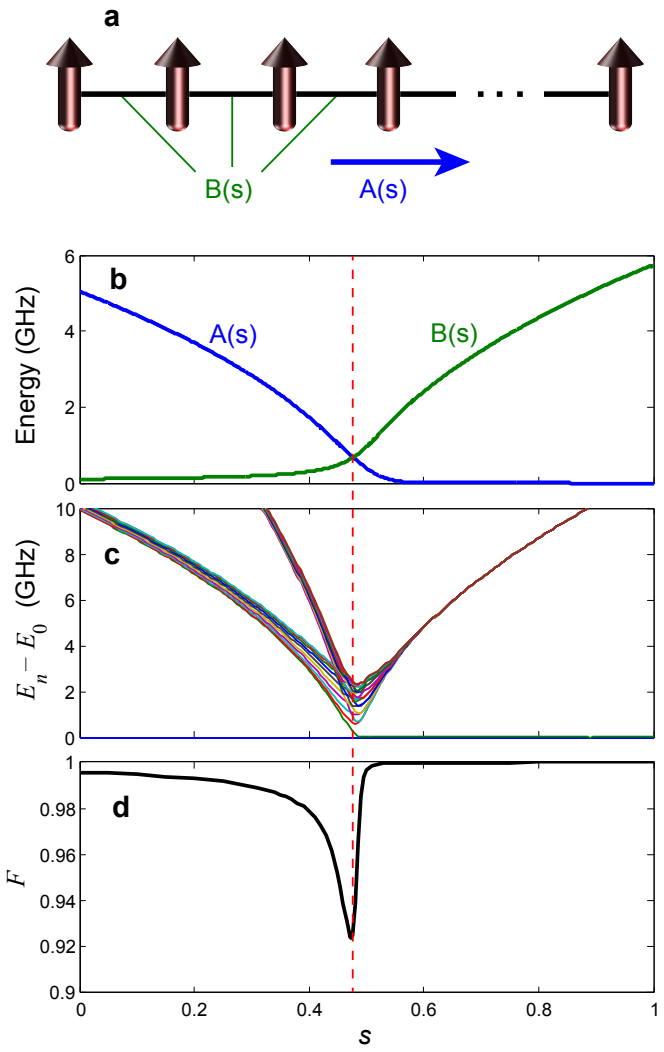


Figure 5.2: Fig **a.** A ferromagnetic spin chain with transverse field and coupling energies given, respectively, by $A(s)$ and $B(s)$ in Fig.(b). **b.** Energy scales $A(s)$ and $B(s)$ extracted from experimental parameters. **c.** The lowest 20 energy levels, relative to the ground state, of a 10-qubit ferromagnetic chain with $J_{ij} = -1$, as a function of the normalized time $s$. **d.** Ground state fidelity of the 10-qubit chain of **c** at $T = 20$ mK. The vertical (red) dashed curve marks the quantum critical point.

in the earlier experiments, which were consistent with the noise being a combination of the $1/f$ low-frequency noise and an Ohmic noise at high frequencies [91]. For calculations of fidelity, we take $S(\omega) = \kappa(s)[S_{HF}(\omega) + S_{LF}(\omega)]$, where $S_{HF}(\omega)$ is the Ohmic spectral density (5.55) and $S_{LF}(\omega) = \gamma^2/|\omega|$. The coefficient $\kappa(s) = B(s)/B(s_m)$ appears because the strength of coupling to flux noise depends on the persistent current of the flux qubits which changes as a function of $s$ (see SI). Here $s_m$ is the bias point at which the measurements of $\eta$ and $\gamma$ are performed. Based on the experimental data, we use $\eta = 0.1$, $\gamma = 20$ MHz and $s_m = 0.636$. We also assume $\omega_c = 100$ GHz for the high-frequency cutoff and $\omega_L = 1$ MHz for the low-frequency cutoff (based on a $t_f \sim 1$ $\mu$s evolution time of an algorithm). We found that for these parameters, the fidelity is dominantly determined by the high-frequency Ohmic noise and not by the $1/f$ noise.

In principle, since the total number of energy levels grows exponentially with $N$, the time required for numerical calculation of $F$ also grows exponentially. Fortunately, the value of $F$ converges rapidly for a finite number of retained energy states. Here, we keep all energy levels for $N \leq 10$, and up to 2000 energy levels for larger chains. The fidelity of the 10-qubit chain is plotted as a function of $s$ in Fig. 5.2**d**. The ground state fidelities of chains with other lengths (and coupled systems other than chains) are qualitatively the same as the one plotted in Fig. 5.2**d**. It is clear from the figure that the fidelity is minimum close to the critical point. Notice also that the fidelity approaches $F = 1$ as $s$ increases, which is the result of $H_P$ commuting with $H_I$, with only $\sigma_j^z$ terms and negligible other types of coupling to environment. This again reflects the fact that the fidelity depends rather on relaxation than dephasing.

Figure 5.3 shows the numerical results for the ground state fidelity for $N$-qubit chains with $N = 1$ to 16 at the critical point. For all chain lengths, the fidelity is better than 90%. It should be emphasized that these are the minimum fidelities at the quantum critical point. The fidelity at all other points is larger, and near $s = 1$, is very close to 1 as shown in Fig. 5.2**d**. We have also plotted in Fig. 5.3 the ground

state fidelity of $N$ uncoupled qubits at different $N$ based on the exponential scaling of Eq. (5.59). The scaling and magnitude of the fidelity at large $N$ is better for the ferromagnetic chain than for the uncoupled qubits. Unfortunately, it was not possible to pursue numerical calculations beyond 16 qubits, as direct perturbation approximation would break down when $F$ strongly deviates from unity. A naive exponential extrapolation of the data points to $N = 128$ (representing the worse case) still yields $F = 0.47$, meaning that the eigenstates could retain their quantum properties without error correction for such a large-size system. As in uncoupled qubits, if one can reduce the noise by a large factor, the size of the chain can be increased by the same factor while keeping the fidelity unchanged. In addition, other techniques such as dynamical decoupling [93] or error correction [94] could be employed to enhance the ground state fidelity at large scales.

Finally, we discuss how the ground state fidelity should affect the performance of AQC. In universal AQC [36, 37], the fidelity of the final ground state determines the quality of the computation. Indeed, deviations of $F$ from 1 mean that the statistics of measurements done on this state will be different from the one that corresponds to the ideal ground state. For instance, in the case of one qubit with $\epsilon = 0$ and the Hamiltonian (5.50), measurement of $\sigma_x$ has a non-vanishing probability $1 - F^2$ of producing the result $\sigma_x = -1$ different from the ground state $\sigma_x = 1$ even at temperatures $T \ll \Delta$. However, this effect is absent in the special case when the coupling to environment via $H_I$ commutes with the final Hamiltonian $H_P$, leading to $F = 1$ at the end of evolution, as in the adiabatic quantum optimization discussed above and shown in Fig. 5.2**d**. In this case, thermal transitions increase the loss of probability due to small fidelity in the middle of the evolution, thereby decreasing the ground state probability even further ($\widetilde{P}_0 = P_0 F^2$). Therefore, the probability will be distributed among the low energy states even more than implied by the thermal equilibrium. Part of the probability can be regained later when the gap is larger and $F$ is closer to 1. However, since the relaxation time becomes exponentially long near the end of evolution, the majority of the probability that is lost may not be

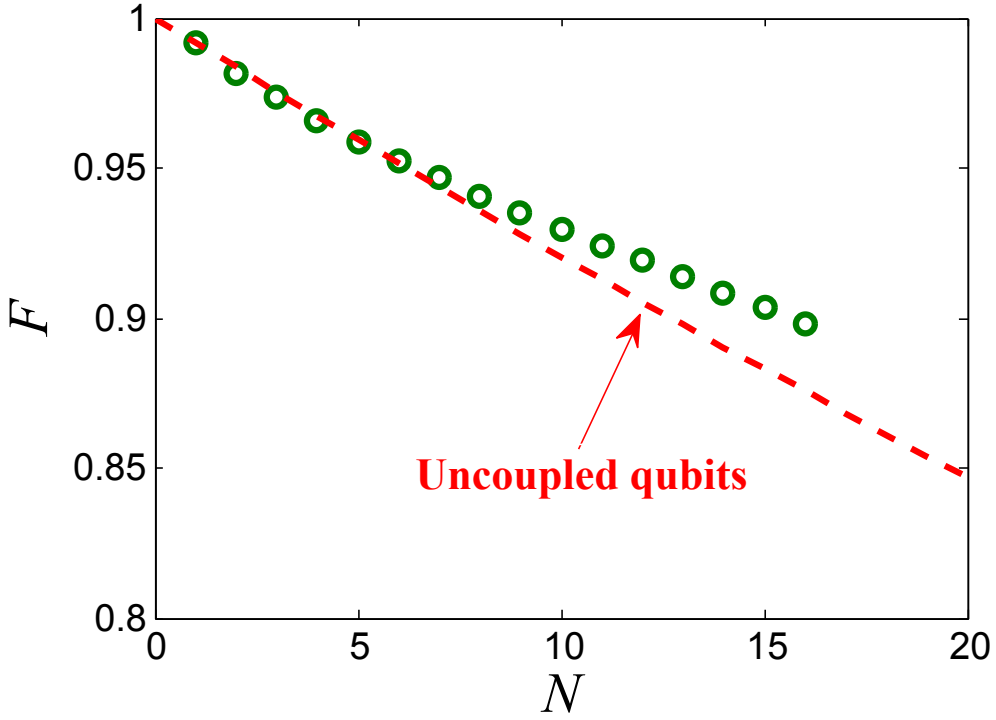


Figure 5.3: Ground state fidelity at the quantum critical point for ferromagnetic chains with $N = 1$ to 16, at $T = 20$ mK. Circles are the numerical results using (5.49). The red dashed curve is fidelity of uncoupled qubits from (5.59) with $k = 0.32$ and $Q = 38.4$.

gained back, thus leading to smaller probability of success. This makes it important to maintain fidelity close to unity throughout the evolution. We stress that most treatments of AQC based on the weak coupling master equation, e.g., [33, 83, 95], do not take into account the effect of deformation of the eigenstates that is captured by our calculation of the fidelity.

## 5.5 Conclusions

In summary, we have proposed using ground state fidelity as a quantity for measuring the strength of decoherence effects in AQC. Fidelity plays a role similar to decoherence time in GMQC, and is determined by the same noise correlator that determines the decoherence time in GMQC. However, fidelity takes into account qualitatively different effects of environment on the ground state relevant to AQC. The fidelity is related to the relaxation processes and is relatively insensitive to the dephasing. Our numerical calculations indicate that fidelity close to unity can be achieved with a moderate qubit quality factor, even for large numbers of qubits. Ground state fidelity should be a useful measure of the environment related quality of AQC systems in the context of further work on important topics in AQC such as quantum error correction or the threshold theorem.

# Bibliography


[1] D. Deutsch, *Proc. Roy. Soc. London Ser.* A, Vol.**400** No.1818 ,97 (1985).

[2] A. Church, *Am. J. Math.* **58**, 345 (1936).

[3] A. Turing, *Proc. Lon. Math. Soc.* **42**, 230 (1936).

[4] P. Shor, *Proceedings 35th Annual Symposium on Foundations on Computer Science*, Los Alamitos, CA, IEEE Press (1994).

[5] L. K. Groover, *Phys. Rev. Lett.* **79**,325 (1997).

[6] D. Simon, *Proceedings 35th Annual Symposium on Foundations on Computer Science*, Los Alamitos, CA, IEEE Press (1994).

[7] R. Calderbank and P. W. Shor, *Phys. Rev. A* **54**, 1098 (1996).

[8] A. Steane, *Proc. R. Soc. London Ser. A* **452**, 2551 (1996).

[9] J. Preskill, *Proc. R. Soc. Lond. A* **454**, 385 (1998).

[10] A. Y. Kitaev, *Russ. Math. Surv.* **52**, 1191 (1997).

[11] D. Aharonov and M. Ben-Or, arXiv:quant-ph/9906129 (1999).

[12] E. Knill, R. Laflamme, and W.H. Zurek, *Science* **279**, 342-345 (1998).

[13] E. Knill, *Nature* **434**, 39-44 (2005).

[14] M. A. Nielsen and I. L. Chuang, *Quantum Computation and Quantum Information*, Cambridge University Press (2010).

[15] L. D. Landau and E.M. Lifshitz, *Quantum mechanics*, Pergamon (1981).

[16] K. Blum, *Density matrix thoery and applications*, Plennum, NY (1981).

[17] B. D. Josephson, *Phys. Lett.* **1**, 251 (1962).

[18] B. D. Josephson, *Rev. Mod. Phys.* **36**, 216 (1964).

[19] J. Clarke, *Scientific American* **271**, 46 (August 1994).

[20] J. Clarke and A. I. Braginski, *The SQUID Handbook*, Vol. **1**, Wiley-VCH (2004).

[21] Y. Nakamura, Yu. A. Pashkin, and J.S. Tsai, *Nature* **398**, 786 (1999).

[22] D. Vion, A. Assime, A. Cotter, P. Joyez, H. Pothier, C. Urbina, D. Estave, and M. H. Devoreti, *Science* **296**, 886 (2002).

[23] Yu. A. Pashkin, T. Yamamoto, O. Astafiev, Y. Nakamura, D. V. Averin, and J. S. Tsai, *Nature* **421**, 823 (2003).

[24] R. Rouse, S. Han, and J. E. Lukens, *Phys. Rev. Lett.* **75**,1614 (1995).

[25] J. R. Friedman, V. Patel, W. Chen, S. K. Tolpygo, and J. E. Lukens, *Nature* **406**, 43 (2000).

[26] C. H. van der Wal, A. C. J. ter Haar, F. K. Wilhelm, R. N. Schouten, C. H. P. M. Harmans, T. P. Orlando, S. Lloyd, and J. E. Mooij, *Science* **290**, 773 (2000).

[27] J. M. Martinis, S. Nam, J. Aumentado, and C. Urbina, *Phys. Rev. Lett.* **89**, 117901 (2002).

[28] J. Clarke, A. N. Cleland, M. H. Devoret, D. Esteve, and J. M. Martinis, *Science* **239**, 992 (1988).

[29] J. Koch, T. M. Yu, J. Gambetta, A. A. Houck, D. I. Schuster, J. Majer, A. Blais, M. H. Devoret, S. M. Girvin, and R. J. Schoelkopf, *Phys. Rev. A* **76**, 042319 (2007).

[30] C. Rigetti, J. M. Gambetta, S. Poletto, B. L. T. Plourde, J. M. Chow, A. D. Crcoles, J. A. Smolin, S. T. Merkel, J. R. Rozen, G. A. Keefe, M. B. Rothwell, M. B. Ketchen, and M. Steffen, *Phys. Rev. B* **86**, 100506(R) (2012) .

[31] E. Farhi, J. Goldstone, S. Gutmann, J. Lapan, A. Lundgren, and D. Preda, *Science* **292**, 472 (2001).

[32] T. Kato, *J. Phys. Soc. Jap.* **5**, 435 (1951).

[33] A. M. Childs, E. Farhi, and J. Preskill, *Phys. Rev. A* **65**, 012322 (2001).

[34] S. Lloyd, arXiv: 0805.2757 (2008).

[35] A. Mizel, M.W. Mitchell, and M. L. Cohen, *Phys. Rev. A* **63**, 040302 (2001).

[36] D. Aharonov, W. van Dam, J. Kempe, Z. Landau, S. Lloyd, and O. Regev, arXiv: quant-ph/0405098 (2004).

[37] A. Mizel, D. A. Lidar, and M. Mitchell, *Phys. Rev. Lett.* **99**, 070502 (2007).

[38] A. Kitaev, A. Shen, and M. Vyalyi, *Classical and Quantum Computation, Graduate Studies in Mathematics*, Vol. **47**, (AMS, Providence, R.I., 2002).

[39] J. Kempe, A. Kitaev, and O. Regev, *SIAM J. Comput.* **35**, 1070 (2006).

[40] R. Oliveira and B. Terhal, arXiv: quant-ph/0504050 (2005).

[41] J. D. Biamonte and P. J. Love, *Phys. Rev. A* **78**, 012352 (2008).

[42] T. Kadowaki and H. Nishimori, *Phys. Rev. E* **58**, 5355 (1998).

[43] A. B. Finnila, M. A. Gomez, C. Sebenik, C. Stenson, and J. D. Doll, *Chem. Phys. Lett.* **219**, 343 (1994).

[44] M. W. Johnson, M. H. S. Amin, S. Gildert, T. Lanting, F. Hamze, N. Dickson, R. Harris, A. J. Berkley, J. Johansson, P. Bunyk, E. M. Chapple, C. Enderud, J. P. Hilton, K. Karimi, E. Ladizinsky, N. Ladizinsky, T. Oh, I. Perminov, C. Rich, M. C. Thom, E. Tolkacheva, C. J. S. Truncik, S. Uchaikin, J. Wang, B. Wilson, and G. Rose, *Nature* **473**, 194 (2011).

[45] D. V. Averin, *Fortschr. Phys.* **48**, 1055 (2000).

[46] Y. Makhlin, G. Schön, and A. Shnirman, *Rev. Mod. Phys.* **73**, 357 (2001).

[47] A. Leggett, *Foundations of Physics* **33**(10), 1469 (2003).

[48] B. S. DeWitt, *Proceedings of the Internation School of Physics "Enrico Fermi" Course IL: Foundations of Quantum Mechanics*, Academic Press (1972).

[49] J. Von. Neumann, *Mathematical Foundations of Quantum Mechanics*, Princeton University Press (1955).

[50] V. B. Braginskym and F. Ya. Khalili, *Quantum Measurement*, Cambridge Univeristy Press (1992).

[51] D. V. Averin, *Quantum Noise in Mesoscopic Physics*, Vol. **97**, Kluwer Academic Publishers (2003). Also in arXic:cond-mat/0301524 (2003).

[52] A. A. Clerk, S. M. Girvin, and A.D. Stone, *Phys. Rev. B* **67**, 165324 (2003).

[53] A. A. Clerk, M. H. Devoret, S.M. Girvin, F. Marquardt, and R.J. Schoelkopt, *Rev. Mod. Phys.* **82**, 1155 (2010).

[54] J. J. Sakur and J. J. Napolitano, *Modern Quantum Mechanics*, Addison-Wesley (2011).

[55] U. Weiss, *Quantum Dissipative Systems*, World Scientific (1999).

[56] H. B. Callen and T. A. Welton, *Phys.Rev.* **83**, 34 (1951).

[57] J. W. Negle and H.i Orland, *Quantum Many-Partilce Systems*, Westview Press (1988).

[58] G. Strang, *Linear Algebra and Its Applications*, Cengage Learning (2005).

[59] A. N. Korotkov and D. V. Averin, *Phys. Rev. B* **64**, 165310 (2001).

[60] O. Astafiev, Yu. A. Pashkin, Y. Nakamura, T. Yamamoto, and J. S. Tsai, *Phys. Rev. Lett.* **93**, 267007 (2004).

[61] F. Yoshihara, K. Harrabi, A. O. Niskanen, Y. Nakamura, and J. S. Tsai, *Phys. Rev. Lett.* **97**, 167001, (2006).

[62] R. Harris, M. W. Johnson, S. Han, A. J. Berkley, J. Johansson, P. Bunyk, E. Ladizinsky, S. Govorkov, M. C. Thom, S. Uchaikin, B. Bumble, A. Fung, A. Kaul, A. Kleinsasser, M. H. S. Amin, and D. V. Averin, *Phys. Rev. Lett.* **101**, 117003, (2008).

[63] J. Bechhofer, *Rev.Mod.Phys.* **77**, 783 (2005).

[64] A. V. Oppenheim and R. W. Schafer, *Discrete-Time Signal Processing*, Prentice Hall (2009).

[65] S. Pligram and M. Büttiker, *Phys. Rev. Lett.* **89**, 200401 (2002).

[66] K. K. Likharev and V. K. Semenov, *IEEE Trans. Appl. Supercond.* **1**, 3 (1991).

[67] V. K. Semenov and D. V. Avein, *IEEE Trans. Appl. Supercond.* **13**, 960 (2003).

[68] V. K. Kaplunenko and A. V. Ustinov, *Eur. Phys. J. B* **38**, 3 (2004).

[69] A. M. Savin, J. P. Pekola, D. V. Avein, and V. K. Semenov, cond-mat/0509318 (2005).

[70] D. V. Averin, K. Rabenstein, and V. K. Semenov, *Phys. Rev. B* **73**, 094504 (2006).

[71] K. G. Fedorov, A. V. Shcherbakova, R. Schäfer, and A. V. Ustinov, *Appl. Phys. Lett.* **102**, 132602 (2013).

[72] C. Bennett, *IBM J. Res. Devel.* **17**, 525 (1973).

[73] P. Benioff, *Phys. Rev. Lett.* **48**, 1581 (1982).

[74] R. Rajaraman, *Solitons and Instantons*, North Holland, New York ( 1982).

[75] S. Coleman, *Aspects of Symmetry: selected Erice Lectures*, Cambridge University Press (1988).

[76] J. Rubinstein, *J. Math. Phys.* **11**, 258 (1970).

[77] M. Steffen, M. Ansmann, R. C. Bialczak, N. Katz, E. Lucero, R. McDermott, M. Neeley, E. M. Weig, A. N. Cleland, and J. M. Martinis, *Science* **313**, 1423 (2006).

[78] J. H. Plantenberg, P. C. de Groot, C. J. P. M. Harmans, and J. E. Mooij, *Nature* **447**, 836 (2007).

[79] V. K. Semenov, G. V. Danilov, and D. V. Averin, *IEEE Trans. Appl. Supecond.* **13**, 938 (2003).

[80] J. Ren, V. K. Semenov, Yu. A. Polyakov, D. V. Averin, and J. S. Tsai, *IEEE Trans. Appl. Supecond.* **19**, 961 (2009).

[81] M. W. Johnson *et al.*, Nature **473**, 194 (2011).

[82] J. D. Biamonte, V. Bergholm, J. D.Whitfield, J. Fitzsimons, and A. Aspuru-Guzik, *AIP Advances* **1**, 022126 (2011).

[83] M. H. S. Amin, C. J. S. Truncik, and D. V. Averin, *Phys. Rev. A* **80**, 022303 (2009).

[84] J. Roland and N. J. Cerf, *Phys. Rev. A* **71**, 032330 (2005).

[85] M. S. Sarandy and D. A. Lidar, *Phys. Rev. Lett.* **95**, 250503 (2005).

[86] M. Tiersch and R. Schützhold, *Phys. Rev. A* **75**, 062313 (2007).

[87] M. H. S. Amin, P. J. Love, and C. J. S. Truncik, *Phys. Rev. Lett.* **100**, 060503 (2008).

[88] M. H. S. Amin, D. V. Averin, and J. A. Nesteroff, *Phys. Rev. A* **79**, 022107 (2009).

[89] A. Uhlmann, *Rep. Math. Phys.* **9**, 273 (1976).

[90] R. Harris, J. Johansson, A. J. Berkley, M. W. Johnson, T. Lanting, Siyuan Han, P. Bunyk, E. Ladizinsky, T. Oh, I. Perminov, E. Tolkacheva, S. Uchaikin, E. M. Chapple, C. Enderud, C. Rich, M. Thom, J. Wang, B. Wilson, and G. Rose, *Phys. Rev. B* **81**, 134510 (2010).

[91] T. Lanting, M. H. S. Amin, M. W. Johnson, F. Altomare, A. J. Berkley, S. Gildert, R. Harris, J. Johansson, P. Bunyk, E. Ladizinsky, E. Tolkacheva, and D. V. Averin, *Phys. Rev. B* **83**, 180502(R) (2011).

[92] J. Dziarmaga, *Phys. Rev. Lett.* **95**, 245701 (2005).

[93] D. A. Lidar, *Phys. Rev. Lett.* **100**, 160506 (2008).

[94] S. Jordan, E. Farhi, and P. Shor, *Phys. Rev. A* **74**, 052322 (2006).

[95] T. Albash, S. Boixo, D. A. Lidar, and P. Zanardi, arXiv:1206.4197.

[96] Z. Bian, F. Chudak, W. G. Macready, L. Clark, and F. Gaitan, arXiv:1201.1842.

[97] J. Dziarmaga, *Phys. Rev. Lett.* **95**, 245701 (2005).